AN INTERNAL FRICTION AND DSC STUDY OF THE Cu-Zn-Al SHAPE MEMORY ALLOYS

BY

TIAN XIAO

A Thesis

Submitted to the School of Graduate Studies

in Partial Fulfilment of the Requirements

for the Degree

Doctor of Philosophy

McMaster University

AN INTERNAL FRICTION AND DSC STUDY OF THE Cu-Zn-Al SHAPE MEMORY ALLOYS

Dedicated to My Dear Parents.

DOCTOR OF PHILOSOPHY (1993) MCMASTER UNIVERSITY

(Materials Engineering) Hamilton, Ontario

TITLE: **An Internal Friction and DSC study of the Cu-Zn-Al Shape Memory Alloys**

AUTHOR: **Tian Xiao**

B.Sc. (Shanghai Jiao Tong University)

M.A.Sc. (University of Windsor)

SUPERVISOR: **Professor G.P. Johari**

NUMBER OF PAGES: xx, 200

ABSTRACT

The temperature and time dependence of the thermoelastic martensitic transformation in Cu-Zn-Al shape memory alloys have been studied by means of internal friction, DSC (Differential Scanning Calorimetry), X-ray diffraction and metallography. A physical model and mathematical treatment have been developed to derive an expression for internal friction associated with the thermoelastic martensitic transformation. This expression has been able to explain the amplitude dependence of the internal friction in various ranges of stress amplitude, where other theories have failed. In the special case where the applied stress amplitude is much higher than the critical stresses for the stress-induced martensitic transformation, the internal friction is found to be linearly proportional to the reciprocal of the stress amplitude, in good agreement with the experimental results. The time evolution of internal friction and shape change has been measured simultaneously in different microstructural states of the shape memory alloys. In the single-martensite phase state, the monotonic decrease of internal friction with time, without any accompanying shape change, has been attributed to the progressive pinning of the martensite/martensite interfaces. When the parent phase is present, the appearance of an internal friction peak, accompanied by an evident shape change, is found to be

associated with the stress-induced martensitic transformation and the subsequent pinning of the martensite/parent and martensite/martensite interfaces.

The effects of aging in both martensite and parent phases have been studied. Aging in parent phase caused the precipitation of α-phase which hindered the subsequent martensitic transformation and resulted in a suppressed internal friction peak and a deteriorated DSC peak. Aging in the martensite phase resulted in the pinning of the martensite/martensite interfaces by vacancies, which significantly obstructed the subsequent transformations upon heating and cooling. This has been evidenced by both internal friction and DSC measurements.

ACKNOWLEDGEMENTS

The author wishes to express his sincere gratitude to the following individuals and organizations:

First and foremost, to Dr. G.P. Johari, for providing the helpful supervision and encouragement throughout the course of this work, and for his numerous criticisms and valuable suggestions, without which this thesis would not be in its present form.

To Professors Gary R. Purdy and George C. Weatherly who accepted to serve on the supervisory committee. Their comments and criticisms were highly appreciated.

To Professor Christian Mai of INSA de Lyon, France, who carefully prepared the Cu-Zn-Al shape memory alloys.

To Mr. Tom Bryner who helped me greatly with the metallographic techniques.

To McMaster University and the Department of Materials Science and Engineering for their financial support in the form of a Teaching Assistantship and Departmental Scholarship.

To the Natural Sciences and Engineering Research Council of Canada for its financial support in the form of a research grant to Dr.G.P. Johari.

Finally, to my parents and sisters, without whose caring and support this work would not have been possible.

TABLE OF CONTENTS

LIST OF FIGURES

CHAPTER 1

INTRODUCTION

The shape memory effect (SME) has brought renewed interest and diversification in martensitic transformations, since its first discovery in AuCd alloy (Chang and Read, 1951). The activity in the SME field did not become extensive until Buehler et al.(1963) found a similar behaviour in Ni-Ti alloy, following early exploratory work on the phase transformations in the Ni-Ti system of nearly equiatomic compositions (Duwez and Taylor, 1950; Poole and Hume-Rothery, 1955; Purdy and Parr, 1961). Between the time of discoveries of SME in Au-Cd and Ni-Ti, came similar findings for β-brass (Reynolds and Bever, 1952) and Cu-Al-Ni alloys (Rachinger, 1958). Many other shape memory alloys (SMA) were discovered later, including Fe_3Pt, NiAl, AgCd and CuSn, etc. (Funakubo, 1987). However, the only ones which could be used, in addition to TiNi, were the copper-based alloys. Currently, the application of SMAs is being considered in many fields and economics of producing devices have therefore become an important factor in determining the possibility of widely using an alloy. The copper-based alloys therefore seem very attractive as a replacement for TiNi, which costs ten times as

much. However, due to the complex nature of the martensitic transformations in these systems and the many variables which can affect their stability, a complete understanding of the transformations and the corresponding shape memory behaviour in these SMAs is still not yet accomplished.

This study is intended to achieve a better understanding of the mechanisms of the thermoelastic martensitic transformation and associated SME and the effects of various variables on them, by combining a variety of different experimental techniques such as internal friction, differential scanning calorimetry, X-ray diffraction and metallography. The internal friction technique is useful for studying martensitic transformations since it is sensitive to the movement of interfaces accompanying the transformation. This method also provides the possibility of studying the effects of various external variables (e.g., frequency, stress amplitude, heating or cooling rate, etc.) on the transformation. The most recent availability of a new instrument for internal friction measurements, namely, Dynamic Mechanical Analyzer (DMA), provides an added, and yet very important advantage of studying the shape changes simultaneously with the changes in internal friction, elastic modulus and other material parameters. Differential Scanning Calorimetry (DSC), on the other hand, provides the possibility of studying the thermodynamics and kinetics of the

transformation. X-ray diffraction analysis of a stressed specimen has been attempted to study the stress-induced martensite from a different perspective, while the in-situ microscopic observation of the forward and reverse martensitic transformation during cooling and heating has provided direct evidence of some of the most important features of the thermoelastic martensitic transformation, such as the structural reversibility and thermal hysteresis.

The thesis is divided into six chapters. This chapter is a brief introduction of the general background and the purpose of this study.

Chapter 2 provides a more in-depth look into the various relevant subjects through a comprehensive literature review.

The preparation of the samples as well as the experimental techniques used for this study are described in Chapter 3.

The experimental results and corresponding discussions are presented in Chapter 4.

Chapter 5 describes the development of a theoretical formulation of internal friction due to thermoelastic martensitic transformation. Interpretation of the experimental results, unaccountable by other existing theories, has been given in the light of the formulation developed.

The conclusions of the thesis are given in Chapter 6.

Since September 1990, when this study began, numerous papers on the internal friction and DSC study of the martensitic transformations have appeared in the literature. Additionally, the International Conference on Martensitic Transformations (ICOMAT-92, July 1992) and the 10th International Conference on Internal Friction and Ultrasonic Attenuation in Solids (ICIFUAS-10, September 1993), as well as a few other meetings on the subject have been held during the course of this study. Therefore, it was necessary to submit for publication an account of this study prior to writing this thesis. This was done, and one paper (Xiao, 1993) has been published in Metallurgical Transactions (A) and another (Xiao et al., 1993) is now in press. Part of this work was also presented at the Symposium on Functional Materials and Energy Source Science (August 1992, Shanghai) and at the poster session of the 4th Canadian Materials Science Conference (June 1992, Kingston). Two more papers are currently being planned for submission to Metallurgical Transactions.

CHAPTER 2

LITERATURE REVIEW

2.1 Martensitic Transformation

2.1.1 Definition and General Characteristics

Martensite was originally the name given to the transformation product in quenched steels, named after the eminent German metallurgist Adolf Martens (Osmond, 1895). Later, the name was extended by Greninger and Mooradian (1938) to include transformation products in copper alloys bearing parallel crystallographic features. Martensitic transformations have since been observed in many other metals and alloys (Petty, 1970) as well as in ceramics (Bansal and Heuer, 1972 & 1974) and inorganic compounds (Kennedy et al., 1979). Today, the term "martensitic transformation" is widely used, and signifies one type of phase transition in solids which is diffusionless and occurs by a crystallographic shear. Bilby and Christian (1956) suggested that, "A structural transformation is classed as martensitic if the atoms on a primitive lattice defined by a selected unit cell of the parent structure move to positions on a primitive lattice defined by some unit cell of the product structure, in such a way that the displacements constitute a homogeneous deformation. This deformation may be different in adjacent

small regions." Christian (1965) later introduced the vivid terminology "military transformation" to describe the coordinated atomic movements during the martensitic transformation. Using the crystallographic theory as a basis for defining a martensitic transformation, Clark and Wayman (1970) noted that, "a martensitic transformation is in general described by an invariant-plane strain relief effect at a free surface, an irrational habit plane and orientation relationship, a lattice correspondence between substitutional atoms which implies the absence of long-range diffusion, and the presence of an internal inhomogeneity such as twinning". A definition by Nishiyama (1978) stated, "A martensitic transformation is a phase transformation that occurs by cooperative atomic movements. The product of a martensitic transformation is martensite. That a given structure is produced by a martensitic transformation can be confirmed by the existence of various characteristics that have been discussed, especially the diffusionless character, the surface relief, and the presence of many lattice imperfections. Such characteristics are therefore criteria for the existence of martensite." According to Cohen et al.(1979), "A martensitic transformation can be considered to be a first-order solid-state structural change which is (a) displacive, (b) diffusionless, and (c) dominated in kinetics and morphology by the strain energy arising from shear-like displacements." The

most recent definition by Funakubo (1987) stated, "Martensitic transformation can be defined simply and precisely: a lattice transformation involving shearing deformation and resulting from cooperative atomic movement. The atoms within the lens- or plate-shaped areas in the parent phase are not shifted independently but undergo shearing deformation as a unit while maintaining a domino-like coordination until the parent lattice transforms into martensite. With this kind of cooperative movement of atoms, a one-to-one correspondence, called 'lattice correspondence', persists between the lattice points in the parent phase and the points in the martensite phase."

The general characteristics listed below follow from the definition of martensitic transformations:

1) Martensitic transformation occurs by a process of shear which forms single crystal plates or sometimes laths (not exceeding the grain size) coherent with the parent phase. The remaining untransformed parent phase matrix constrains the extremities of these martensite plates resulting in lenticular shapes. Martensites thus appear acicular on a polished and etched surface.

2) Martensitic transformation is diffusionless, which means that the parent and product phases have the same composition. For instance, an ordered parent phase would transform to an ordered martensite.

3) A martensite crystal has a specific "habit plane", along which shear occurs during the transformation. Habit planes are specified by indices of planes in the parent phase. There are many cases in which they are irrational.

4) There is a definite orientation relationship between the parent and martensite phase lattices.

5) The lattice shear and volume changes produce distortion between the product and the matrix and result in surface relief effects observed on pre-polished surfaces.

6) Lattice defects necessarily exist in the martensite crystal. Even if a shearing deformation equal to the measured shape change is induced along the habit plane in the parent phase lattice, a true martensite phase lattice can not be obtained, unless complementary deformations (slip or twinning) are also introduced. Such complementary deformations are also called inhomogeneous shear or lattice invariant strain, and their traces, such as dislocation and stacking or twinning faults have been observed by electron microscopes. It should be mentioned that the twin faults especially play a major role in the shape memory effect.

2.1.2 Classification

Martensitic transformations can be classified in different ways depending on which kinetic feature is of primary interest. The following summarizes the three most

commonly used classifications.

1) Athermal and Isothermal Transformations:

Martensitic transformations are often divided into athermal and isothermal ones. Most martensitic transformations are described as athermal, i.e., the transformation begins at a certain temperature (M_s) on cooling and progresses only if the temperature is continually lowered until a completion temperature (M_f) is reached. If cooling is interrupted, transformation stops, but resumes again with further cooling. In some cases, martensite can form isothermally, above or below the M_s temperature. A classical example of an isothermal martensitic transformation was reported by Cech and Holloman (1953) who studied an iron-nickel-manganese steel and found the TTT curves showing typical C-shapes. Many other examples are now known, and the isothermal characteristics generally result from slow nucleation at constant temperature rather than slow growth.

2) Reversible and Non-reversible Transformations

In steels, when the martensite is heated, it undergoes tempering and eventually decomposition into equilibrium phases, ferrite and carbide. This happens since the temperature at which reversion to austenite occurs on heating lies in a region where diffusion of carbon is rapid. Consequently decomposition of martensite to ferrite and

carbide occurs before the austenite can reform. Martensitic transformations in steels are therefore called non-reversible. However, in carbonless ferrous alloys and many non-ferrous alloys exhibiting shape memory effect, the martensitic transformations are reversible, i.e., when the martensite is heated it transforms back to the parent phase. The martensite to parent phase transformation also occurs martensitically.

3) Thermoelastic and Non-thermoelastic Transformations:

According to the nature of the martensite/parent phase interface, the martensitic transformations can be characterized as thermoelastic or non-thermoelastic.

In non-thermoelastic transformations, during cooling, a martensite plate instantaneously springs full size into existence and then its interface becomes sessile due to plastic accommodation of transformational shape and volume changes. Therefore, the martensite crystals do not continue to grow on further cooling and the transformation proceeds by nucleating more and more new martensite crystals. Conversely, in thermoelastic transformations, once martensite crystals are nucleated they grow at a velocity proportional to the cooling rate, i.e., the martensite growth is synchronous with the temperature drop.

On the other hand, during heating, for non-thermoelastic transformations the martensite plates do not exhibit "backwards" movement but instead the reverse

transformation takes place by nucleating parent phase platelets within the martensite plates. For thermoelastic transformation, the reverse transformation occurs by the "backwards" movement of the martensite/parent interfaces and the martensite plates revert completely to the parent phase and to the original lattice orientation. Another significant difference between the thermoelastic and non-thermoelastic transformations is the magnitude of the thermal hysteresis. Thermoelastic transformation is characterized by a small transformation hysteresis while non-thermoelastic transformation features a very large one. This happens because a large chemical driving force is required, in non-thermoelastic transformation, to provide the energy necessary for plastic deformation whereas only very small chemical driving force is necessary in thermoelastic transformation, where the transformational shape and volume changes are accommodated elastically. Moreover, in thermoelastic transformation, the stored elastic energy during the forward transformation can be recovered during heating and actually helps the reverse transformation, further decreasing the transformation hysteresis.

2.1.3 Thermodynamics and Kinetics of Thermoelastic Martensitic Transformation

Thermoelastic martensitic transformation is

characterized by a local balance between chemical and non-chemical forces. The condition of local thermoelastic equilibrium is reached at the interfaces at a given temperature, during both forward and reverse transformations. The local character of the thermoelastic (energy) balance explains that growth and shrinkage of the martensite plates take place in a well defined sequential order. Chemical forces arise from the difference in Gibbs free energy between austenite and martensite, and act as a driving force promoting the phase with lower free energy at each temperature.

Non-chemical forces can be further divided into two main different contributions. The first one is the need to accommodate the transformational shape and volume changes. If accommodation takes place elastically, the associated elastic energy is stored in the specimen during the forward transformation (austenite to martensite) and reversibly recovered during the reverse transformation. Therefore this contribution opposes the forward transformation and promotes the reverse one. The second contribution is the energy dissipated in the specimen as internal work during the transformation. This contribution is used in overcoming frictional barriers opposing the interfacial motions, either during growth or during shrinkage of the martensite plates. It represents the irreversible part of the non-chemical energies and constitutes a resistive force opposing both forward and

reverse transformations. The heat exchanged between the sample and the surroundings during a thermally-induced thermoelastic martensitic transformation results therefore from three contributions, which are measured together in a typical DSC experiment.

A detailed thermodynamic analysis by Ortin and Planes (1988) has separated the three energy terms by application of the first and second thermodynamic principles to a complete cycle. Each individual contribution can therefore be evaluated quantitatively from heat-flow DSC data. For the multiple-interface forward transformation, the formulations are summarized as follows:

(1) Chemical Enthalpy Change:

$$\Delta H_{ch} = T_o \int_{M_s}^{M_f} \frac{dQ_c}{T} \qquad (2.1)$$

(2) Frictional Energy:

$$\Delta H_{fr} = \frac{1}{2}(Q_h - Q_c) \qquad (2.2)$$

(3) Elastic Strain Energy:

$$\Delta H_{el} = \Delta H_{ch} - \Delta H_{fr} - Q_c \qquad (2.3)$$

where Q_c and Q_h represent the total heat measured by DSC during the forward and reverse martensitic transformation, respectively, and T_o is the temperature where the Gibbs free energy of martensite equals that of parent phase. If the frictional energy is zero, the thermoelastic transformation would be ideally reversible and an already existing martensite plate would grow and shrink in a true thermoelastic equilibrium, following a single thermal path, i.e., without any hysteresis in temperature (Ortin and Planes, 1988). Olson and Cohen (1977) have shown that in this situation only a small hysteresis could arise due to the fact that the martensitic nucleation and initial growth as well as the final reversion occur away from true thermoelastic equilibrium because of the shape dependence of the strain energy. However, in reality, significant thermal hysteresis is at play even for the already existing martensite plates in most alloy systems generally acknowledged to transform thermoelastically. Therefore the total thermal hysteresis of the transformations results from both the presence of irreversible contributions to the free energy change (frictional energy) and the inherent hysteresis associated with the elastic barriers for nucleation of martensite plates.

The elastic strain energy term plays an important role in determining the kinetic features of the thermoelastic

martensitic transformations (Salzbrenner and Cohen, 1979). In a single-crystal, single-interface transformation, no elastic strain energy is stored because the transformational shape change freely alters the external shape of the specimen as the single interface traverses the crystal. Fig.2.1(a) illustrates the forward and reverse single-interface transformations, where the hysteresis is a manifestation of frictional resistance to the interfacial motion.

Moreover, during such motion there is no change in interfacial energy since the interface which extends across the specimen section remains constant in area. Clearly T_o lies unambiguously between T_f and T_r, the temperatures at which the forward and the reverse transformations occur (as shown in Fig.2.1a), and can be theoretically taken as $T_o=(T_f+T_r)/2$ assuming that the frictional resistance is the same in both directions. If the same crystal used for single-interface experiments in a temperature gradient is made to undergo multiple-interface transformations into different martensite variants by cooling the specimen uniformly instead of in a thermal gradient, typical results are shown in Fig.2.1(b). The influence of stored elastic strain energy is then reflected in the differences between the transformation characteristics represented by Fig.2.1(b) vs.(a). An obvious change is in the lowering of M_f and A_s, whereas M_s and A_f lie rather close to T_f

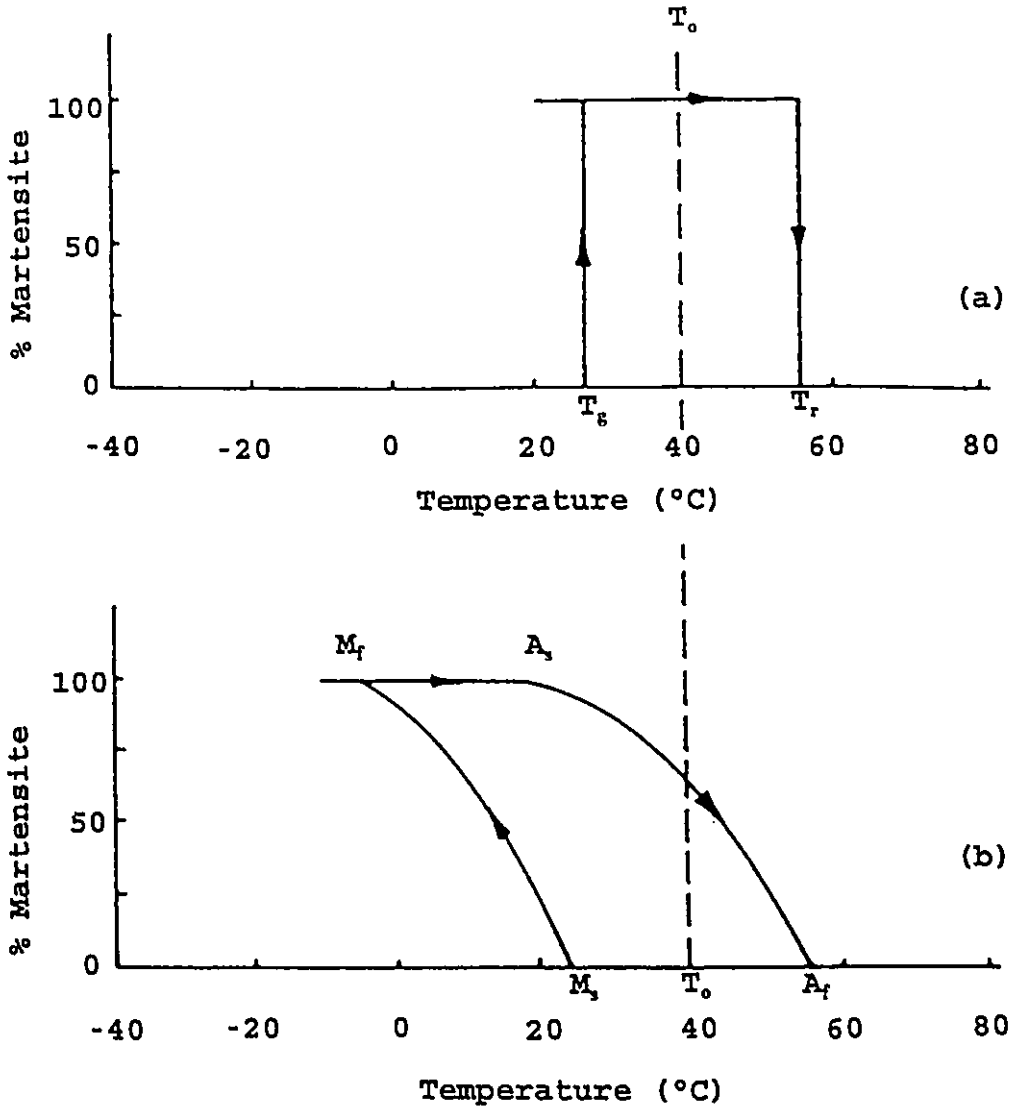

Fig.2.1: Transformation hysteresis in a single crystal of Cu-14%Al-2.5%Ni. (a) Single-interface transformation and (b) multiple-interface transformation (Salzbrenner and Cohen, 1979).

and T_r, respectively, in the single-interface experiments. The reason for this correspondence is that, in the multiple-interface case, strain energy is not generated when the first martensite plate forms at M_s because the nucleation takes place at a "free" corner or edge of the crystal; a similar geometric situation prevails for the last plate to revert at A_f. Therefore for the single-crystal, multiple-interface situations, $T_o=(M_s+A_f)/2$, in agreement with the analysis by Tong and Wayman (1974). The role of stored elastic strain energy is revealed even more clearly in polycrystalline specimens of different grain sizes. The transformation characteristics, for specimens with various grain sizes as well as for a single crystal, are shown in Fig.2.2. It is concluded that the downward shift of the transformation temperatures with decreasing grain size arises from the increasing elastic constraints of the smaller grains.

2.2 Shape Memory Effects

2.2.1 Overview

As described in Section 2.1, martensitic transformations are due macroscopically to a pseudo-shearing deformation, and therefore operate as a deformation mode similar to slip or twinning in ordinary metals and alloys under stress. However, since a martensitic transformation has

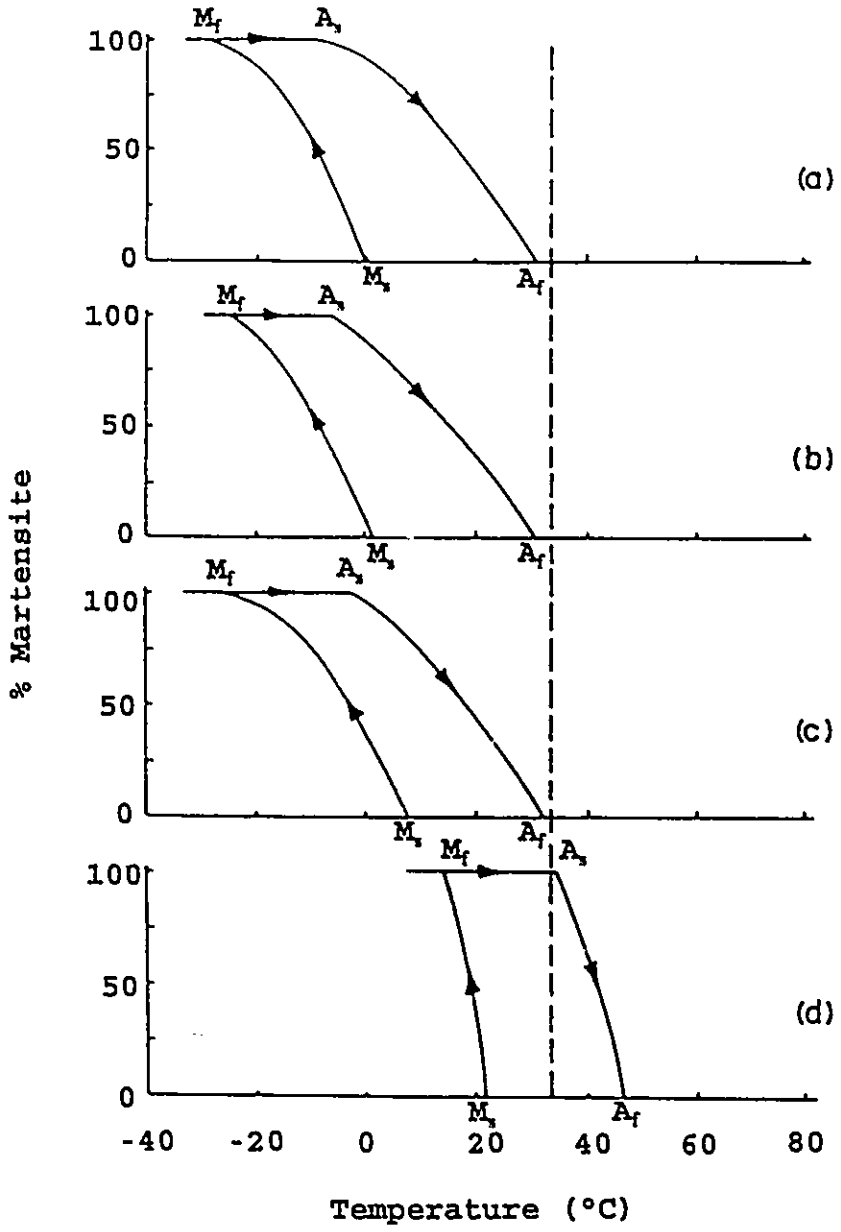

Fig.2.2: Transformation hysteresis curves for Cu-14%Al-2.5%Ni with different grain sizes: (a) fine-grained (d=0.5mm), (b) intermediate-grained (d=1.5mm), (c) coarse-grained (d=4.0mm) and (d) single crystal cut from the coarse-grained sample (Salzbrenner and Cohen, 1979).

a characteristic of reverse transformation, which is absent in deformation by slip or twinning, the deformation behaviour of alloys which undergo martensitic transformations can be remarkably different from ordinary metals and alloys.

The shape memory effect (SME) occurs in materials undergoing a martensitic transformation. Shape memory alloys are found to have common characteristics such as atomic ordering, a thermoelastic martensitic transformation which is crystallographically reversible, and a martensite phase which forms (on cooling) in a self-accommodating manner (Wayman, 1990).

2.2.2 Phenomena and Mechanisms

In addition to the familiar "one-way" memory, shape memory alloys also exhibit a "two-way" memory, as well as a "mechanical" shape memory resulting from the formation and reversal of stress-induced martensite (Wayman, 1990 and Friend, 1991). Some shape memory alloys also exhibit "rubberlike" behaviour (Wayman, 1990). The various types of shape memory effects and related phenomena are described separately below.

(1) One Way Shape Memory Effect

The process of one way shape memory effect is schematically illustrated in Fig.2.3 (Wayman, 1990). Upon cooling a single crystal of the parent phase, typically 24

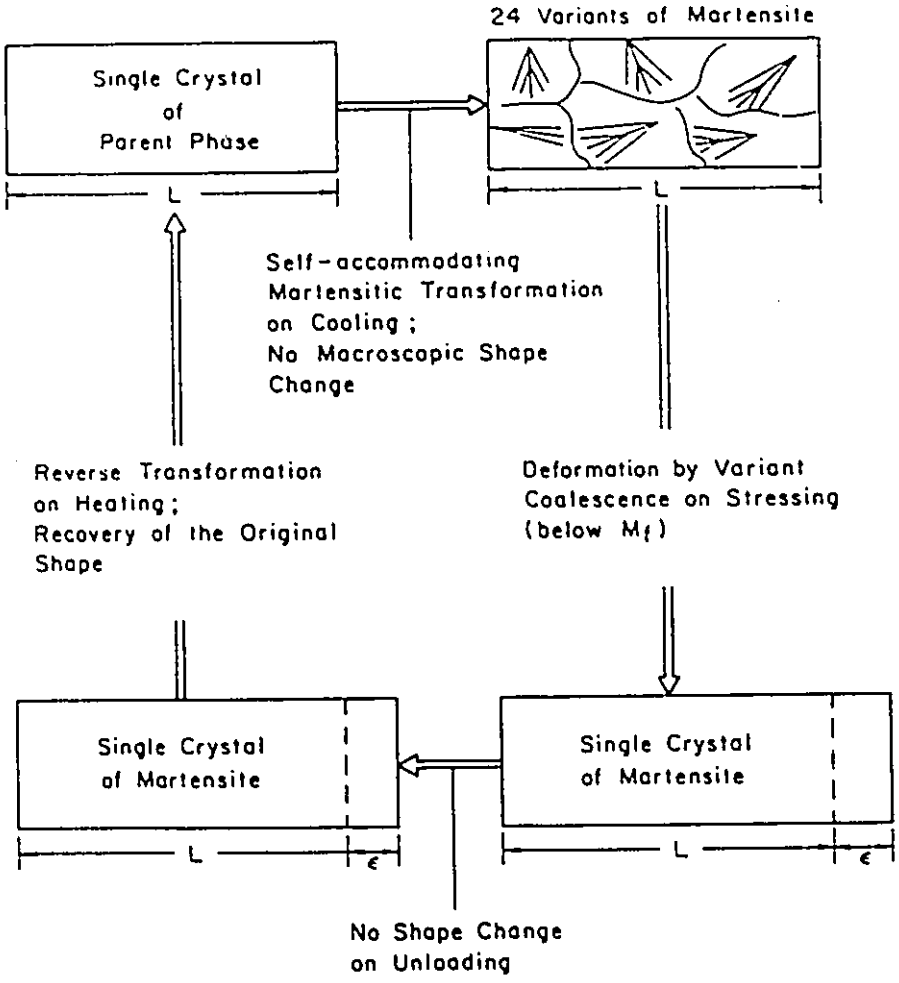

Fig.2.3: Schematic representation of one way shape memory process (Wayman, 1990).

variants of martensite form. They form in self-accommodating groups of four variants in a diamond-like morphology. As the martensite phase is deformed some variants grow at the expense of others and eventually only one variant persists. The surviving variant is the one whose shape strain direction (parallel to the habit plane) is most parallel to the tensile axis, thus permitting maximum elongation of the specimen. When this resultant single crystal of martensite is heated between A_s and A_f, the original specimen shape and parent single crystal are regenerated. Because of crystallographic restrictions and the necessity to maintain ordering, the single crystal of martensite has only one way to undergo the reverse transformation. In other words, there are numerous variants (up to 24) of the Bain strain (Petty, 1970) during the forward transformation but only one during reversal. The "one-way" shape memory just described is a one time only occurrence, but can be revived by reforming the martensite and deforming it, etc.

(2) Two Way Shape Memory Effect (TWSME)

With the "one way" shape memory effect, as previously described, a specimen "deformed' in the martensitic condition will "undeform" and regain its original shape after heating from A_s to A_f. This shape, however, will not change when the specimen is again transformed into martensite by cooling. In

contrast, the two way shape memory effect (TWSME) involves a reversible deformation: a specimen will spontaneously deform during cooling from M_s to M_f and then undeform during heating from A_s to A_f. There are various "training" techniques for inducing TWSME. The principle involved in all of these techniques is that (A) sites of internal stress are created by some mechanism inside the high-temperature parent phase and (B) these sites control the martensitic transformation instigated by cooling. Thus, after appropriate training, when the high-temperature parent phase is cooled down, only certain preferential variants of martensite nucleate and grow, whereas other variants do not appear. This gives rise to a net macroscopic shape change which depends on the training process. Heating, by reverse transformation, restores the initial parent-phase shape as in the one way memory effect.

(3) Superelasticity

When a stress is applied above the M_s temperature, a mechanically elastic martensite can be stress-induced in most thermoelastic alloys, and when the stress is released the stress-induced martensite (SIM) will disappear. This behaviour results in a mechanical type of shape memory. A typical stress-strain curve for a shape memory alloy showing superelastic behaviour is shown in Fig.2.4 (Funakubo, 1987). The strain up to the point labelled b in the stress-strain

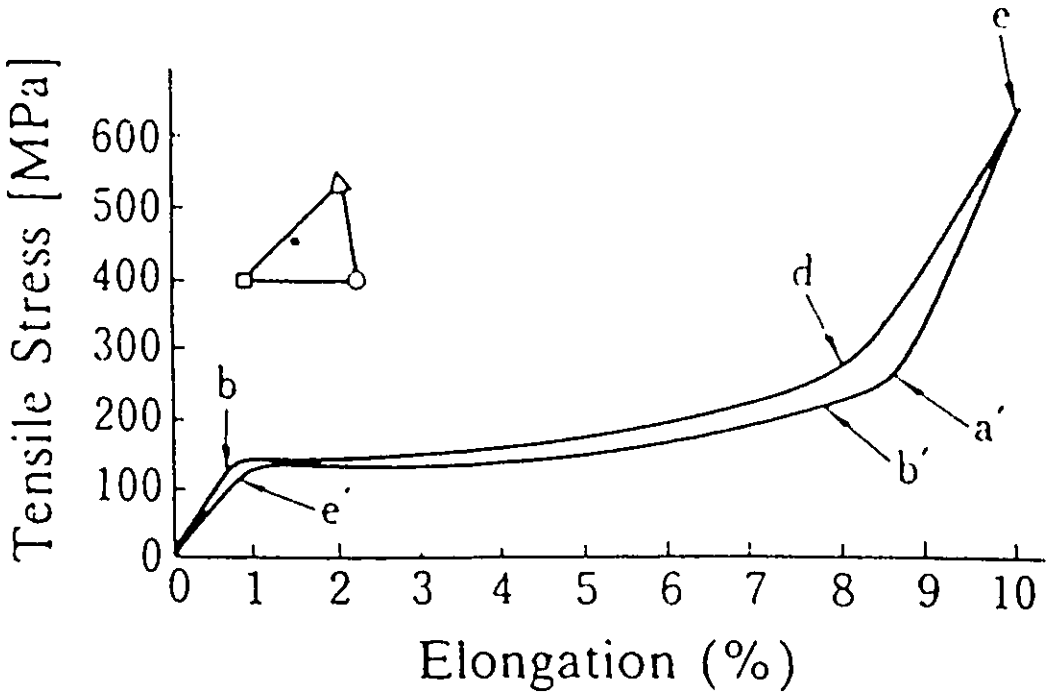

Fig.2.4: Superelastic behavior shown by the stress-induced martensitic transformation in a single crystal of Cu-14.1%Al-4.2%Ni alloy (Funakubo, 1987).

curve is due to elastic deformation of the parent phase. At point b, stress-induced martensites begin to appear, which are confirmed by neutron diffraction and by observations with optical microscopes. The strain increase between b and d is the result of the progression of the stress-induced martensitic transformation. At point d, the specimen becomes almost a single crystal of martensite. The strain between d and e is due to the elasticity of the martensite. When the stress is removed, the strain in the specimen first propels an elastic recovery to point a', and then recovers as far as the neighbourhood of e' due to the reverse transformation. Finally, the specimen completely returns to zero strain due to elastic recovery in the parent phase. The reverse transformation occurs upon unloading because at temperatures above M_s unstressed martensite is thermodynamically unstable when under no stress. Comparing superelasticity with one way shape memory, it is obvious that in either case shape recovery is driven by the reverse transformation and only the way in which the reverse transformation is induced differs.

(4) Rubberlike Behaviour

Some SMAs, after being deformed in the fully martensitic state, are able to recover their original shape upon release of the applied stress. This is referred to as "rubberlike behaviour", and was first reported in Au-Cd alloy

(Olander, 1932), long before the other more obvious signs of shape memory effect were discovered. This behaviour was later confirmed by Chang and Read (1951) and Burkhart and Read (1953) in Au-Cd and In-Tl alloys respectively.

Rubberlike behaviour also constitutes a mechanical type of shape memory as does the superelasticity associated with the SIM formation. But rubberlike behaviour is characteristic of a fully martensitic structure whereas superelastic behaviour is associated with a phase transformation under stress. These two types of behaviour collectively fall in the category of "pseudoelasticity". Rubberlike behaviour does not involve a phase transformation and appears to be related to the reversible movement of transformation twin boundaries or martensite boundaries, but the exact nature of the restoring force still remains unclear. Wayman (1990) commented recently, "It is ironic that even today, 57 years later, the origin of rubberlike behaviour remains obscure. Why does a freshly transformed specimen exhibit the shape memory effect and then after sitting around at room temperature for a few hours switch to rubberlike behaviour?"

2.2.3 Aging Effects in Copper-based Shape Memory Alloys

Copper-based shape memory alloys are susceptible to aging effects which can radically alter their transformation

behaviour (i.e., the extent and temperature of the transformation) and may limit their reliability as temperature-sensitive components. Both the parent and the martensite phase are susceptible to aging effects, due to the metastable nature of both phases.

The aging effects in martensite have recently been reviewed by Ahlers (1986). The effects appear to be related to multiple mechanisms and are differentiated between a decomposition process dominating at high temperature and a stabilization effect at low temperature. The low temperature stabilization effect involves structural changes on a finer scale or in a homogeneous manner so that a single phase martensite is retained. Evidence suggests that the following processes may be responsible:

(1) Martensite interface pinning due to the clustering of quenched-in defects (Mantel et al., 1986a, Morin et al., 1987 and Morin and Guenin, 1990).

(2) Changes in long range order (Delaey et al., 1984, Scarsbrook and Stobbs, 1987 and Arab and Ahlers, 1988).

(3) Martensite structural modification leading to a more stable stacking sequence (Stobbs, 1983), smaller β angle modification and interface relaxation (Delaey et al., 1984).

The quenched-in defects, such as vacancies, appear to have significant effects on the stabilization of direct-quenched martensites.

Aging in the parent phase can also be differentiated into a reversible ordering process at low temperatures and irreversible decomposition at high temperatures (Dunne and Kennon, 1981). Schofield and Miodownik (1980) and Planes et al.(1981) both found that, in Cu-Zn-Al alloys, low temperature aging (in the range of 39-67°C and at 22°C) of the parent phase increased its degree of ordering and resulted in an increase in the martensitic transformation temperature. Schofield and Miodownik also found that these aging effects are reversible. However, further work remains to be done regarding the explanation of the direction in which M_s (and all the associated transformation temperatures) are moved by the ordering change. For example, Fe_3Pt system (Berkowitz et al., 1957) also exhibits both an ordering reaction and a thermoelastic martensitic transformation, but heat treatments which decrease the degree of long-range order increase the martensitic transformation temperatures, in contrast to the results of Schofield and Miodownik and Planes et al.(1981). At this stage, it can only be stated qualitatively that ordering phenomena have important effects on the precise values of the martensitic transformation temperatures, and that particular systems may yield either a decrease or an increase in these characteristic temperatures.

Despite the differences in the rate, mechanism and

reversibility of the processes occurring on low and high temperature aging, the measured activation energies are approximately the same and are consistent with diffusional processes assisted by a supersaturation of vacancies (Dunne and Kennon, 1981).

2.3 Internal Friction Associated with the Martensitic Transformations

2.3.1 Experimental Observations and Theoretical Interpretations

The internal friction of martensitic alloys, measured as a function of temperature, usually shows a sharp maximum around the transformation temperature, for both thermoelastic (Dejonghe et al., 1976, Mercier and Melton, 1979 and Evsyukov et al., 1991) and non-thermoelastic (Delorme et al., 1971 and Xie et al., 1988) martensitic transformations. The main origin of internal friction in these martensitic alloys is believed to be the reversible movement of the martensite and/or twin plate boundaries. Factors that are generally recognized as affecting the internal friction during martensitic transformations include interface mobility, cooling (or heating) rate, amplitude and frequency of oscillating stress. The effects of cooling (or heating) rate ($\partial T/\partial t$) and frequency (f) on the internal friction were described first by Belko et al.(1969) and later by Delorme et al.(1971), while the

influence of stress amplitude (σ_o) was formulated by Dejonghe et al.(1976). Both Belko's and Delorme's formulations predicted a linear relationship between $(\partial T/\partial t)f^{-1}$ and internal friction, while Dejonghe's formulation further included the effect of stress amplitude (σ_o) and can be written as:

$$\tan\phi = \frac{A}{2\pi}\left(\frac{\partial m}{\partial T}\frac{\partial T}{\partial t}f^{-1}+\frac{4}{3}\sigma_o\frac{\partial m}{\partial \sigma}\left[1-\left(\frac{\sigma_c}{\sigma_o}\right)^3\right]\right) \qquad (2.4)$$

where $\tan\phi$ is the internal friction, σ_c is the critical stress for inducing the martensitic transformation, σ_o the amplitude of the applied oscillating stress (σ), m the amount of martensite transformed and A a material constant.

Equation (2.4) is known as Delorme-Dejonghe theory and has been able to explain many experimental observations (Zhao et al., 1991). This formulation shows clearly that the following five factors can influence the internal friction accompanying the martensitic transformation:

(1) $\partial m/\partial T$: the quantity of material that transforms per unit temperature change. This is related to the width of the transformation interval in that a narrow interval gives a larger $\partial m/\partial T$ for a given amount of material transformed.

(2) $\partial T/\partial t$: the heating or cooling rate.

(3) f: oscillation frequency.

(4) σ_o: the amplitude of oscillating stress.

(5) $(\partial m/\partial \sigma)$: the quantity of material that transforms per unit stress. This is related to the mobility of the interfaces (two types of interfaces have to be considered: parent/martensite and martensite/martensite).

2.3.2 Limitations of the Existing Theories:

While the Delorme-Dejonghe theory is generally regarded as the most comprehensive formulation for internal friction associated with martensitic transformation, it fails to explain and in some cases even contradicts the experimental results. For example, Gremaud et al.(1987) found that the internal friction accompanying the martensitic transformation in pure cobalt decreases with increasing stress amplitude (σ_o), in contradiction to the prediction by equation (2.4). A number of researchers have also found that the internal friction associated with the martensitic transformations in Mn-Cu (Xie et al., 1988), Ni-Ti (Zhu et al., 1988) and pure cobalt (Bidaux et al., 1989) do not depend linearly on $\partial T/\partial t$, $1/f$ or $(\partial T/\partial t)f^{-1}$ as predicted by equation (2.4). An alternative theory (Mercier and Melton, 1976) for internal friction due to martensitic transformation, which is based on dislocation damping, is able to explain the appearance of the internal friction peak when $\partial T/\partial t=0$ (Mercier and Melton, 1979), which is not obvious from equation (2.4). However, this

theory also has serious limitations in that its predictions of frequency, amplitude and cooling rate dependence of internal friction are in contradiction with most experimental observations.

CHAPTER 3

EXPERIMENTAL PROCEDURES

3.1 Alloy Selection and Heat Treatment

In this study, ternary Cu-Zn-Al alloys of two different compositions were selected for their convenient temperature ranges of phase transformation. Most of the experimental work has been concentrated on the samples of one composition, Cu-13%Zn-9%Al (hereafter called alloy A). However, parallel experiments on the alloy of another composition, Cu-23%Zn-5%Al (hereafter called alloy B), were also carried out in some cases, where the generality of important results needed to be confirmed. Both alloys were prepared by induction-melting pure (99.9%) metals of Cu, Zn and Al, followed by casting and extrusion. All compositions throughout this thesis are expressed in weight percent.

The equilibrium microstructures and phase transformations in a ternary brass can be conveniently predicted by using the concept of "zinc equivalent" (West, 1982). If the zinc equivalent coefficient of aluminum is taken as 6, then the equivalent zinc content of the two ternary alloys can be determined as follows:

Alloy A: $Zn\%(Equivalent) = (13+6\times9)/(13+6\times9+78) = 46.2\%$

Alloy B: $Zn\%(Equivalent) = (23+6\times5)/(23+6\times5+72) = 42.4\%$

Therefore, the equilibrium microstructures in a ternary brass can now be conveniently predicted by looking at the Cu-Zn binary phase diagram, Fig.3.1.

From Fig.3.1, the appropriate heat treatment procedures can be determined. For both alloys, a temperature of 850°C was selected for homogenization treatment (or solution treatment). The homogenization time for all samples (1.2mm in diameter) was 10 minutes, which was long enough to homogenize the sample into a single β phase. This was confirmed by the X-ray diffraction and metallographic examination of samples quenched to room temperature water after the homogenization treatment. The rapid cooling rate during quenching suppresses the precipitation of the α-phase at lower temperatures, and a supersaturated β' phase, which is ordered, forms. This ordered β' phase subsequently transforms to martensite at lower temperatures. The β' phase in Fig.3.1 has a B2 (CsCl-type) ordered structure and it is generally accepted that the $\beta \rightarrow \beta'$ ordering, which is a second order transition, can not be suppressed even by drastic quenching (Schofield and Miodownik, 1980). The ordering phenomena in Cu-Zn-Al ternary alloys, however, are more complicated than shown in Fig.3.1. In the Cu-Al binary system at compositions near Cu_3Al, DO_3 order (Fe_3Al-type) occurs in the metastable β-phase on cooling below about 500°C (Swann and Warlimont, 1963). It

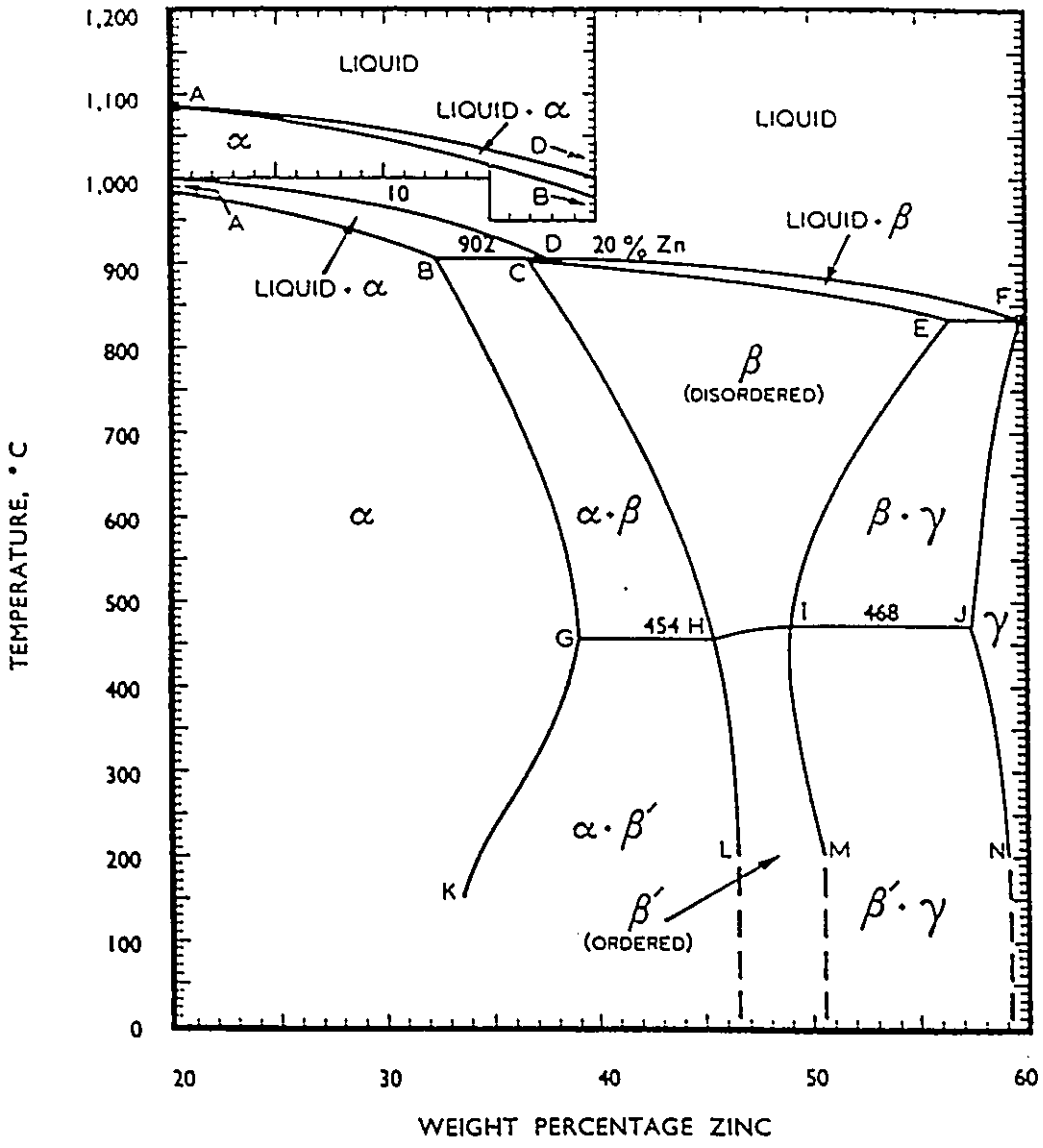

Fig.3.1: Copper-Zinc equilibrium phase diagram (West, 1982).

is apparent, therefore, that at some position across the Cu-Zn-Al phase diagram, a B2→DO_3 transition must be expected (Schofield and Miodownik, 1980). B2 order results in 9R martensite (a 9-layered periodic stacking order structure) while DO_3 order results in 18R martensite (a 18-layered periodic stacking order structure) on subsequent cooling (Funakubo, 1987). In general, both the transformation temperatures and the prevalence of 18R martensite increase as Al content increases at the expense of Zn (Dunne and Kennon, 1981).

3.2 Internal Friction Measurements

3.2.1 Dynamic Mechanical Analyzer

A Dynamic Mechanical Analyzer, DMA-7, made by Perkin-Elmer Corporation, was used for most of the internal friction measurements. The sample was oscillated in a three-point bending mode by means of an assembly which is schematically shown in Fig.3.2 (Pascheto, 1991). In it, a sample (1) is placed on a gold-plated stainless steel platform (3) and is sinusoidally deformed in a bending mode by a probe tip (2), which imposes a dynamic stress at a frequency ranging from 0.01 to 51 Hz. A static stress, which is always 1.2 times the amplitude of the dynamic stress, is also applied to ensure good contact between the sample (1), the probe tip (2) and the

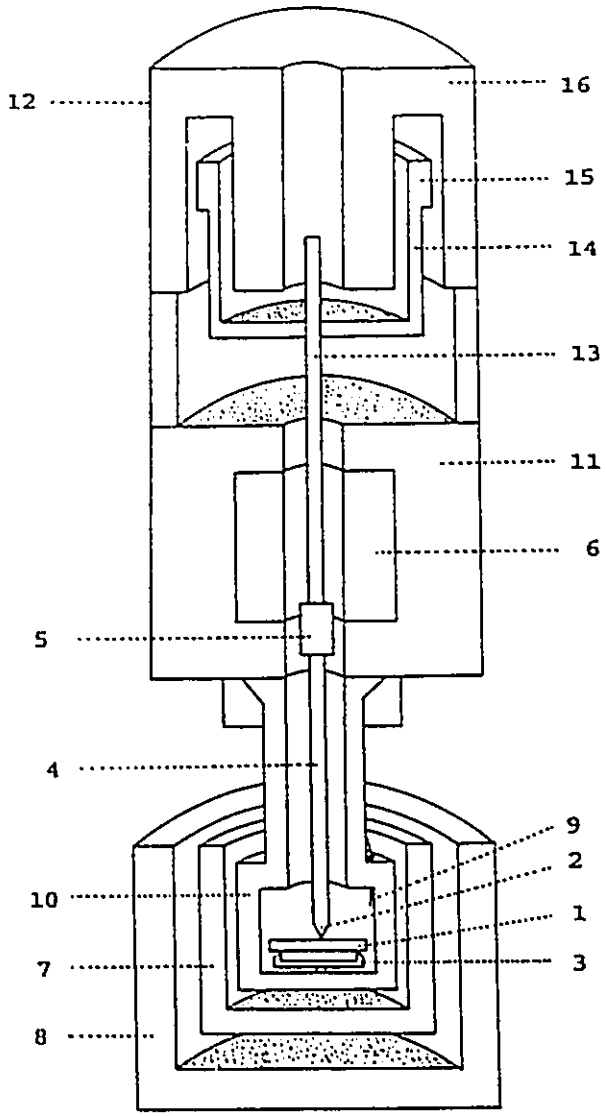

1. Sample
2. Probe Tip
3. Platform
4. Probe
5. Probe Holder
6. Displacement Detector
7. Furnace
8. Dewar
9. Thermocouple
10. Housing
11. Temperature Encloser
12. Force Motor
13. Rod
14. Armature
15. Coil
16. Magnets Assembly

Fig.3.2: Schematic of the vertical section of the dynamic mechanical analyzer (Pascheto, 1991).

platform (3). The stress is applied by a linear force motor (12) located at the upper end of the apparatus. This linear force motor consists of a cylindrical magnet assembly (16) coaxially mounted above the probe. It also includes a movable armature of aluminum (14) coaxial with the magnet assembly, which encloses an energizable coil (15) at its upper end. This energizable coil generates a magnetic field which interacts with the magnet assembly leading to a vertical axial force on the armature. The lower end of the armature is fixed to a non-magnetic actuator rod (13) which is coaxially mounted on the probe. The force generated by the linear force motor is proportional to the current in the coil and to the magnetic field strength. A constant current is used to produce the static stress on the sample. An additional, sinusoidally oscillating current is superimposed to generate an oscillating dynamic stress on the sample. The three point bending assembly is supported by, and enclosed in, a metal housing (10). The housing also acts as a channel for the flow of helium gas for providing an inert environment during the experiments. Between the probe holder (5) and the linear force motor there is a high sensitivity displacement detector (6). This is a conventional linear variable differential transformer, LVDT, which provides a voltage output indicating the position of the probe with respect to the platform edges. The oscillating dimensional response of the sample is therefore detected by

the LVDT which produces another oscillatory sinusoidal signal. The internal friction is then measured from the phase lag between the sine wave generated by the linear force motor and the sine wave generated by LVDT as a result of the detected deformation in the sample. A low mass furnace (7) based on a resistance-heating design and a dewar (8) allows one to perform experiments over the temperature range of -160°C to 500°C. The heating and cooling rate is controllable from 0.1°C/minute to 40°C/minute. A thermocouple (9) made of chromel-alumel alloy is placed at a distance of about 5mm from the sample to monitor the temperature. For measurements at subambient temperatures, the dewar (8) is filled with liquid nitrogen.

The entire measurement unit described above is connected to a control assembly which includes a Perkin-Elmer Analyzer Controller, model TAC 7, which is a microprocessor that links the measurement module to a computer. It continuously monitors and analyzes all system functions, such as the frequency, stress, strain, temperature and the heating or cooling rates.

A personal computer, Perkin-Elmer PE 7700, collects all the data sent by the Analyzer Controller and performs calculation of the dynamic functions related to the internal friction measurement. In a typical experiment, a method previously used can be recalled from the directory stored on

the hard disk. During the experiment, the stress amplitude, strain, internal friction, modulus and probe position etc. are all observed in real-time on the computer monitor.

For measurements in the three point bending mode, the cylindrical sample, with a dimension of 1.2mm(Diameter)x25mm (Length) was placed on its mount so as to remain centered and perpendicular to both the platform edges and the probe tip edge. Once the sample was properly mounted, the probe tip was lowered until it contacted the sample's surface. Thereafter, the furnace was raised to enclose the three point bending assembly and various parameters for measurements were entered into the computer. Helium gas was then allowed to flow through the measurement system at a rate of 40cc/minute. This prevented condensation of humidity and formation of ice on the sample, which might affect the internal friction results.

Internal friction and other material parameters have been measured on DMA-7 in three different operating modes : (1) Temperature Scan, (2) Time Scan and (3) Frequency Scan. All measurements are carried out in the three point bending configuration. The instrumental accuracy for the measurements of internal friction and probe position are 1.8×10^{-5} and 2×10^{-4} mm, respectively, and in the temperature ±0.6° at a rate of 5°C/min. The latter is determined from measurements of the melting point of ice.

3.2.2 Inverted Torsional Pendulum

A Dynamic Mechanical Spectrometer, MARK IV, constructed by Metravib Instruments (France), was used for the measurement of internal friction in the torsional oscillation mode. It mainly consists of an inverted torsional pendulum, the schematic of which is shown in Fig.3.3 (Pascheto, 1991). The sample (5) is held between two clamps (11) made of stainless steel. The upper clamp is attached to a rotatable rod (12) made of tantalum, while the lower clamp is rigidly attached to a fixed mount.

A torque created by the interaction between the magnets (2) and the Helmholtz coils (3) carrying a current I, is transmitted by the rotatable rod (12) to the sample. The suspension system (6) acts to counterbalance the axial load on the sample, and a bar-shaped damper (7) made from tantalum reduces the effect of parasitical vibrations induced by the surroundings. The strain on the sample is then detected by a light beam (10) reflected from a mirror (8) rigidly mounted on the rod (12). The reflected light is directed at a photovoltaic cell (9), which is connected to a low drift amplifier (13) supplying a voltage proportional to the sample strain.

A removable resistance furnace (4) axially encloses the sample during the measurements. The temperature is monitored by means of a platinum resistance thermometer (17)

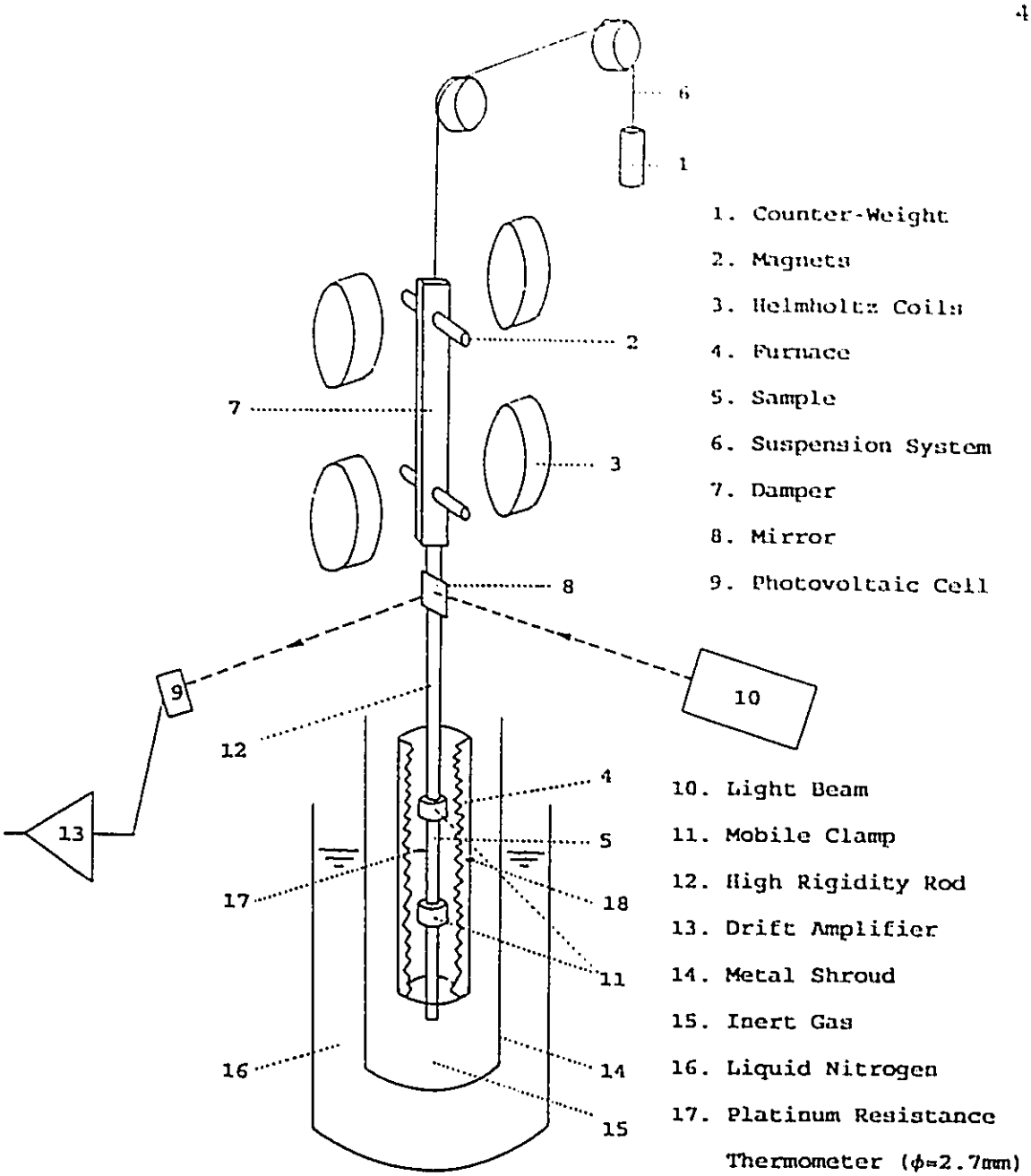

Fig.3.3: Schematic of the inverted torsional pendulum (Pascheto, 1991).

kept at a distance of about 1mm from the sample. The furnace is hermetically sealed by means of a metal shroud (14) which allows the sample to be studied either in vacuum or in an inert environment of argon gas. The metal shroud is immersed in a dewar containing liquid nitrogen (16). The thermal control enclosure allows measurements of the mechanical properties both under isothermal conditions and during heating or cooling over a temperature range of -173°C to 397°C.

Dynamical mechanical measurements are monitored by an automatic data acquisition system which consists of several modules. Among them, the interface module consists of a generator which provides a sinusoidal excitation signal to the sample, the frequency of which can be selected either manually or through a computer. A power amplifier allows the adjustment of the excitation power between 10^{-4} and 1 A. A control system enables the selection of operation under either constant stress amplitude or constant strain amplitude. In this study, all measurements were made under a constant stress amplitude. A view-meter on the interface module allows one to observe the approximate magnitudes of stress and strain. This enables one to adjust the stress and strain amplitude as well as to mechanically adjust the sample's mean position for zero distortion.

A digital controller model Microcor II made by Coreci,

France, was used to regulate the temperature of the furnace (4). It controls the power input and the heating rate of the furnace by sensing the temperature through a platinum resistance thermometer (18) located inside the ceramic wall of the furnace. This module also contains the power supply which keeps the light source operating at a constant voltage.

An oscilloscope model 1020 made by Leader Electronics Corporation, USA, was added to the instrument to precisely determine the magnitude of the stress and strain signals, and more importantly, to ensure that the oscillations of the sample remained sinusoidal. It also allowed adjustment of the excitation levels before and during the course of measurement.

A PC compatible computer model Data train 2801 made by Data Translation Inc., USA, was also connected to the assembly. It controls the experiments by using a data acquisition interface to allow an interactive dialogue with the measurement system. During the experiments, the computer receives from the generator information related to the sample stress, strain and temperature. The computer then performs calculation of the internal friction. The computer was also connected to a printer and a plotter which provided a means for following the mechanical properties of the sample during the course of the measurements. For measurements in torsional pendulum, the sample was first carefully mounted between the clamps and then attached to the rod by fixing the clamps to

the rod. The proper alignment of the axis of the sample with the axis of the rod was necessary since a poor alignment causes the oscillations of the sample to become nonsinusoidal, leading to inaccurate results. The appropriate alignment can be checked by observing the signal on the oscilloscope. After the sample was mounted, the reflected light beam was directed at the center of the photovoltaic cell by means of an adjustment screw that rotated the entire assembly with respect to the photovoltaic cell. This was first done visually. A fine adjustment was then made with the help of the oscilloscope and the view-meter. A centered, sinusoidal signal on the oscilloscope and the view-meter ensured the axial alignment of the sample. The magnitude of the stress and strain on the sample were then adjusted by examining the signals on the view-meter. It was found that the optimum magnitude of stress amplitude for the sample of dimension 0.5mm(Diameter)x 22mm(Length) was 1.2MPa, which was kept constant throughout the measurement. After the necessary adjustments, the pendulum assembly was hermetically sealed in the metal shroud, which was then immersed in liquid nitrogen. Air was evacuated and argon gas was introduced into the assembly, which was kept at a pressure of 0.4 bar. Relevant parameters for the experiments such as oscillation frequency, temperature range and sample dimensions were then entered into the computer. Accurate measurements of the sample's dimensions were

necessary for purpose of shear modulus calculation. The internal friction was measured from the energy input to the mechanical system per cycle needed to maintain the constant amplitude as a percentage of the maximum energy stored in the sample in a cycle. All internal friction measurements were performed as a function of temperature while keeping the frequency and stress amplitude constant. In all cases, an oscillation frequency of 1Hz was used.

3.3 Differential Scanning Calorimetry (DSC)

A Perkin-Elmer DSC-4 was used for all DSC measurements in this study. The schematic of the instrumentation for the Differential Scanning Calorimetry is shown in Fig.3.4(a) (Daniels, 1973). It differs fundamentally from DTA (Differential Thermal Analysis) in that the sample and reference are both maintained at the temperature predetermined by the program even during a thermal event in the sample. The amount of energy which has to be supplied to or withdrawn from the sample to maintain zero temperature differential between the sample and the reference is the experimental parameter displayed as the ordinate of the thermal analysis curve, as shown in Fig.3.4(b).

The sample and reference are placed in identical environments, i.e., metal pans on individual bases which each contain a platinum resistance thermometer and a heater. The

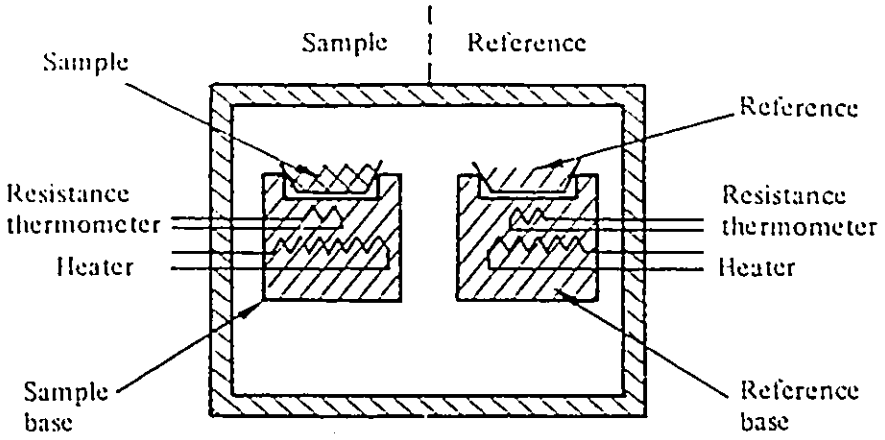

(a) EXPERIMENTAL ARRANGEMENT

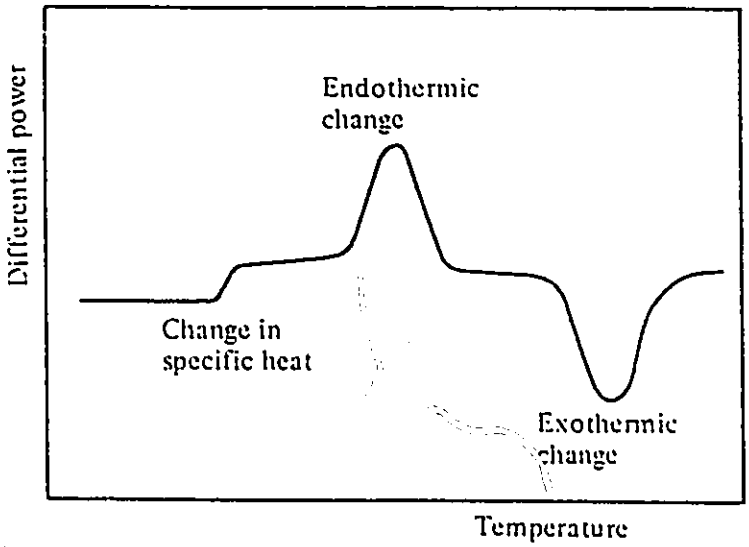

(b) TYPICAL CURVE (PERKIN-ELMER CONVENTION)

Fig.3.4: Schematic of the DSC instrumentation (a) and typical curve measured by the DSC technique (b) (Daniels, 1973).

thermal mass of the holders is minimized so that the response of the resistance thermometers is rapid. The temperatures of the two thermometers are compared, and the electrical power supply to each heater adjusted so that the temperatures of both the sample and the reference remain equal to the programmed temperature, i.e. any temperature difference which would result from a thermal event in the sample is "nulled". Unlike DTA, DSC does not require the thermal masses of the sample and reference to be closely matched, since a power difference, not a temperature difference, is measured.

The ordinate signal, i.e., the rate of energy absorption or evolution by the sample, is proportional to the specific heat of the sample since the specific heat at any temperature determines the amount of thermal energy necessary to change the sample temperature by a given amount. Thus any transition accompanied by a change in specific heat produces a change in the differential power signal and exothermic or endothermic enthalpy changes give rise to peaks whose areas are proportional to the total enthalpy change of the phase transitions, Fig.3.4(b).

Since DSC measures the energy change in the sample directly, not as a temperature change, it is consequently more suitable than DTA for quantitative measurement of heat of transition or specific heat, etc. Another major advantage of DSC is its capability of measurements under isothermal

conditions, which may be used for isothermal studies in which the energy changes occurring at constant temperature are recorded as a function of time.

The sample containers used in DSC measurements of this study were shallow metal pans (platinum or aluminum) without pan cover. The sample and reference containers were placed on individual bases thermally isolated from each other, each base containing a separately controllable heater and a resistance thermometer. Any inert material may be used as reference, but an empty sample pan is generally preferred and was therefore used in this study. In this way, if the sample and reference pans are matched, the thermal capacity of the sample pan is balanced and the DSC curve records changes in only the sample. The sample pans and the pan holders were chosen so that they will neither undergo phase transitions nor react with the sample in the temperature range of operation. The sample chamber was maintained in an inert atmosphere to prevent oxidation. This was achieved by supplying a flow of helium gas at 20 PSI through the sample chamber. The flowing helium also prevented any moisture from condensing on the sample, especially during subambient operations where liquid nitrogen was used to cool the sample.

The typical sample size for DSC measurements is approximately 2.5mmX1.0mmX0.8mm with a weight of about 20 mg. Larger sample improves the sensitivity of the differential

power signal, but also increases the thermal resistance and therefore the temperature lag between the sample and the thermometer. The sample size was chosen so that an optimum combination of high sensitivity and low thermal lag was achieved.

A one point calibration procedure was used to calibrate the temperature (abscissa). This procedure is possible due to the advanced electronics which automatically linearizes the temperature calibration using only a single transition point. The standard which was used for temperature calibration is distilled water, with a melting point lying in the middle of the temperature range of operation, i.e., -100°C to 100°C. The energy (ordinate) calibration was carried out with an automatic ordinate calibration procedure using a standard power signal (10 mcal/sec) generated by DSC at 50°C.

For DSC operation in a wide temperature range, there is usually an element of curvature in the curve obtained unless the DSC baseline has been optimized. The undesirable curvature could lead to confusion in curve interpretation and inaccurate quantitative results. This reproducible curvature can be eliminated by storing a Scanning Autozero (SAZ) baseline which will be subtracted from subsequent runs. The SAZ baselines are obtained simply by making a temperature scan with empty sample and reference holders. In this study, all DSC measurements are made by employing the Scanning Autozero

function of the instrument.

3.4. X-ray Diffraction Analysis

The instrument used for X-ray diffraction studies was a Nicolet I2 automated diffractometer. This system consists of a two-circle diffractometer with x-ray tube, detector and counter, and a LSI-11/23 computer for analysis and instrument control. The instrument was operated at 40 KV and 20 mA, using Cu $K_{\alpha 1}$=1.5406Å and $K_{\alpha 2}$=1.5448Å radiation.

The basic geometry of the X-ray diffractometer is shown in fig.3.5 (O'Reilly, 1988). The focusing circle has the X-ray source (s), sample and receiving slit of the detector (F) on its circumference. The diffractometer circle has the sample at its centre and the detector scans around its circumference. The size of the diffractometer circle is fixed. Since the surface of the sample must stay tangential to the focusing circle the sample is coupled to the detector so that as the detector scans 2θ, the sample rotates θ in the same direction.

One sample used for X-ray diffraction studies was a flat plate specimen (25mmX2.5mmX0.5mm) in as-quenched condition. The same sample was then bent into a semicircle by fixing its two ends at two holes drilled on a steel plate and then studied at the same central spot. Another metallographic

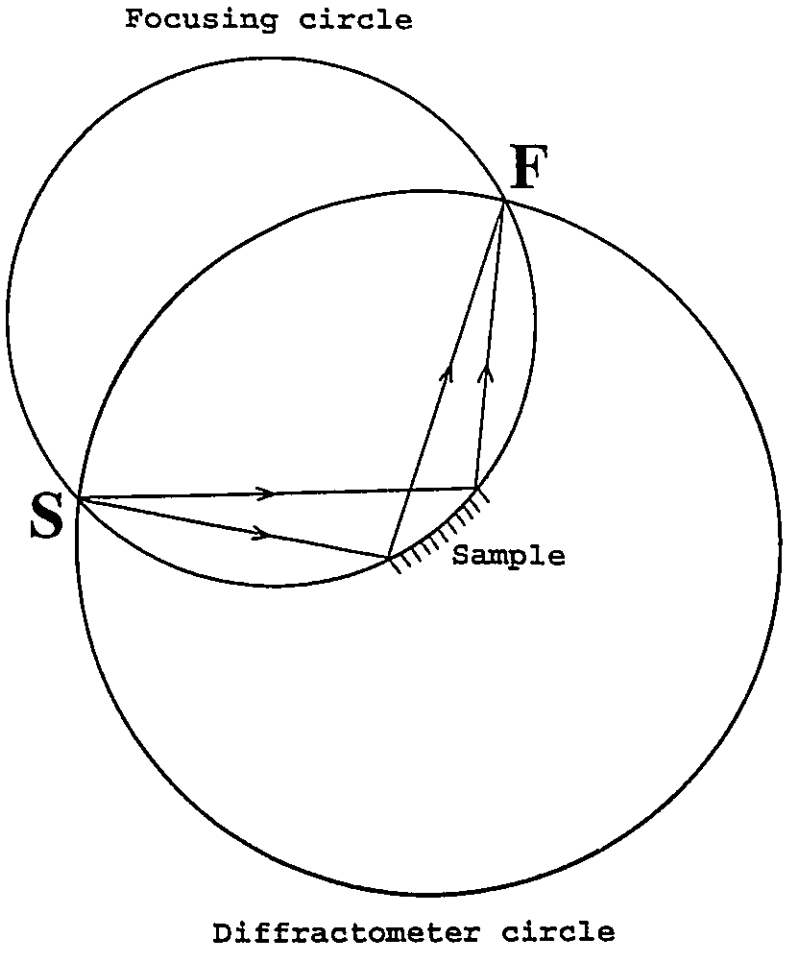

Fig.3.5: Geometry of the two-circle X-ray diffractometer (O'Reilly, 1988).

specimen (15mmX2mmX0.5mm) mounted with epoxy resin was also used for X-ray diffraction in order to confirm the existence of α-phase precipitation, which had been observed by metallography.

3.5 Metallography

For static observation under optical microscope, the samples are prepared as follows:

(1) mechanical polishing with emery paper (grit 2) was used to remove about 0.5mm from the cylindrical surface of the heat-treated sample.

(2) The sample was then mounted using epoxy resin with the polished surface facing outwards.

(3) The mounted sample was ground on silicon carbide paper on a Metaserv Hand Grinder starting with grit 220 and ending with grit 600.

(4) The sample was then polished with 6 μm and 1 μm diamond paste, with oil as lubricant, on a Metaserv Universal Polisher with a low speed of 150 RPM.

(5) Finally the sample was polished with 0.3μm alumina suspension on a rayon cloth, with distilled water as lubricant.

The polished sample was then etched with a reagent consisting of a mixture of $FeCl_3$ (5 g), HCl (50 ml) and H_2O

(100 ml) and observed under a Leitz optical microscope with photographic facilities. Photomicrographs were taken using type 53 medium contrast Polaroid Instant Sheet Films.

For in situ observation of surface relief during cooling and heating, the preparation of samples is somewhat different:

(a) The samples were mounted using a low melting point alloy consisting of 55.5%Bi and 44.5%Pb, with a melting point of 124°C. The good thermal conductivity of metals ensured an accurate measurement of the sample temperature during cooling and heating, when the thermocouple was placed in a hole drilled beside the sample on the mounting alloy. The low melting point of the mounting alloy ensured that no decomposition of the microstructures would take place during mounting.

(b) The cylindrical samples were vertically mounted so that the circular cross sections were polished. This ensured that the samples would not peel off the mounting alloy during repeated heating and cooling while being observed under the microscope.

(c) No etchant was used to reveal the microstructures, since etching would disturb the coherent and glissile interfaces between martensite and parent phase. The surface relief effect accompanying the martensitic transformation creates enough contrast on a polished surface to be clearly

observed under the optical microscope.

The mounted sample for in situ observation during cooling and heating was put face dow.. on an Olympus optical microscope. A stainless steel mould coaxially enclosed the mounting. A Thermolyne Model CN-A 8005M heating tape, whose temperature is controlled by a stepless input control device, was snugly wound around the mould. A thermocouple was placed in a small hole drilled closely beside the sample on the mounting alloy to monitor the temperature change. The cooling and heating was controlled by slowly adding liquid nitrogen into the mould and/or adjusting the dial on the stepless input control.

CHAPTER 4

RESULTS AND DISCUSSION

4.1 General Features of the Martensitic Transformations

The general features of the reversible martensitic transformation studied by DMA (Dynamic Mechanical Analysis) and DSC (Differential Scanning Calorimetry) are schematically shown in Fig.4.1. The internal friction ($\tan\phi$) and probe position (d) curves are simultaneously measured in a typical DMA experiment while the heat flow (dH/dt) curves are measured from DSC. Typically, the martensitic transformation during cooling is accompanied by a significant internal friction peak, an abrupt decrease in probe position and an exothermic DSC peak. The reverse transformation on heating is characterized by an internal friction peak, an abrupt increase in probe position and an endothermic DSC peak. The appearance of the internal friction peak arises from the hysteretic movement of martensite/parent interfaces in response to the oscillating stress (Xiao, 1993). The abrupt change in probe position suggests that the transformation is stress-oriented, i.e., only certain martensite variants which are favourably oriented with respect to the applied stress are formed during the martensitic transformation.

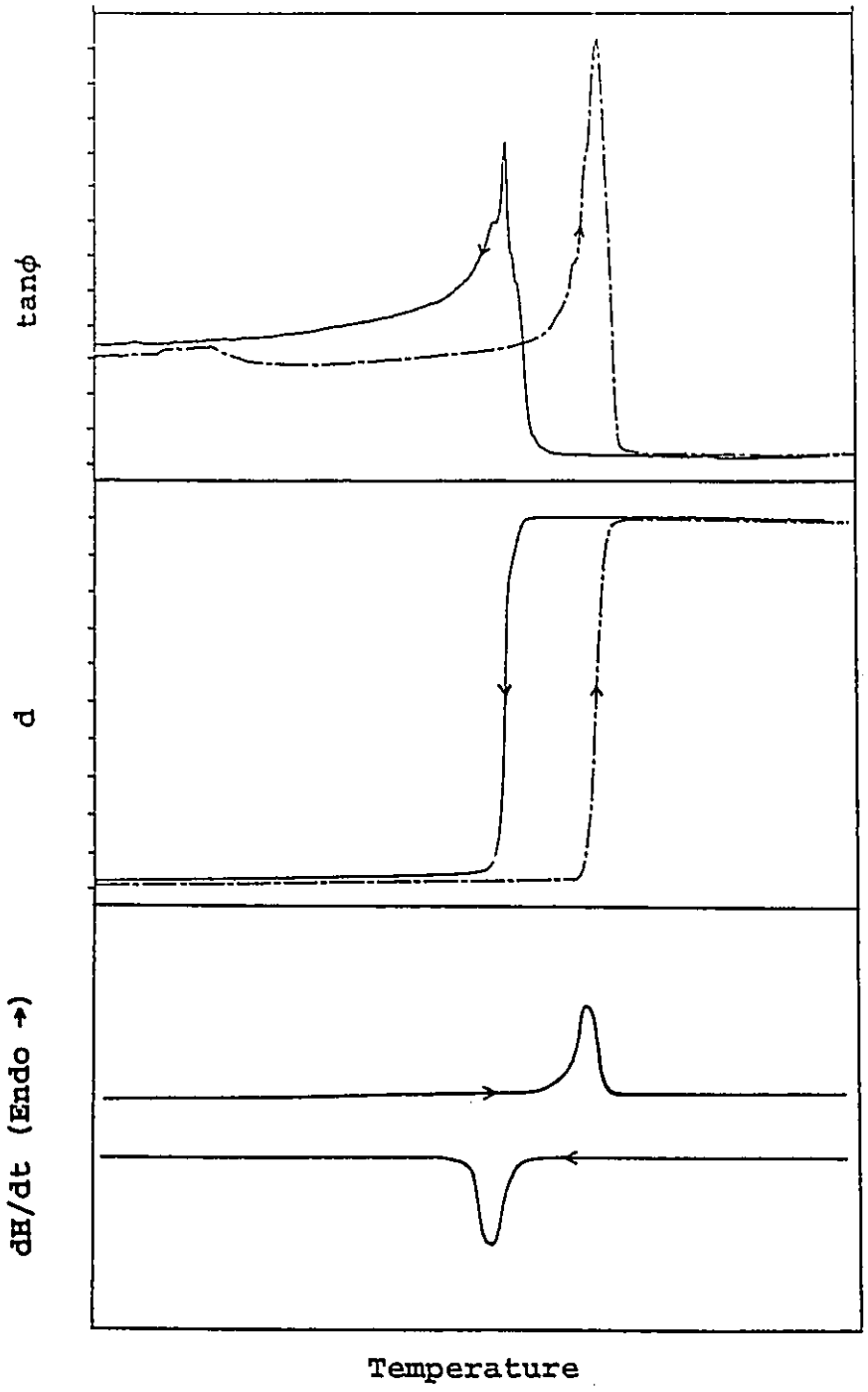

Fig.4.1: Schematic temperature dependence of internal friction (tanϕ), probe position (d) and heat flow (dH/dt) during the reversible martensitic transformation.

4.2 Internal Friction Studies

4.2.1 Study of the Temperature Dependence of Internal Friction

4.2.1.1 Determination of Temperature Range for Reproducible Martensitic Transformation

Before studying the effects of various experimental parameters on the internal friction due to martensitic transformation, it is necessary to first determine the temperature range in which the forward and reverse transformation can occur repeatedly in a reproducible manner, without deterioration due to thermally-induced decomposition. For this purpose, samples of alloy A were thermally cycled in different temperature ranges and the internal friction was measured using the inverted torsional pendulum during cooling and heating at a constant rate of 2°C/minute. The results of the study are as follows:

(1) Cycling Between -173°C and 107°C

The quenched specimen (from 850°C to 18°C water) was mounted in the inverted torsional pendulum at room temperature and its internal friction and elastic modulus were measured during cooling to -173°C, and the results are shown in Fig.4.2 (curves marked "a"). Subsequent measurements during heating to 107°C are shown by curves "b". It is seen that during cooling the retained parent phase at room temperature transforms to

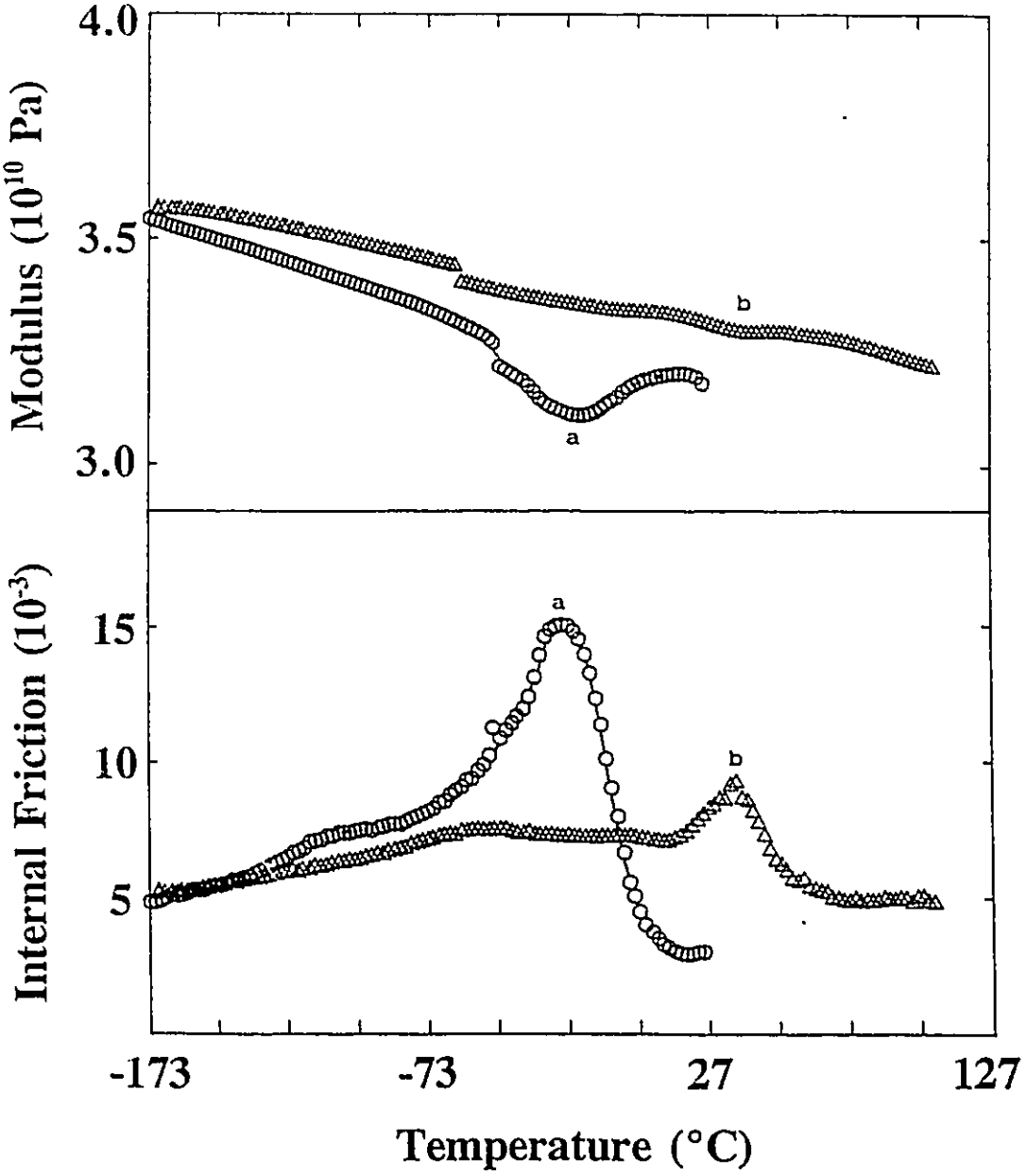

Fig.4.2: Internal friction and modulus measurements of alloy A (-173°C-107°C) immediately after quenching. (a) Cooling, (b) Heating.

martensite resulting in a modulus minimum and an internal friction peak centered around -23°C. During heating, a smaller corresponding minimum and peak appears at about 37°C, indicating a reverse transformation. Internal friction and modulus measurements for the second cooling from 107 to -173°C (curve a) and second heating to 107°C (curve b) are shown in Fig.4.3. The peaks appear at -20°C and 36°C respectively (it should be noted that the modulus discontinuities in Figs.4.2 & 4.3 were caused by disturbances when adjusting the sample's alignment and were not related to any changes in the sample itself). Comparing curves "b" in Fig.4.2 and Fig.4.3, it is apparent that both the internal friction peak and the modulus minimum corresponding to the reverse transformation (heating) is significantly depressed in the first thermal cycle . This is explained to be a result of the partial stabilization of martensite due to the pinning of the variant interfaces by quenched-in vacancies (Morin et al., 1987, 1989 & Morin and Guenin, 1990). The pinning effect is evidenced by a weak internal friction peak at the lower temperature side of both the forward and the reverse transformation peaks during the first thermal cycle as can be seen in Fig.4.2. It is noted, by comparing Fig.4.2 and Fig.4.3, that only curve b, but not curve a, is significantly depressed in the first thermal cycle. This suggests that the pinning of the interfaces, being dependent on the diffusion of vacancies and thus both time and

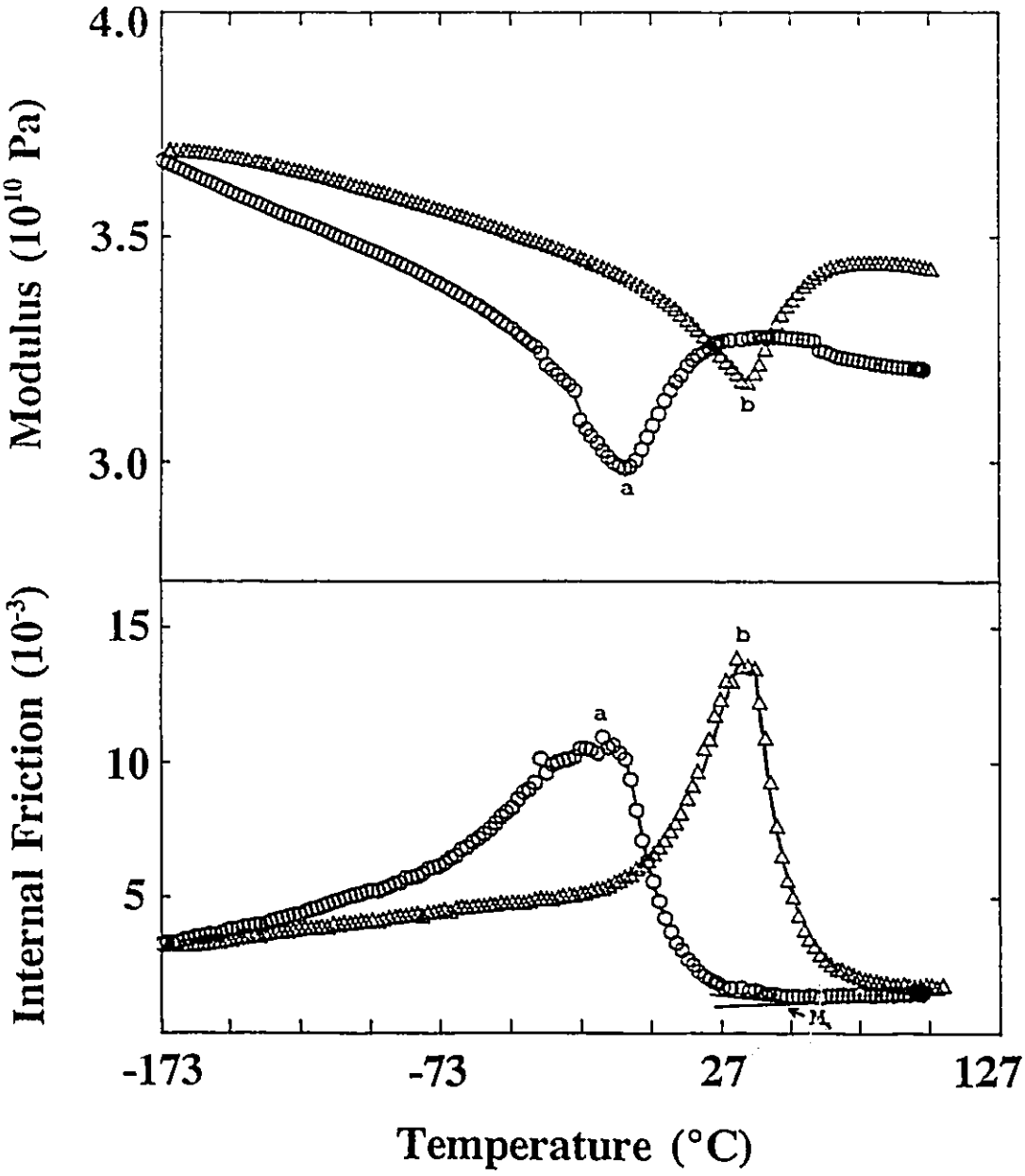

Fig.4.3: Internal friction and modulus measurements of alloy A (-173°C-107°C) for the second thermal cycle. (a) Cooling, (b) Heating.

temperature dependent, has not yet occurred during the initial cooling (curve a in Fig.4.2) due to lack of thermal activation, but becomes more developed during the subsequent heating. The depression of modulus minimum during heating in the first thermal cycle can be explained by the interaction of quenched-in vacancies with soft mode** centers (localized strain centers) to offset the soft mode phenomenon (Zhao et al., 1991). Heating to and holding at 107°C for about five minutes, however, obviously eliminates most of the quenched-in vacancies, evidenced by the disappearance of the vacancy-related peak seen at low temperatures in Fig.4.2 but not in Fig.4.3 and the restoration of the "normal" transformation peaks in Fig.4.3 in the subsequent cooling and heating cycle. In the following thermal cycles, both the cooling and heating curves for the internal friction and modulus became reproducible. A further aging of 9.25 hours at 107°C in the pendulum did not cause any significant changes in the cooling and heating curves, which indicates that the upper limit of 107°C is a "safe" one for repeated thermal cycling without causing immediate aging effects. However, with prolonged aging at 107°C, the M_s temperature, taken as the onset of the internal friction peak during cooling (as shown in Fig.4.3), as well as the peak height, decrease rapidly after an initial incubation period of about 25 hours, as Figs.4.4 and 4.5

** Soft mode here refers to the decrease of elastic modulus.

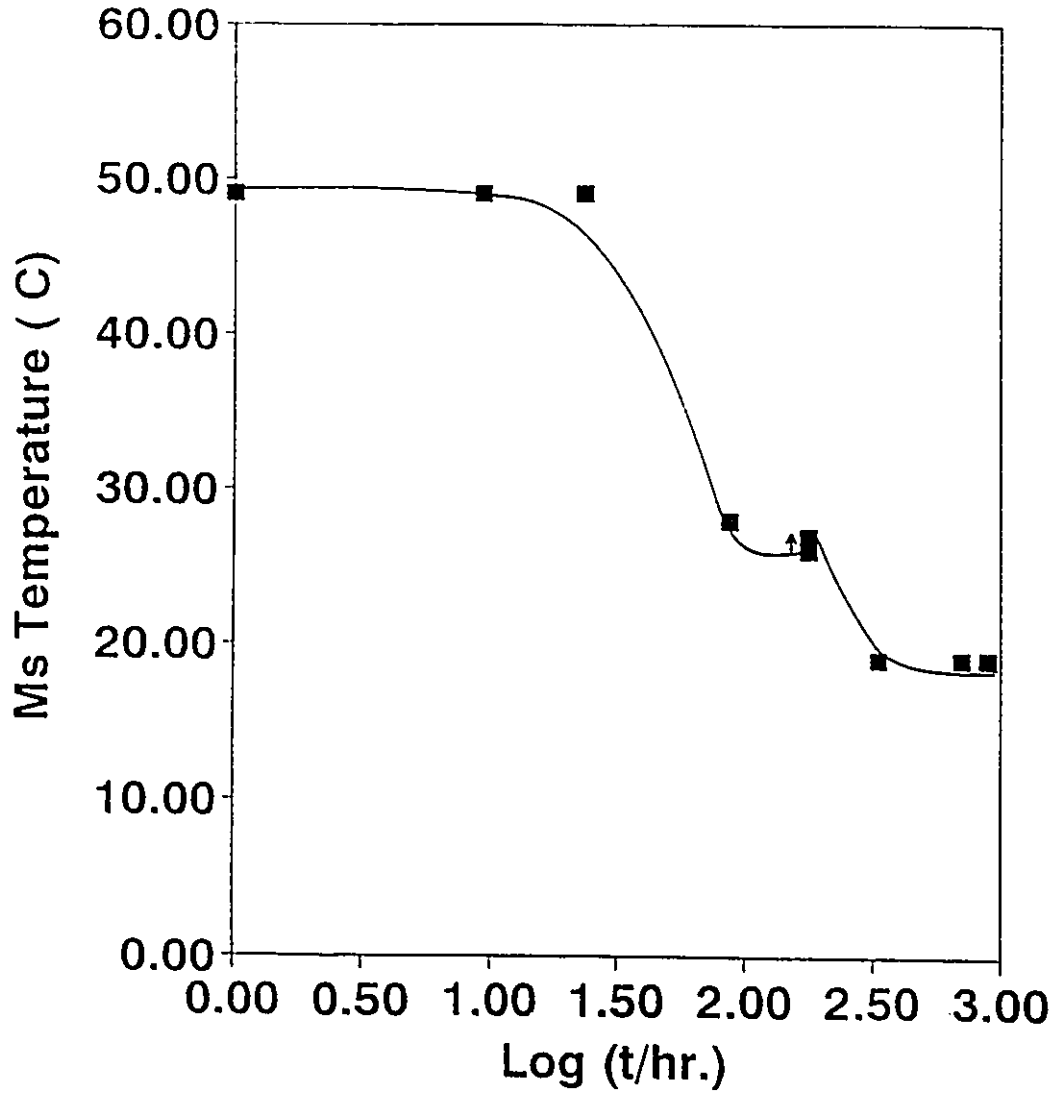

Fig.4.4: M_s temperature as a function of aging time at 107°C.

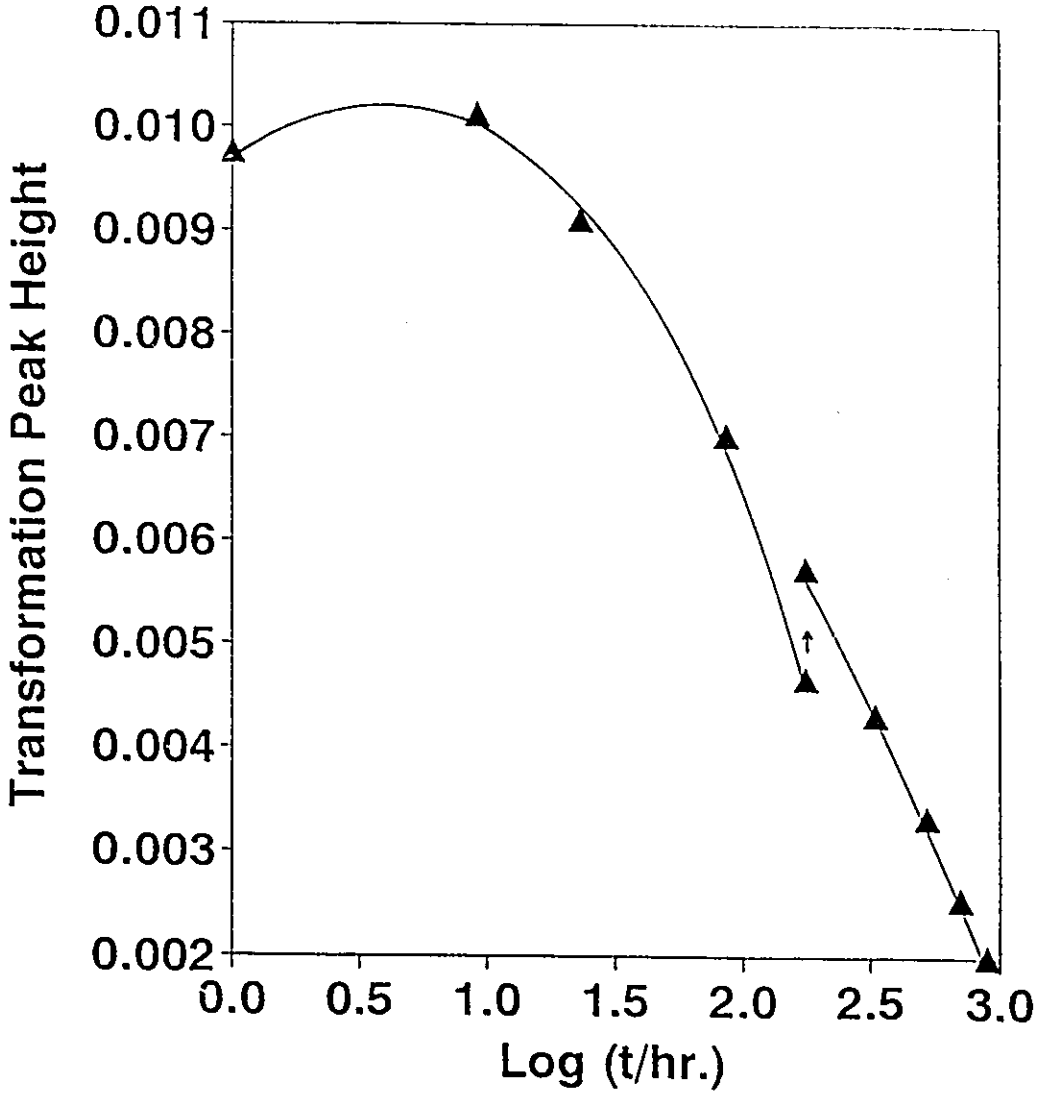

Fig.4.5: Internal friction due to martensitic transformation as a function of aging time at 107°C.

indicate. To give an idea of these changes, Fig.4.6 shows the internal friction and modulus curves before and after aging at 107°C for 187 hours. (Note that the discontinuities in the modulus curves were again due to disturbances while adjusting the sample's alignment as mentioned before). To determine the reversibility of these changes, the specimen was aged at room temperature for 95 hours after an accumulated aging time of 177.5 hours at 107°C and measured again. Both the M_s and the peak height, however, are only partially restored (see arrows in Figs.4.4 & 4.5) before decreasing again with further aging at 107°C. Therefore prolonged aging at 107°C introduces both reversible and irreversible changes in M_s and peak height.

According to Cook and Brown (1978) and Dunne and Kennon (1981), the reversible effects are most likely due to a change in the equilibrium degree of order in the β parent phase while the irreversible effects may originate in the thermally activated decomposition of the parent phase. At temperatures below B2 to DO_3 transition point (417°C in alloy A), the equilibrium degree of DO_3 order decreases with increasing temperature and therefore aging at the upper temperature limit of 107°C would result in a decrease of DO_3 order, which in turn decreases the M_s temperature according to Suzuki et al.(1990) and Rapacioli and Ahlers (1979). This may account for the part of M_s decrease which is reversible by

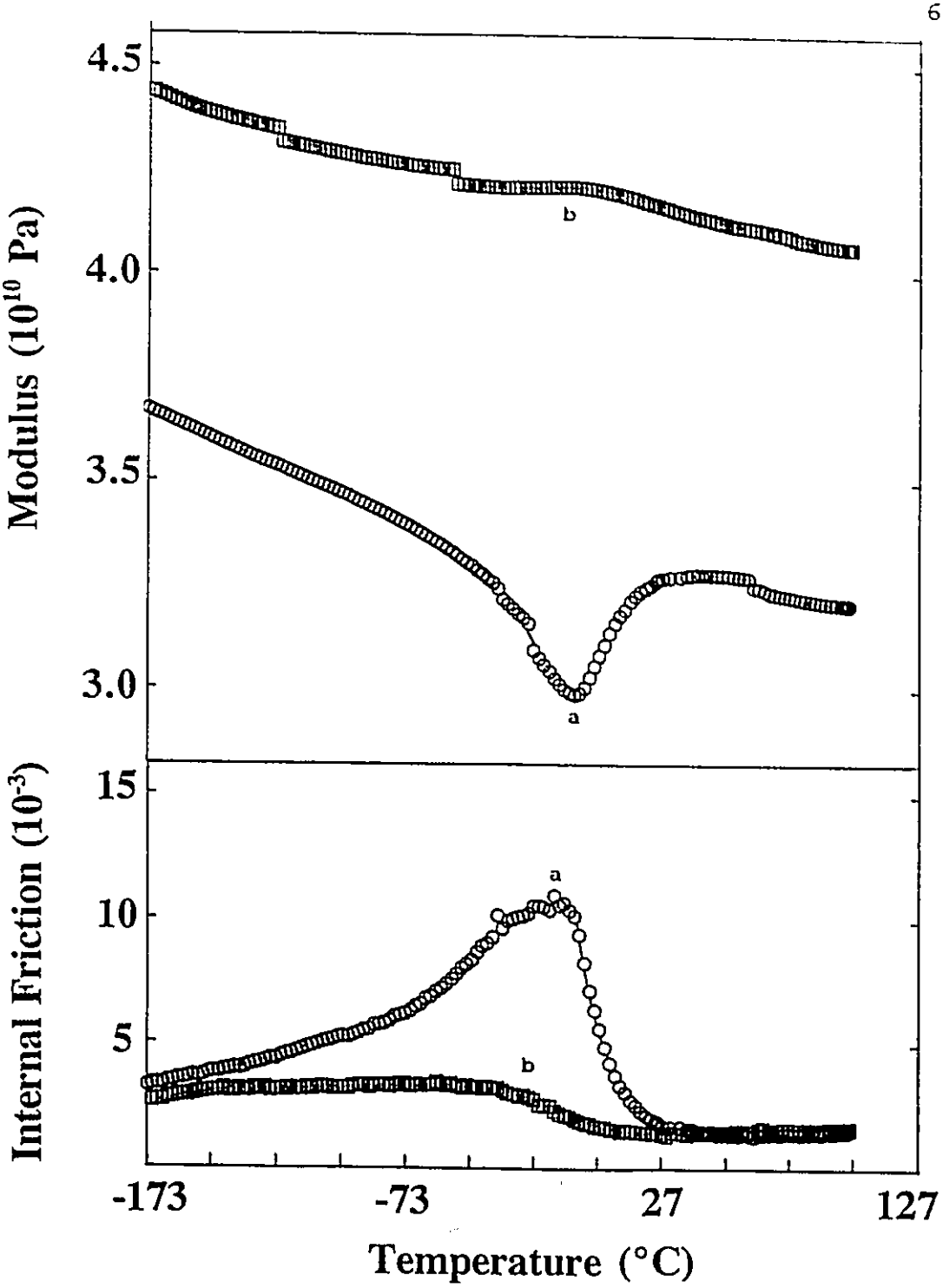

Fig.4.6: Internal friction and modulus of alloy A (-173°C-107°C) during cooling. (a) Second thermal cycle, (b) After 187 hour aging at 107°C.

subsequent aging at room temperature. The irreversible decrease of M_s and internal friction peak height can be explained by the formation of fine segregates or precipitates of α phase which interfere with the martensitic nucleation process (Dunne and Kennon, 1981). The metallographic examination (described in Section 4.4) and X-ray diffraction analysis (described in Section 4.5) has detected the existence of α phase precipitates in the specimen after prolonged aging, as will be later shown.

(2) Cycling between -123°C and 177°C

When the alloy A is heated from 25°C to 177°C and then cooled, the internal friction and modulus measured during cooling and subsequent heating (curve a, Fig.4.7) have quite different features from those observed in Figs.4.2 & 4.3. As seen in Fig.4.7, the transformation on second heating appears to occur in two stages. The features of the internal friction and modulus during the second and sixth heating run are compared in Fig.4.7, and those during the third and seventh cooling run are compared in Fig.4.8. From curves "a" in Fig.4.7 it is interesting to note the distinctly different features of modulus change accompanying the two internal friction peaks. For the low temperature peak, there is a sudden drop in modulus at the temperature of the fastest

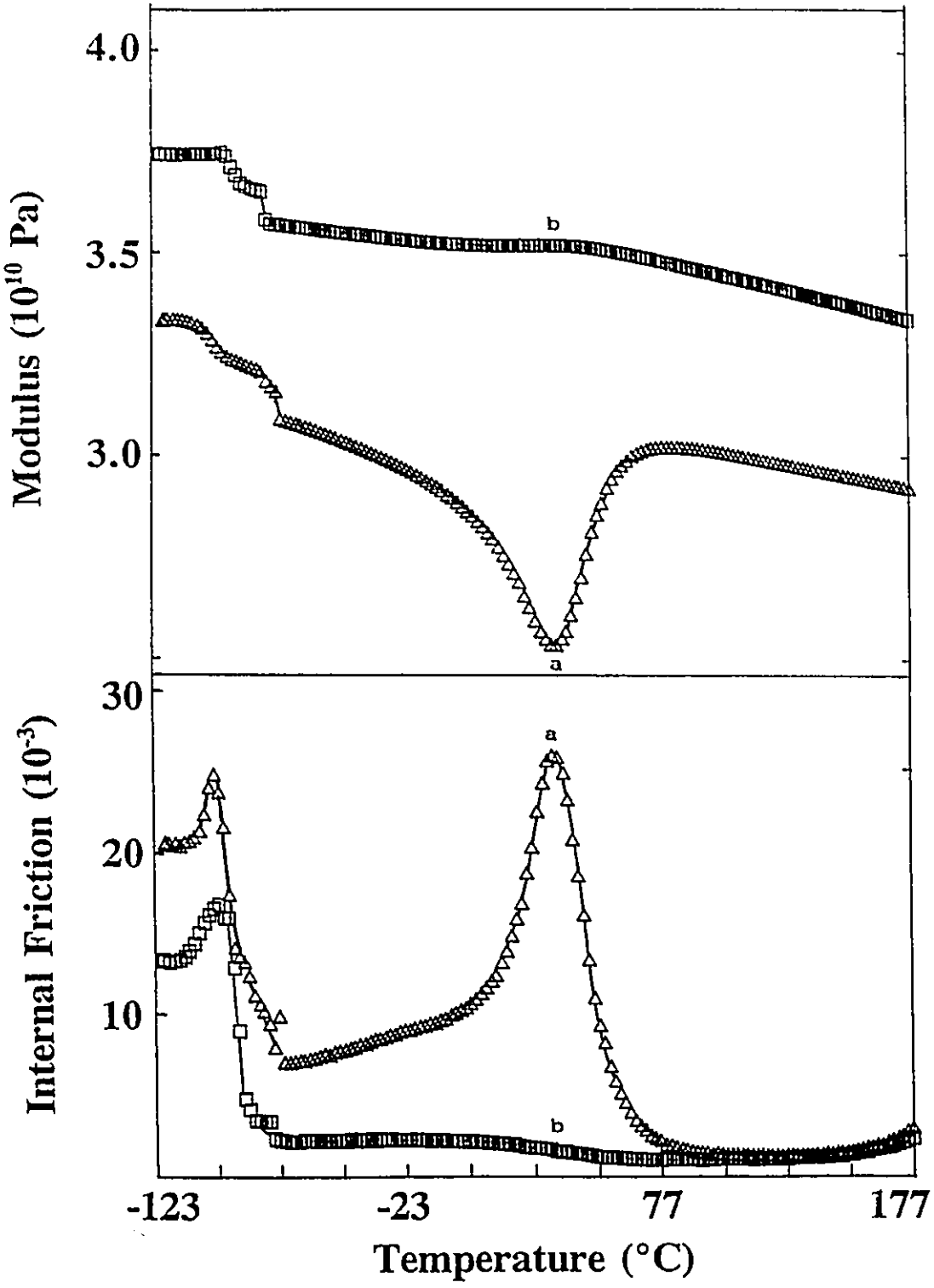

Fig.4.7: Internal friction and modulus of alloy A (-123°C-177°C) during heating. (a) Second thermal cycle, (b) Sixth thermal cycle.

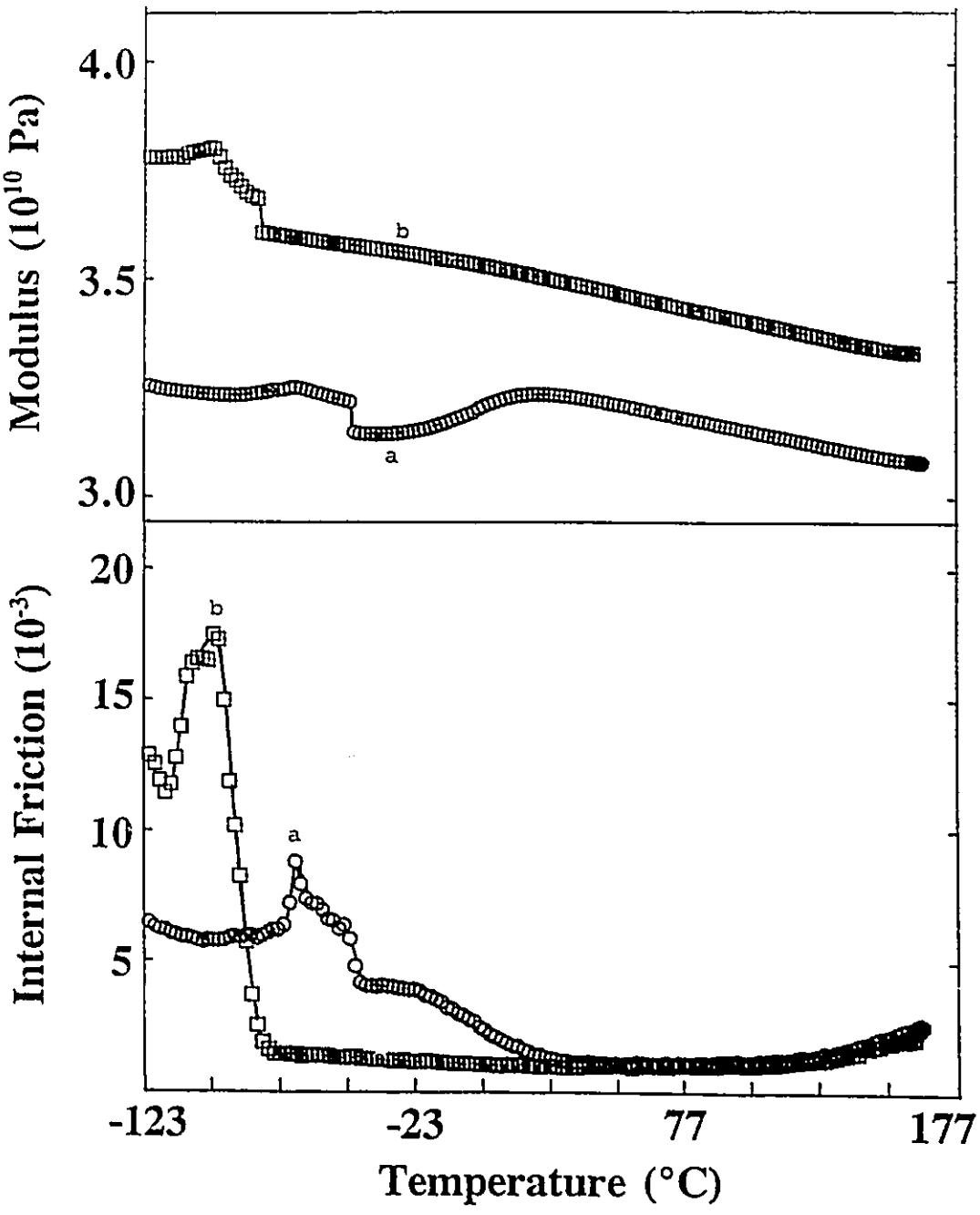

Fig.4.8: Internal friction and modulus of alloy A (-123°C-177°C) during cooling. (a) Third thermal cycle, (b) Seventh thermal cycle.

decrease of internal friction, whereas for the high temperature peak, a modulus minimum characteristic of martensitic transformation occurs at the peak temperature. During cooling (curves "a" in Fig.4.8), the sequence of the internal friction and modulus change is reversed. With the increase of the number of cycling between -123°C and 177°C, the magnitude of the low temperature peak first increases and then saturates after five cycles while that of the high temperature peak keeps decreasing until it almost disappears after six cycles. The modulus minimum corresponding to the high temperature peak also gradually diminishes until it disappears after six cycles.

In analogy to the classical model of dislocation breakaway hysteresis (Batist, 1972), a model based on a mechanism of breakaway** of the martensite/parent interfaces from the precipitates is proposed to account for the observed low temperature internal friction peak. During cooling from 177°C, the internal friction first begins to increase at about 45°C (Fig.4.8a), which is identical to the onset of normal martensitic transformation observed earlier in Fig.4.3(a). This increase in internal friction is due to the nucleation and subsequent movement of martensite/parent interfaces in the region free of precipitates. With further cooling, the martensite plates continue to grow and the martensite/parent interfaces push further towards the surrounding parent matrix

** This is supported by the stress-amplitude dependence of I.F. in Fig.4.19.

and their relative motion begin to become progressively more influenced by the fine α-precipitates formed earlier at higher temperature. This is expected to lead to a breakaway hysteretic process which results in a drastic increase in both the internal friction and the modulus. With further cooling, the density of precipitates on the interfaces becomes too high and the interfaces are completely pinned, resulting in a decrease of the internal friction. Since, during the subsequent heating run, a displacement of the interfaces in the opposite direction occurs, a gradual unpinning of the interfaces from the precipitates results thereby causing a small increase in internal friction, Fig.4.7. When the interfaces become completely free from the pinning at a higher temperature (around -73°C in Fig.4.7), the internal friction as well as the modulus abruptly decrease. Subsequent transformation peak occurs at around the same temperature and in a same manner as that observed earlier in part (1), as shown by a comparison of Fig.4.3(b) and Fig.4.7(a).

With increased thermal cycling, more precipitates develop in the parent phase, resulting in a progressive decrease in the magnitude of the "normal" transformation peak and a simultaneous increase in that of the low temperature peak associated with precipitate-interface interaction. This is evident by comparing curve a and b in Figs.4.7 and 4.8.

(3) Cycling between -173°C and 277°C

Heating to 277°C completely eliminates the "normal" forward and reverse martensitic transformation peaks on further thermal cycling, while producing two other peaks. Fig.4.9 shows the internal friction and modulus during the second heating run. As can be seen, the low temperature peak is situated at about the same temperature (around -90°C) as the one discussed in part (2) and is accompanied by a modulus discontinuity. The high temperature unresolved peak (or a shoulder) occurring at around 187°C, however, is not accompanied by any obvious change in modulus, which suggests that it can not be associated with the reverse martensitic transformation. (This shoulder becomes resolved in the further experiments shown in Fig.4.10). Further cycling showed (data not included here) that the magnitude of the low temperature peak becomes constant after it first appears, whereas the high temperature peak becomes better resolved with increased cycling between -173°C and 277°C.

The low temperature peak in Fig.4.9 has features similar to the ones discussed in Figs.4.7 and 4.8, and this similarity suggests that it has the same origin. It should be pointed out that the absence of the "normal" transformation peak in Fig.4.9 (which occurs at 37°C in Fig.4.3) does not necessarily mean that martensitic transformation is absent. According to Zhao et al.(1991), the martensitic transformation

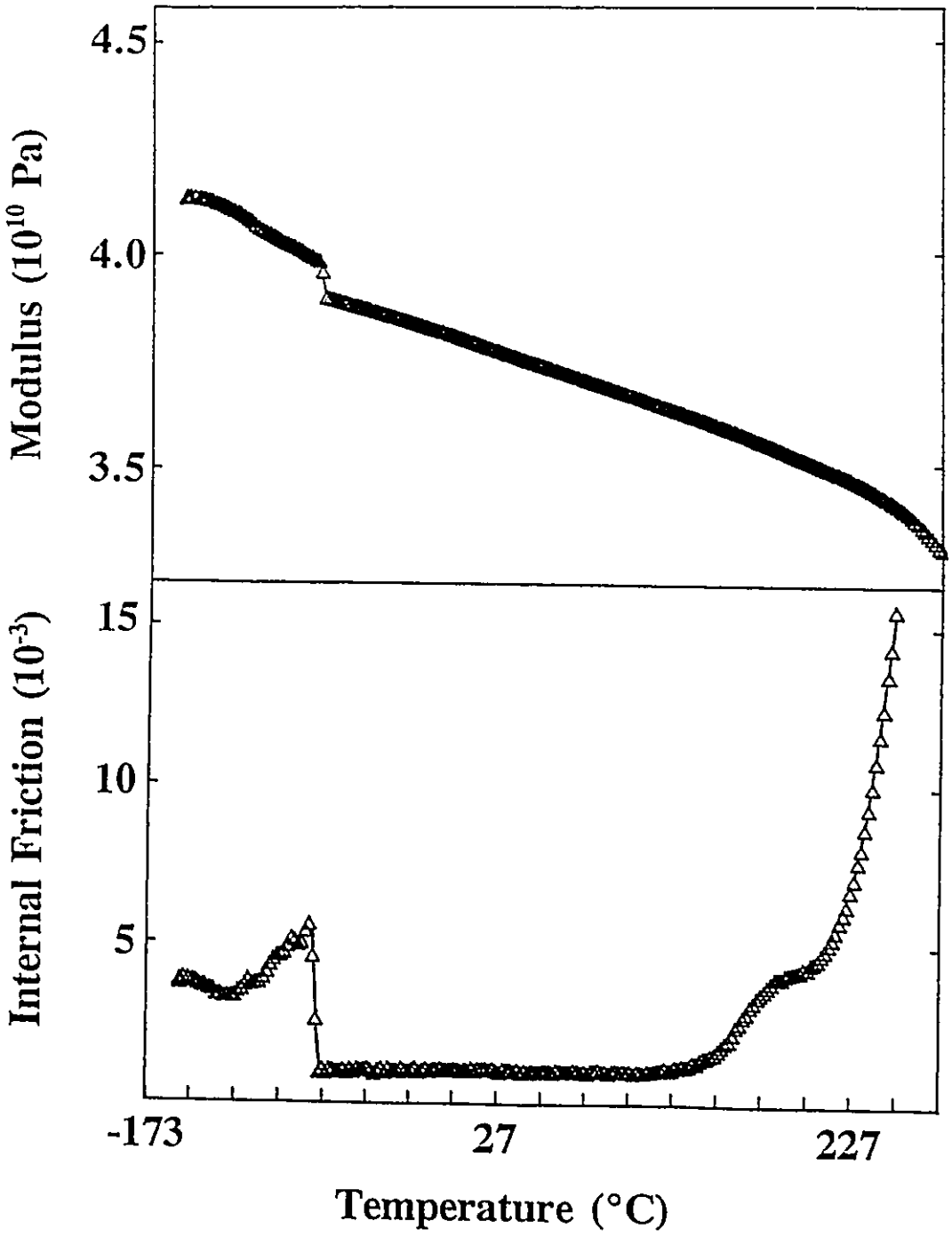

Fig.4.9: Internal friction and modulus of alloy A measured during the second heating run (-173°C-277°C).

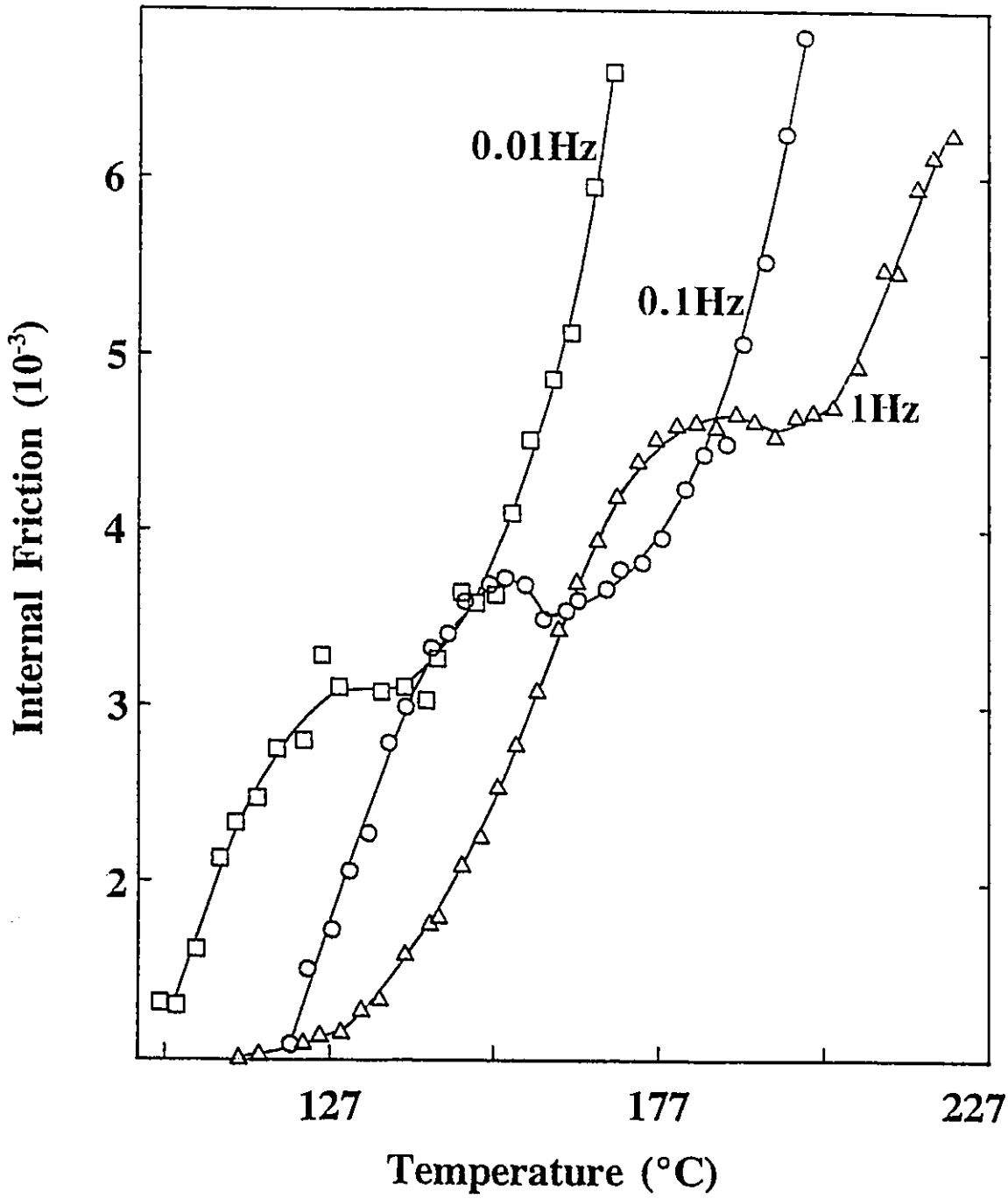

Fig.4.10: The "high temperature peak" measured at 0.01, 0.1 and 1 Hz frequencies.

may still take place, as the appearance of the low temperature peak implies, but does not show a soft mode phenomenon due to the influence of the precipitates on the localized soft mode centers, and therefore no modulus minimum or internal friction peak appears even though the transformation occurs.

The high temperature peak is further studied at three different oscillation frequencies (f), as shown in Fig.4.10. The increase in the temperature of the peak (T_p) with frequency clearly indicates that it is associated with a relaxation process. This leads to an activation energy of about 28.4 kcal/mol, obtained from the slope of the Arrhenius plot of Ln(f) versus $1000/T_p$ shown in Fig.4.11. Zhao et al.(1989) have recently observed a relaxation peak occurring at 190°C at a frequency of 0.6Hz in DO_3 ordered β phase of a Cu-Zn-Al alloy and found an activation energy of 26 kcal/mol, close to that of the high temperature peak found in this study. Combining the results of earlier studies (Ghilarducci and Ahlers, 1983 and Zhao et al., 1988), Zhao et al. attributed the peak to the movement of defects around anti-phase domain boundaries under a vibrating stress. Judging from the similar features between their peak and the one observed here, the latter is therefore thought to have the same origin.

The effects of temperature range of thermal cycling on the internal friction can be summarized as follows:

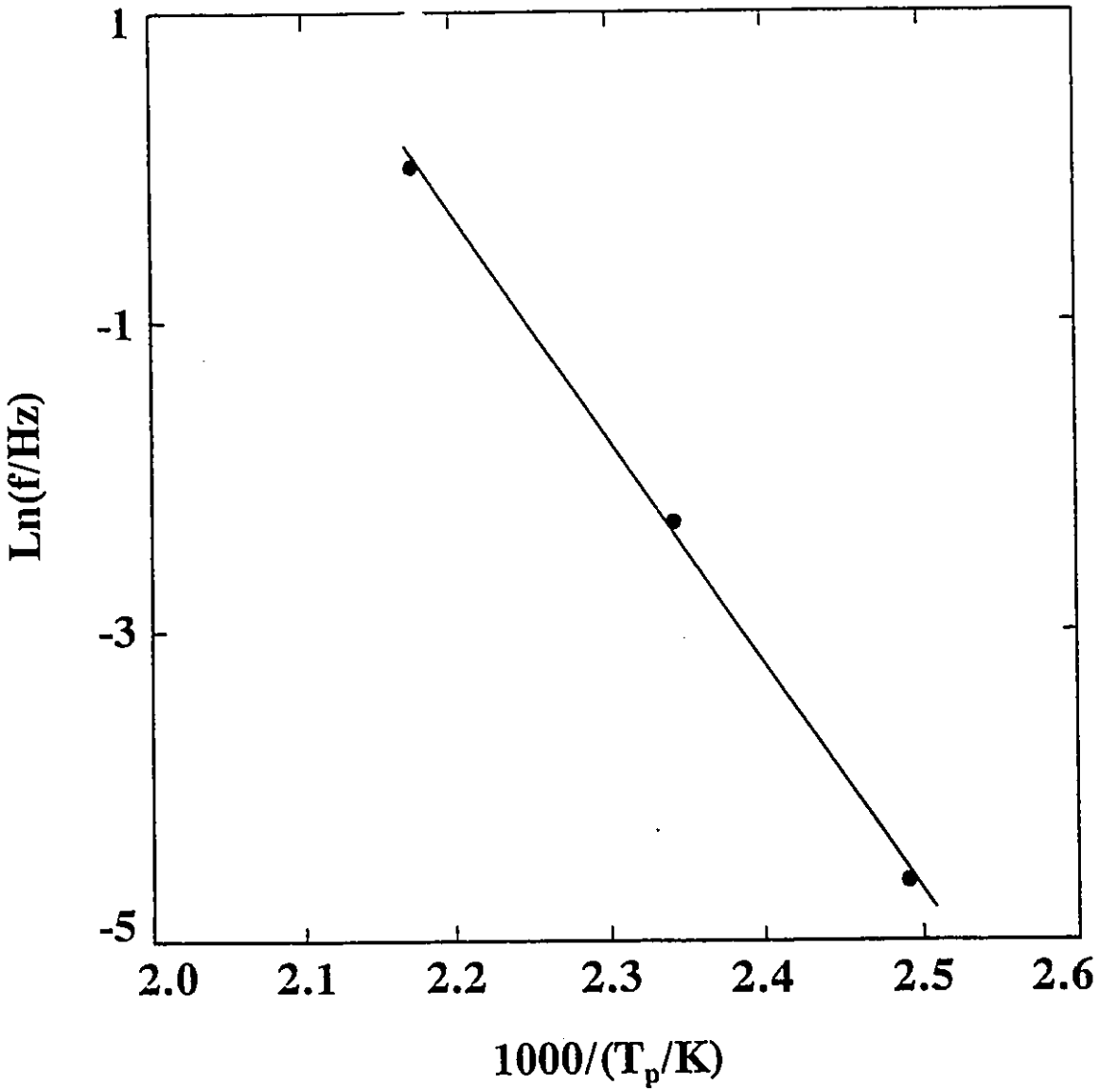

Fig.4.11: Arrhenius plot of Ln(f) vs. $1000/T_p$.

(a). Thermal cycling to a relatively low temperature (107°C) results in a reproducible internal friction peak and modulus minimum due to the martensitic transformation, once the quenched-in vacancies are annealed out. Deterioration of the transformation occurs only after prolonged aging (more than 25 hours) at 107°C, as indicated by an irreversible decrease of M_s and the peak height at the transformation.

(b). Thermal cycling to medium temperature (177°C) progressively decreases the magnitude of the internal friction peak associated with the martensitic transformation and increases that of another low temperature peak originating from the interaction of α precipitates with martensite/parent interfaces.

(c). Thermal cycling to a higher temperature (277°C) results in immediate elimination of the "normal" martensitic transformation peak and the appearance of a low temperature peak similar to that observed in (b).

To conclude, an upper temperature limit of 107°C is "safe" for repeated measurements of internal friction due to martensitic transformation during thermal cycling of a given alloy A sample. Therefore in all further studies of the effects of stress amplitude, cooling rate and frequency on the internal friction, the upper temperature limit of thermal cycling is kept below 107°C.

4.2.1.2 Effects of Stress Amplitude

After a reproducible internal friction peak due to martensitic transformation had been measured in alloy A by using the Dynamic Mechanical Analyzer in an appropriate temperature range (-100°C to 100°C), the dynamic (and the corresponding static) stress was varied in two different sequences, and the results are separately presented in the following:

(1) Decreasing Stress Amplitude:

When the initial stress amplitude applied was large enough to cause stress-induced martensitic transformation, and then progressively decreased, the internal friction peak due to martensitic transformation increased monotonically, as shown in Figs.4.12 and 4.13. The internal friction peak height $(\tan\phi)_{max}$ and peak temperature (M_p) are plotted against the stress amplitude in Fig.4.14. It can be seen that while internal friction peak height $(\tan\phi)_{max}$ increases monotonically with the decrease of stress amplitude, the peak temperature (M_p) first decreases with decreasing stress amplitude until it reaches a minimum, and then increases again with further decrease of stress amplitude. This dependence can not be explained by any currently available theories including that by Dejonghe et al.(1976), which predicts that the internal friction increases monotonically with the increase of stress

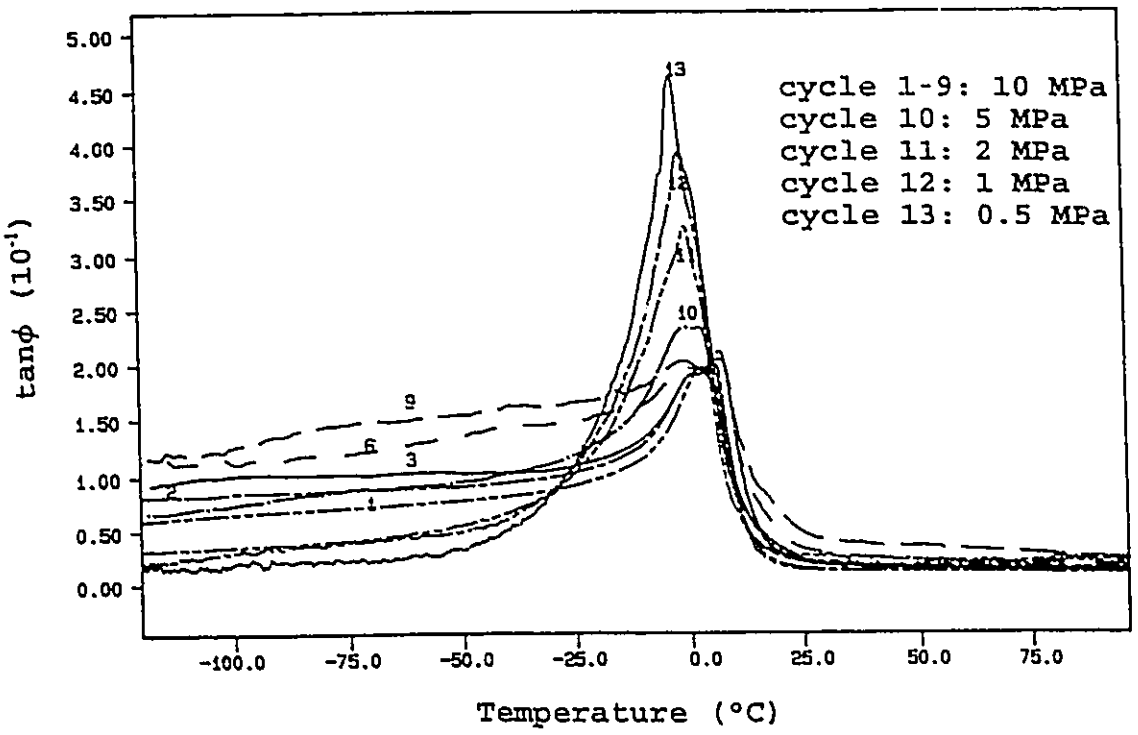

Fig.4.12: Internal friction of alloy A as a function of temperature at various thermal cycles and stress amplitudes measured during cooling. Stress amplitude was kept constant from thermal cycle 1 to 9 and then progressively decreased in the following cycles.

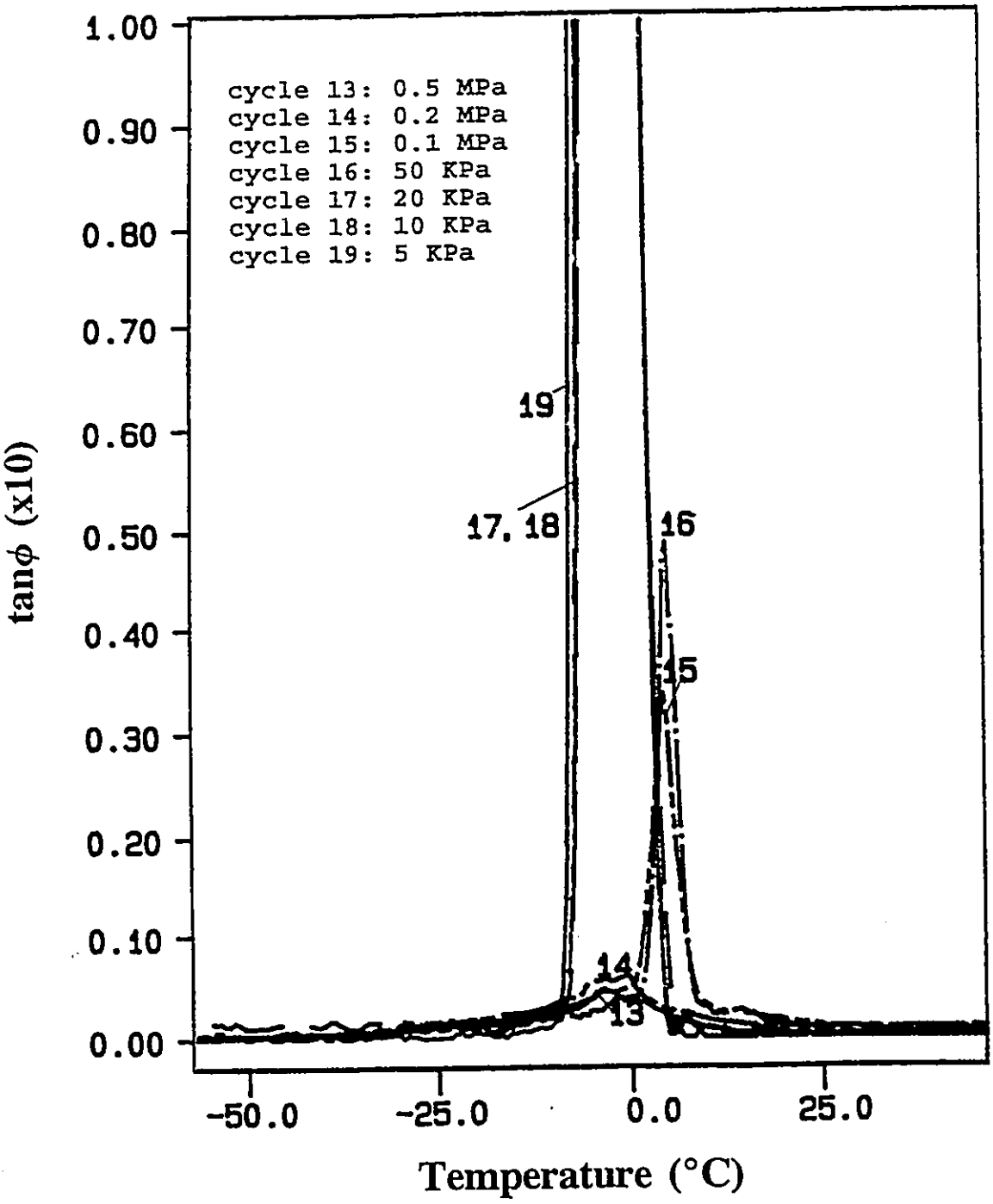

Fig.4.13: Internal friction of alloy A as a function of temperature at various stress amplitudes.

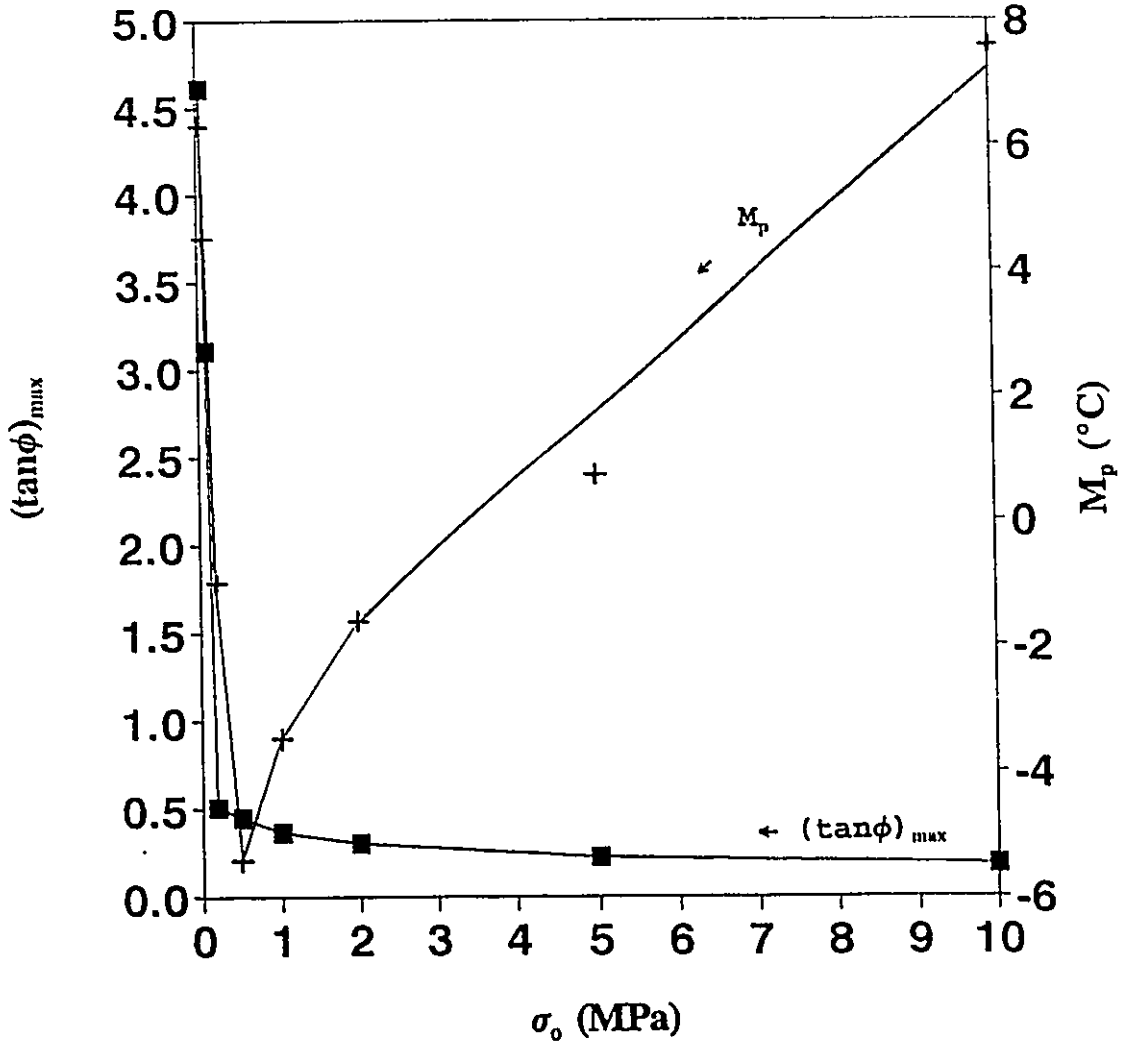

Fig.4.14: Internal friction peak height $[(\tan\phi)_{max}]$ and peak temperature (M_p) as a function of stress amplitude (σ_o).

amplitude. A physical model and mathematical treatment (Xiao, 1993) is therefore developed to interpret this and other experimental results. This will be discussed in detail in Chapter 5.

The average probe position versus temperature curves were also simultaneously obtained during the measurements of internal friction shown in Figs.4.12 and 4.13. These curves for the first nine cooling cycles, given in Fig.4.15, show that the sample becomes bent during the martensitic transformation and that the bending increases with increasing number of thermal cycles, as indicated by a decrease in the probe position, although the stress amplitude is kept constant at 10 MPa. However, the rate of increase is gradually lessened with increase in the number of such cycles. It is believed that thermal cycling under a static and dynamic stress would promote the nucleation and growth of the stress-oriented martensite variants which helps to increase the bending deformation. Indeed, transmission electron microscopy observations by Ritter et al.(1979), Nakata et al.(1985) and Rios-Jara et al.(1985) showed that oriented dislocations are created during such martensitic transformation, the density of which increases rapidly at the beginning and steadily afterwards. These dislocations are supposed to produce oriented internal stresses which help the externally applied stress to induce the stress-oriented martensites, thus

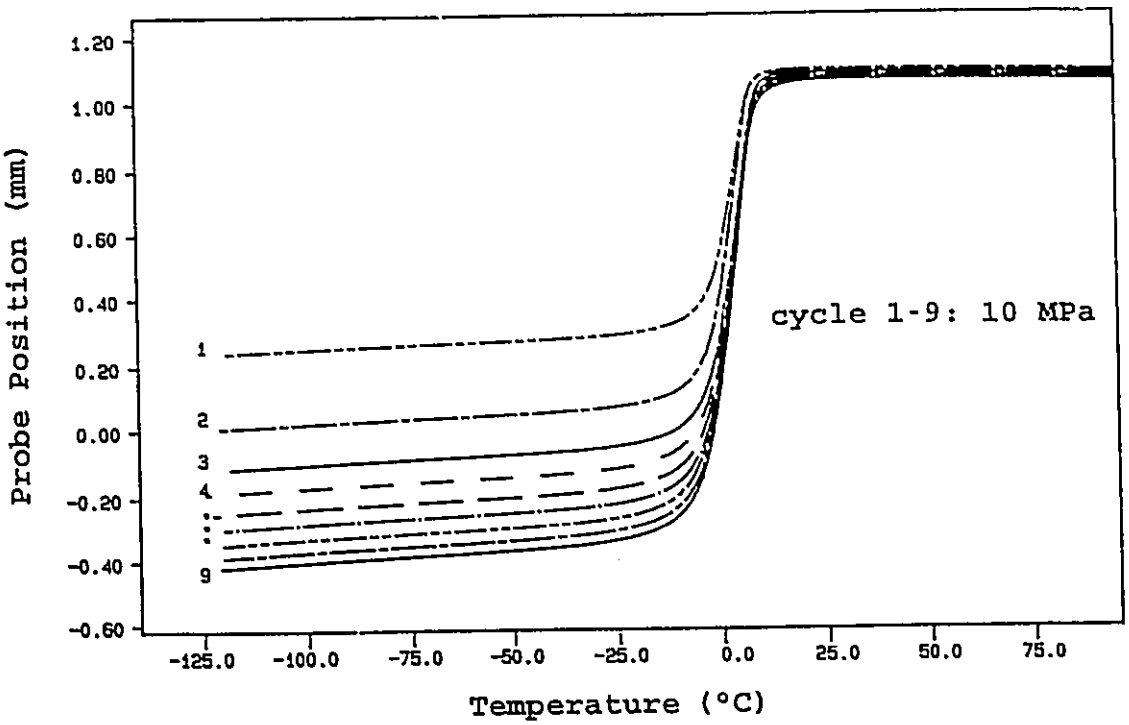

Fig.4.15: Average probe position as a function of temperature at various thermal cycles.

resulting in an additional bending strain during each new thermal cycle. This is supported by the probe position versus temperature curves measured at successively smaller stress amplitudes following the ninth cycle, as shown in Fig.4.16. It is evident, by comparing Fig.4.15 and Fig.4.16, that increasing the number of thermal cycles has the same effect on the transformational shape change as increasing the stress amplitude. However, the effects of these two variables on the temperature dependence of internal friction (Fig.4.12) are somehow different. In the martensitic region, it is seen that the internal friction increases with both the increase in the number of thermal cycles and the increase in stress amplitude, which may be attributed to the increased mobility of the martensite/martensite interface on an increase in stress (internal and external). However, in the region of phase transformation, the internal friction increases rapidly with the decrease of stress amplitude, but remains insensitive to the number of thermal cycles. This behaviour will be explained in Section 5.2, where a model describing the origin of the internal friction due to martensitic transformation is presented and an inverse relation between the internal friction and the stress amplitude is derived.

It is also noted that both the internal friction and the deformation (probe position decrease) in the parent phase region, in contrast to those in the martensite region, are

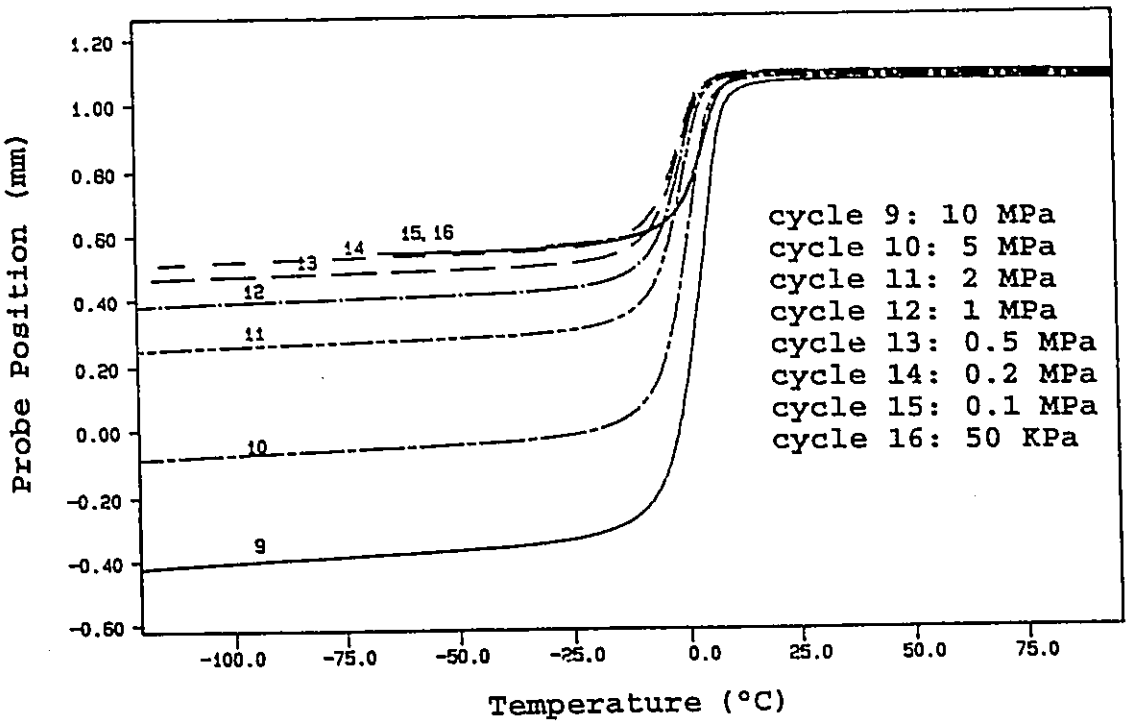

Fig.4.16: Average probe position as a function of temperature at various stress amplitudes.

much less affected by either the number of thermal cycles or the magnitude of stress amplitude. This is clearly related to a lack of mobile interfaces in the β parent phase, thereby reducing the sensitivity of internal friction and deformation to either the magnitude of stress amplitude or the number of thermal cycles. The weak amplitude dependence of internal friction in the β phase may be attributed to dislocation damping.

(2) Increasing Stress Amplitude:

To study the effect of increasing stress amplitude, plots of internal friction vs. temperature (cooling) and probe position vs. temperature (cooling and heating) were obtained at progressively higher stress amplitudes, as shown in Figs.4.17 and 4.18, respectively. From these plots Fig.4.19 was drawn, where the error bars for the internal friction peak curve are based on repeat measurements at a fixed stress amplitude which give a standard deviation of 5×10^{-3}. Fig.4.19 shows that when the stress amplitude was initially at a level not high enough to induce stress-oriented transformation and was later progressively increased, the change in internal friction peak height was no longer monotonic, but three distinct stages were present. With the increase of stress amplitude, the internal friction peak height first increases to reach a maximum (stage I), and then begins to decrease

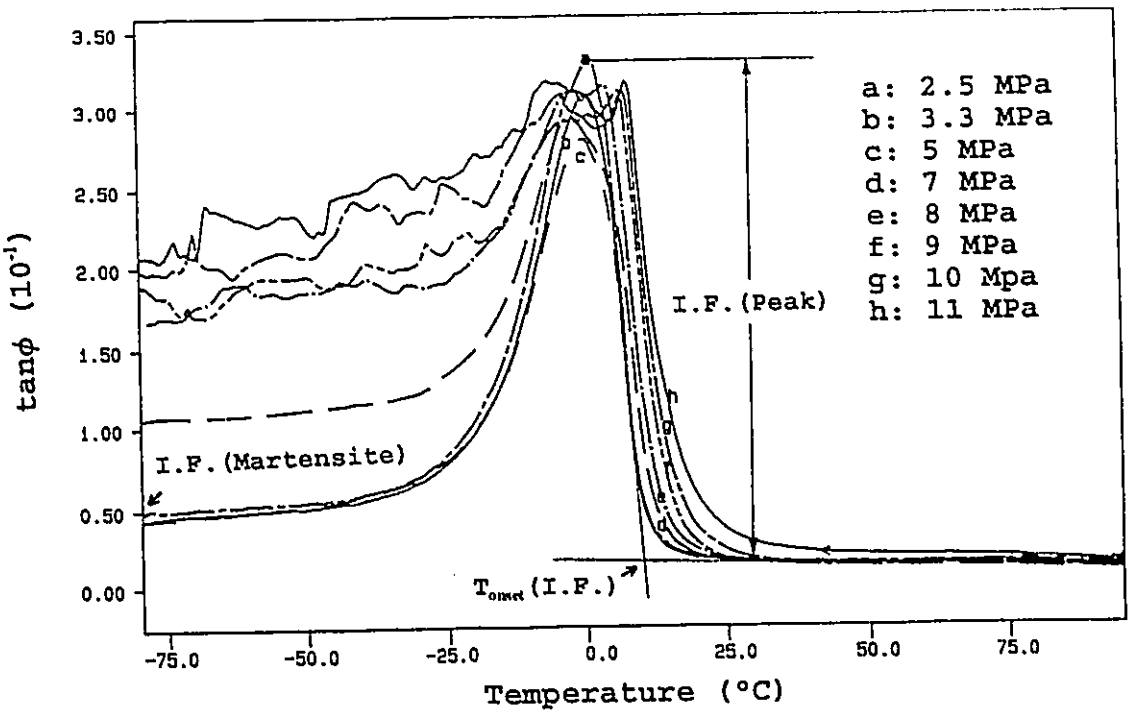

Fig.4.17: Internal friction of alloy A as a function of temperature (cooling) at various stress amplitudes.

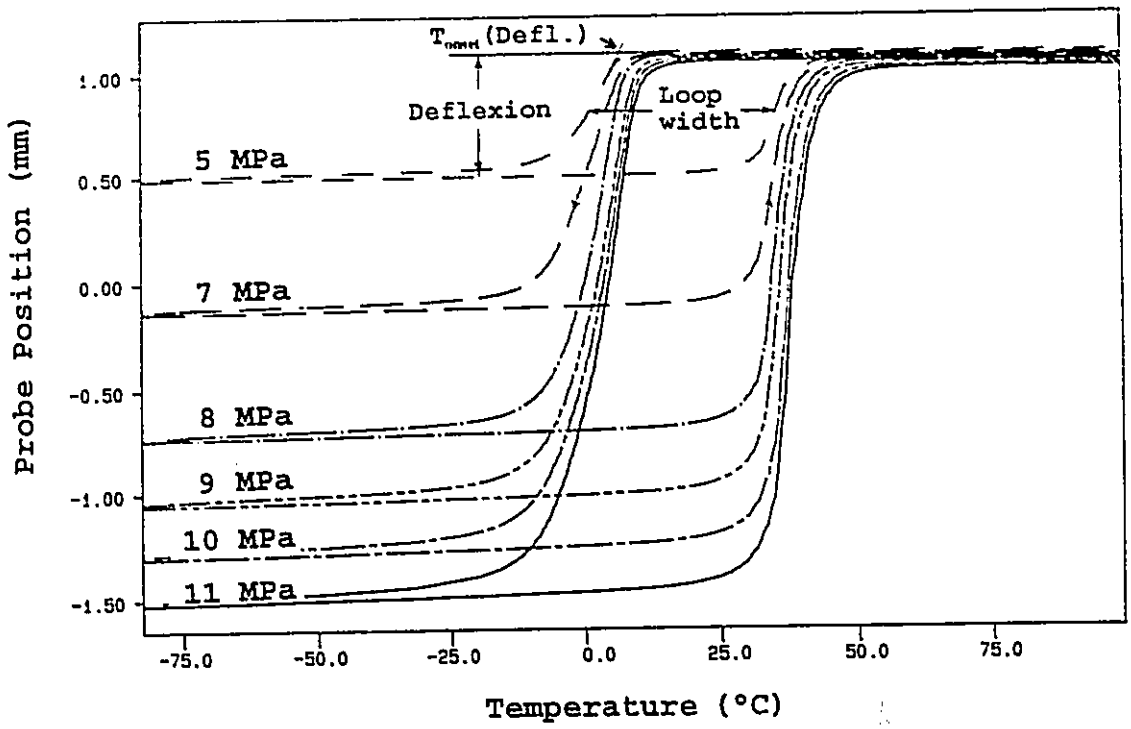

Fig.4.18: Probe position (alloy A) as a function of temperature (cooling and heating) at various stress amplitudes.

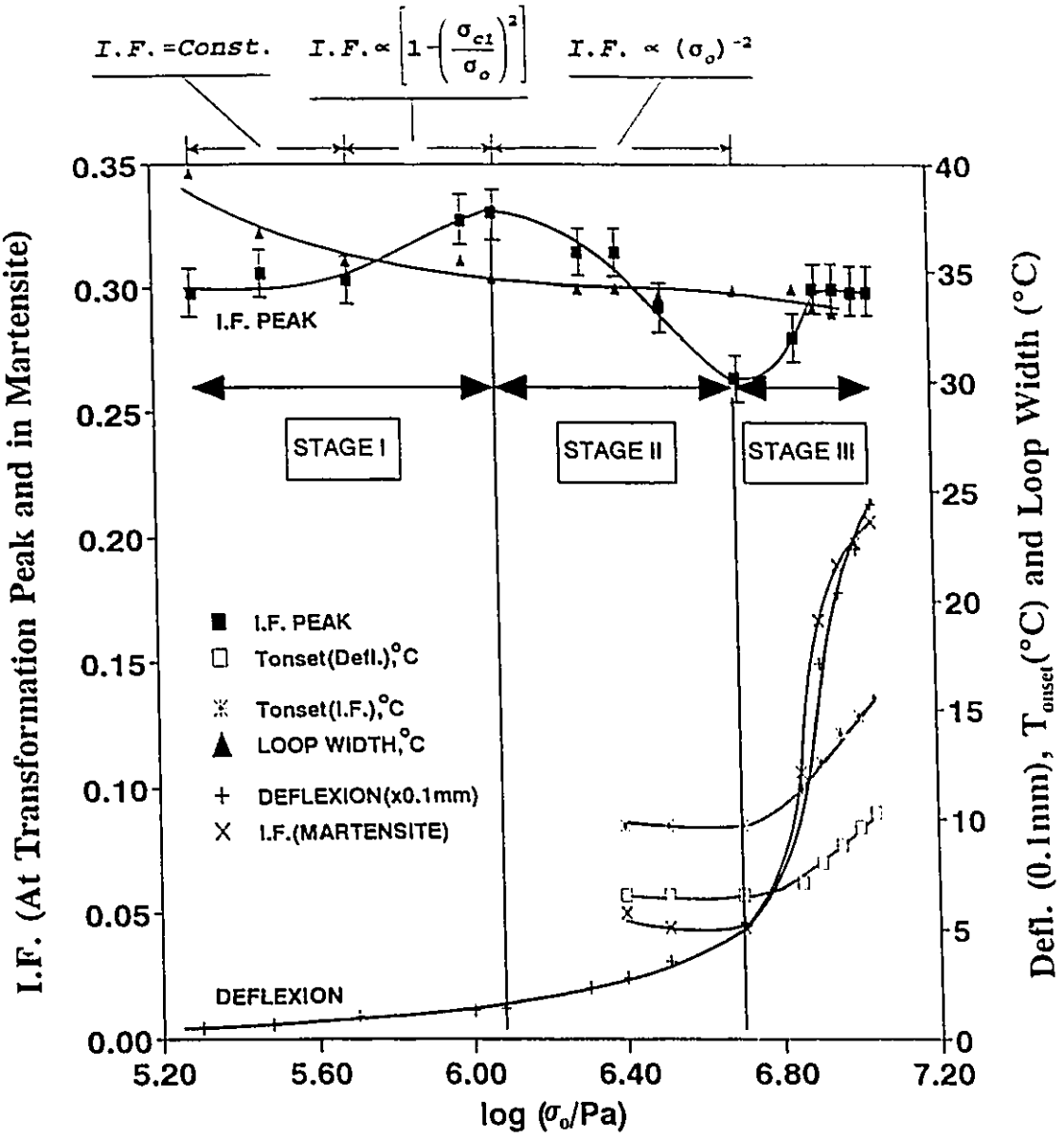

Fig.4.19: Internal friction (of transformation and of martensite), deflexion (maximum probe position change), T_{onset} (I.F. and deflexion) and loop width as a function of increasing stress amplitude (alloy A).

(stage II), before rising again to finally reach a saturation value (stage III). It is observed that the internal friction peak height variation in the three distinct stages correlates with the shape change (deflexion) occurring simultaneously with the martensitic transformation. In stage I, there is little deflexion accompanying the martensitic transformation and it is assumed that thermally-induced, and therefore randomly oriented, martensite variants are dominant in this stage. In stage II, however, there is a noticeable increase of the deflexion suggesting formation of massive stress-induced martensites which are preferentially oriented to give rise to a net shape change. In stage III, the deflexion rises rapidly with the stress amplitude, suggesting that another mechanism of deformation may be activated, giving a much faster rise of deflexion with stress. The concurrent rapid rise of internal friction in the martensite region of the tanϕ vs. temperature curve in Fig.4.19 indicates that this mechanism is most likely the re-orientation of existing martensite variants into more favourable orientation under application of the stress. Therefore, the three different stages should be dealt with individually according to the mechanism operating at each stage.

Comparing case (1) to (2), it is clearly seen that by applying a higher stress first, as in case (1), so as to "train" the shape memory alloy, a very low critical stress can

result so that stress-induced martensitic transformation becomes the dominant mechanism operating during subsequent lower stress measurements. Therefore only features of stage II are observed in case (1), as evident in Fig.4.14.

The dependence of the internal friction and shape change (deflexion) on stress amplitude in Fig.4.19, was only qualitatively reproducible when the same specimen was measured again after another identical heat treatment, as shown in Fig.4.20. The feature of three-stage internal friction change will be discussed and interpreted in detail in Chapter 5.

4.2.1.3 Effects of Cooling Rate

The internal friction peaks measured at σ_o=2MPa and f=1Hz at different cooling rates are shown in Fig.4.21. It is seen that the peak height increases with increase in the cooling rate. The plot of internal friction peak height vs. cooling rate is shown in Fig.4.22. This is consistent with the equation for internal friction due to martensitic transformation proposed by Dejonghe et al.(1976):

$$\tan\phi = \frac{A}{2\pi}\left(\frac{\partial m}{\partial T}\frac{\partial T}{\partial t}f^{-1}+\frac{4}{3}\sigma_o\frac{\partial m}{\partial \sigma}\left[1-\left(\frac{\sigma_c}{\sigma_o}\right)^3\right]\right) \qquad (2.4)$$

where the terms are described in Section 2.3.1. The equation suggests a linear relation between cooling rate

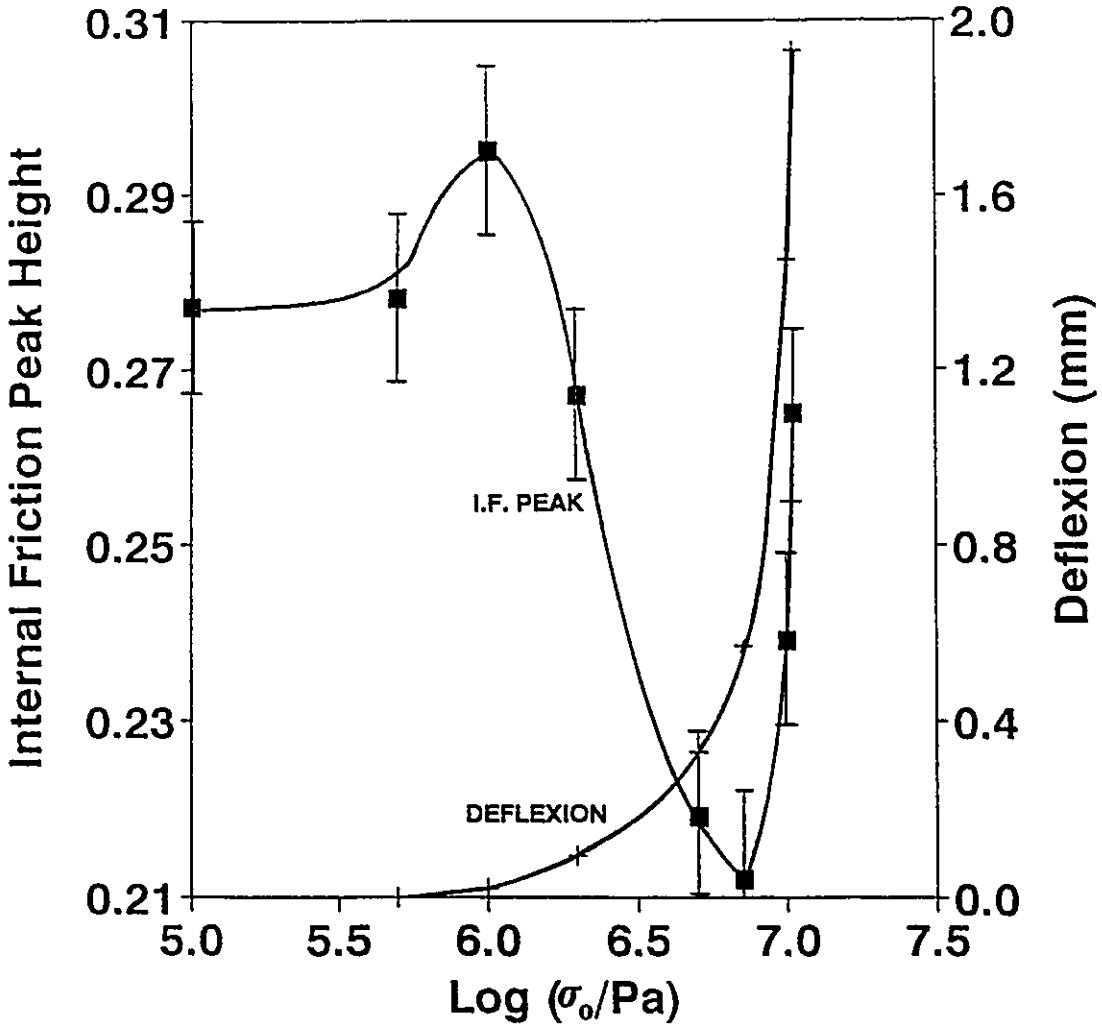

Fig.4.20: Internal friction peak height and deflexion as a function of stress amplitude (alloy A).

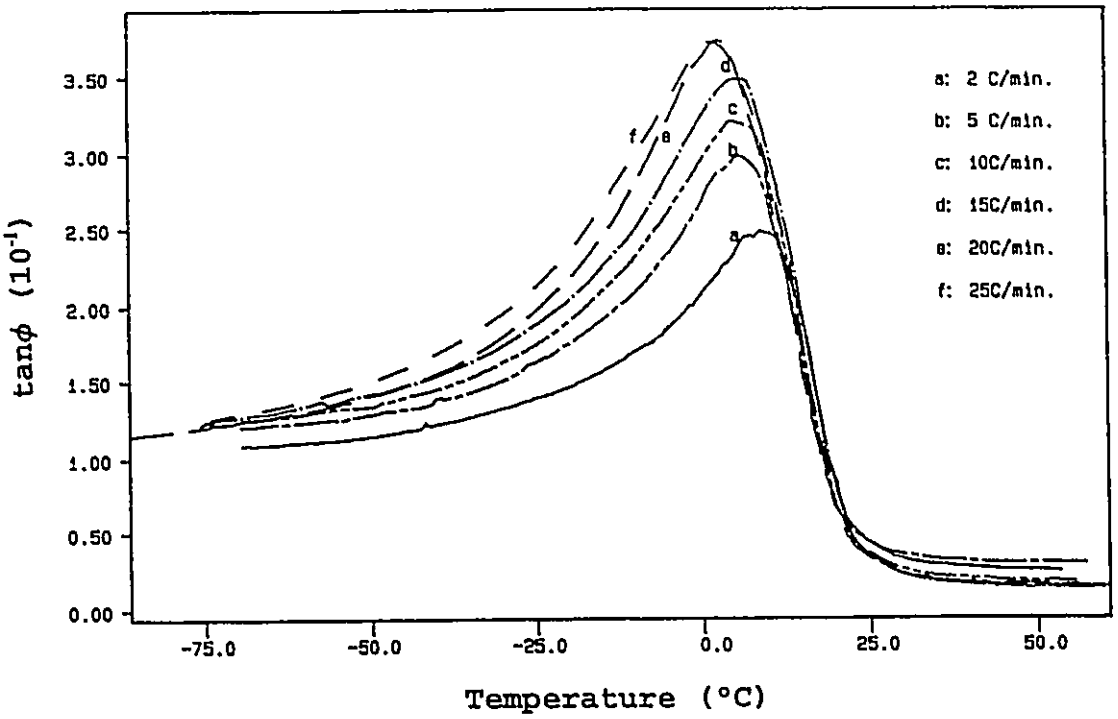

Fig.4.21: Internal friction vs. temperature (alloy A) at various cooling rates with σ_o=2MPa.

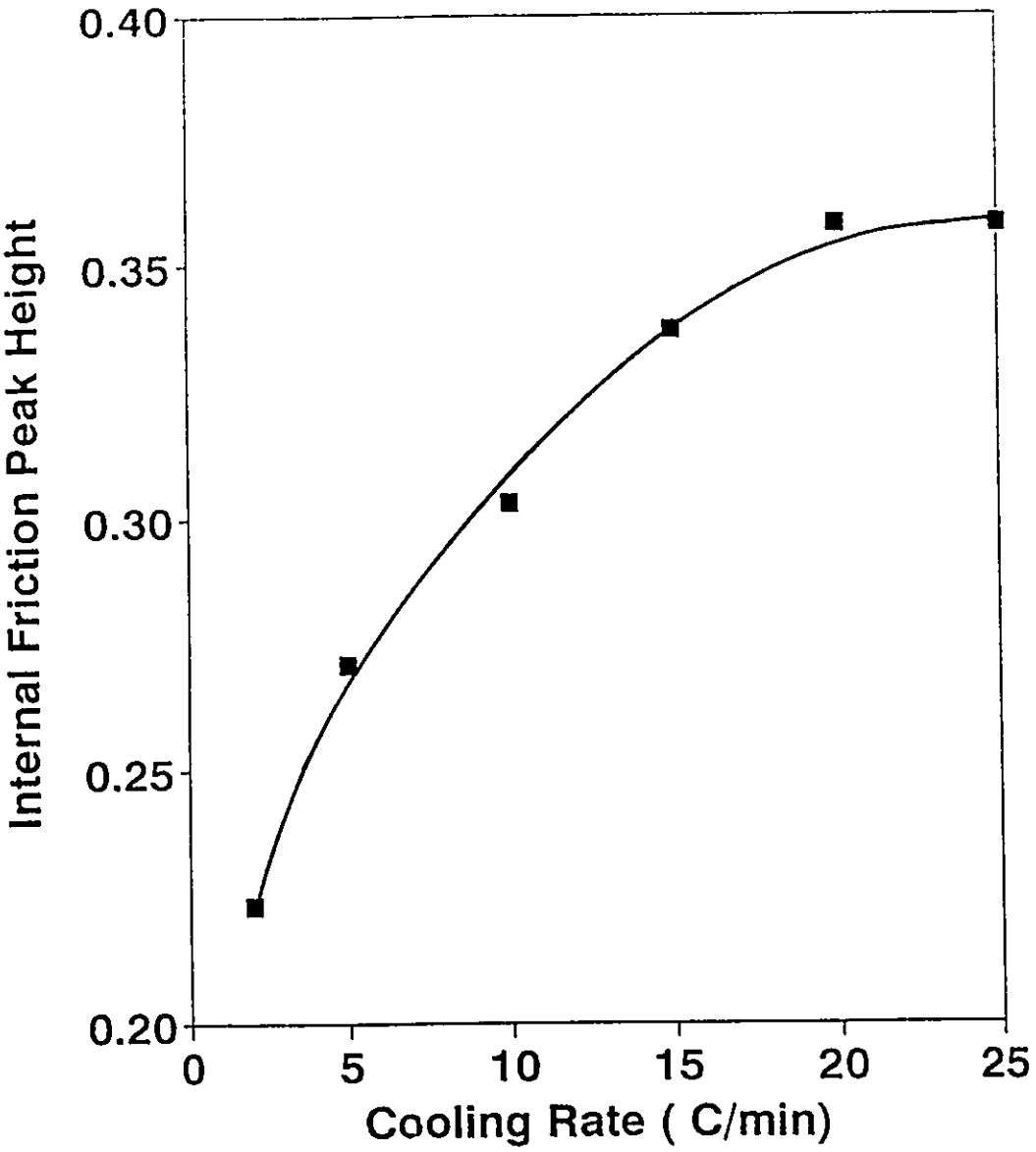

Fig.4.22: Internal friction peak height as a function of cooling rate at σ_o=2MPa.

$(\partial T/\partial t)$ and internal friction peak height $(\tan\phi)_{max}$ if the terms σ_c, σ_o, $(\partial m/\partial T)$ and $(\partial m/\partial \sigma)$ were all constant. $\partial m/\partial T$ represents the amount of parent phase that transforms to martensite per unit temperature change. By examining Fig.4.21 closely, one notes that the temperature spread between the onset and the maximum of the internal friction peak, which is proportional to transformation interval, increases with increasing cooling rate. Obviously, as the transformation interval (ΔT) increases, the amount of material that transforms per unit temperature $(\partial m/\partial T)$ decreases. Therefore, instead of a straight line, Fig.4.22 shows a curve exhibiting decreasing slope $(\partial m/\partial T)$ with increasing cooling rate.

An earlier investigation (Mercier et al., 1979) of the internal friction of martensitic transformation in Ni-Ti alloy found a linear relationship between the peak height and the cooling rate from 0.5 to 3°C/min. That might be due to the fact that the $(\partial m/\partial T)$ term is constant for the small range of cooling rate investigated. More recently, similar cooling rate dependence as that in Fig.4.22 has also been reported for the martensitic transformation in Ni-Ti (Zhu et al., 1988) and Mn-Cu (Xie et al., 1988) alloys. However, no explanation has been given for the observed decreasing slope with increasing cooling rate for these plots. It seems that the deviation from a straight line of the internal friction against cooling rate

plot, as found in Fig.4.22, is rather general, and may arise from the existence of a cooling rate dependence of the temperature spread of the martensitic transformation.

4.2.1.4 Effects of Frequency

Figs.4.23 & 4.24 show the effect of frequency on the internal friction of alloy A measured at σ_o=12MPa during cooling and heating at 10°C/min. It is observed that while the peak height due to both forward and reverse martensitic transformation decreases with increasing frequency, the background internal friction in both martensite and parent phase region increases steadily with frequency.

The peak height in Fig.4.23 is plotted against the reciprocal of the oscillation frequency in Fig.4.25. The curve in Fig.4.25, exhibiting a decreasing slope with the increase of 1/f, is in agreement with the results of Xie et al.(1988), but contradicts those of Belko et al.(1969) who suggested a linear relation between the peak height and 1/f. From equation (2.4), it is clear that under constant stress amplitude (σ_o) and cooling rate ($\partial T/\partial t$), a linear relation between $\tan\phi$ and f^{-1} exists only if $\partial m/\partial T$, $\partial m/\partial \sigma$ and σ_c are all independent of frequency. While no obvious frequency dependence of transformation interval (ΔT) is observed in Figs.4.23 and 4.24, the $\partial m/\partial T$ term may be assumed independent

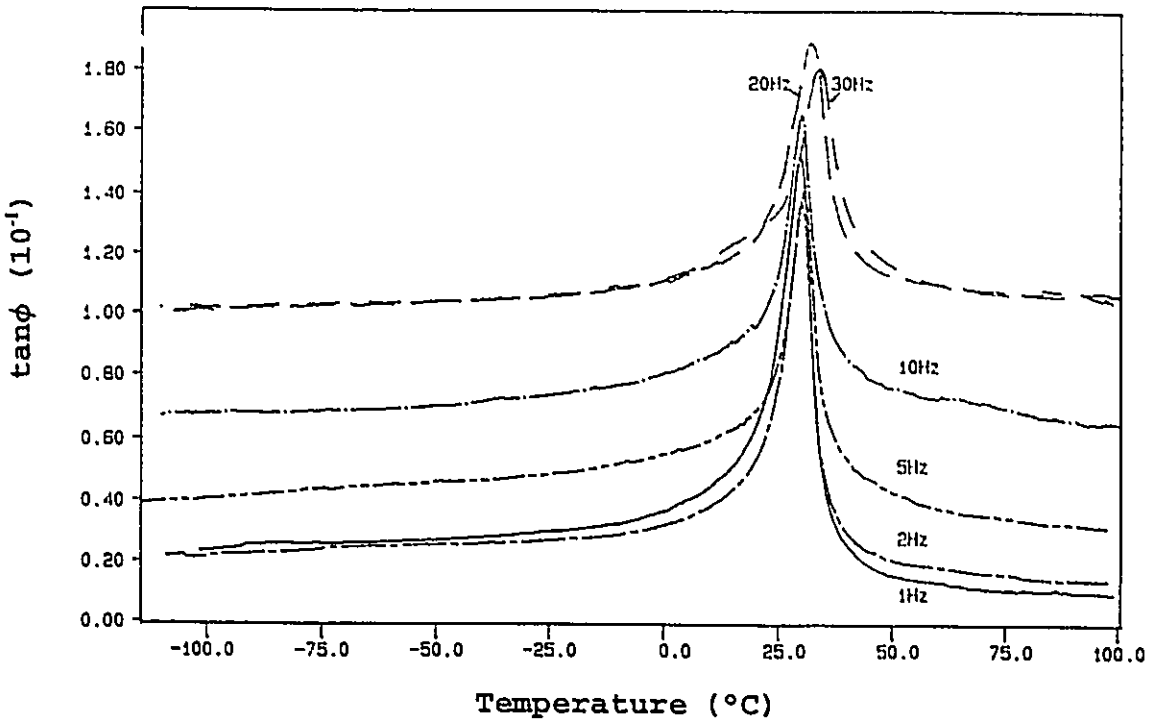

Fig.4.23: Internal friction of alloy A measured during cooling at 10°C/min with σ_o=12MPa at various frequencies.

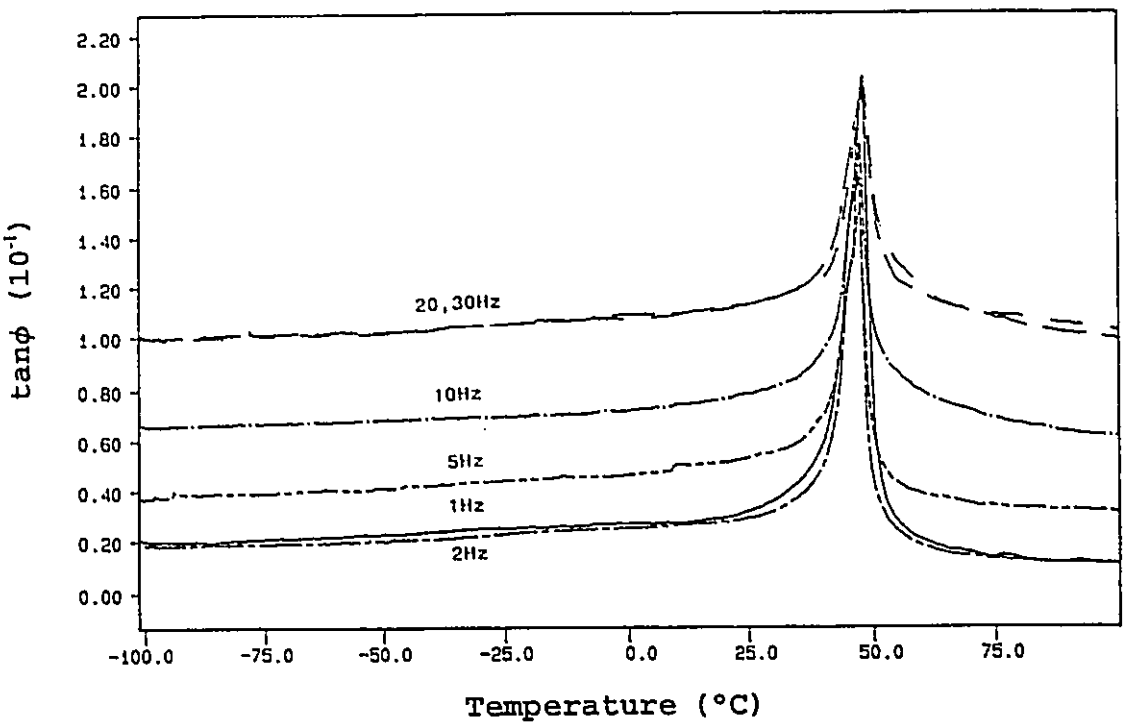

Fig.4.24: Internal friction of alloy A measured during heating at 10°C/min with σ_o=12MPa at various frequencies.

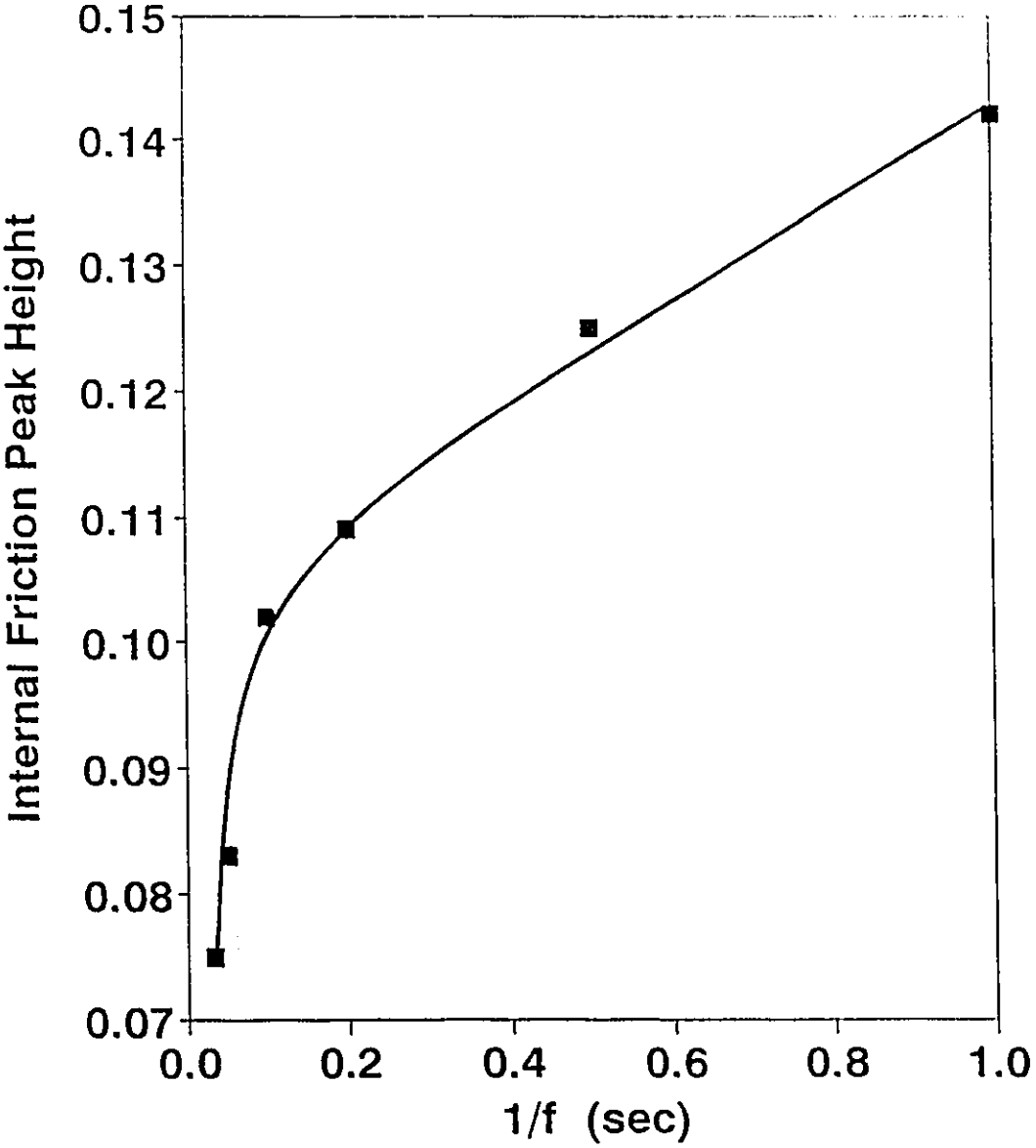

Fig.4.25: Internal friction peak height vs. reciprocal of oscillation frequency.

of frequency. However, both $\partial m/\partial \sigma$ and σ_c are related to the mobility of the martensite/parent interfaces and are likely affected by the oscillation frequency, especially when the frequency becomes high. From Fig.4.25, it is noted that a relatively good linear relation exists between the internal friction peak height and 1/f when the frequency is relatively low (1-10Hz). At higher frequency, however, there is a drastic downward deviation of internal friction from the linear plot, suggesting that at higher frequencies the mobility of martensite/parent interfaces are greatly reduced due to a decrease in $\partial m/\partial \sigma$ or increase in σ_c.

4.2.2 Training and Deterioration of Two Way Shape Memory Effect (TWSME)

4.2.2.1 Training of Optimum TWSME

The two way shape memory effect (TWSME) corresponds to a reversible change between two shapes by heating or cooling without any stress application. This behaviour is obtained after certain thermomechanical treatments called training. It is now widely accepted that TWSME arises from the oriented dislocations generated during the training process (Rodriguez and Guenin, 1990 & Contardo and Guenin, 1990) so that on subsequent cooling with no stress, only certain particular variants of martensite nucleate and grow in response to the

internal stress field created by these dislocations. In this study, two typical training procedures have been investigated to see how these dislocations can be generated more efficiently so that a large and stable TWSME can be developed.

(1).Training with A Single Thermomechanical Cycle:

Fig.4.26 shows the deformation loop for the training cycle (with a static stress of 8.4MPa and dynamic stress of 7.0MPa) and the corresponding TWSME cycle, at a cooling and heating rate of 25°C/minute. It can be seen that the "training efficiency", defined as the ratio of the TWSME loop height to the training loop height, is only as low as 4.8%. Moreover, the TWSME loop deteriorates rapidly with the increase of TWSME cycles, as shown in Fig.4.27. It is interesting to note that a minimum in probe position occurs during heating, and it becomes more significant with increase in the number of cycling. It is believed that after the training with only a single thermomechanical cycle, not enough oriented dislocations are created so that only a fraction of the martensite variants formed in TWSME cycle are preferentially oriented with respect to the applied stress. The rest of the variants may be oriented in the opposite way (due to "residual training") so as to give a shape change in the opposite direction when reverted on heating. The small maximum on the cooling curve can be explained in the same way. Experiments on

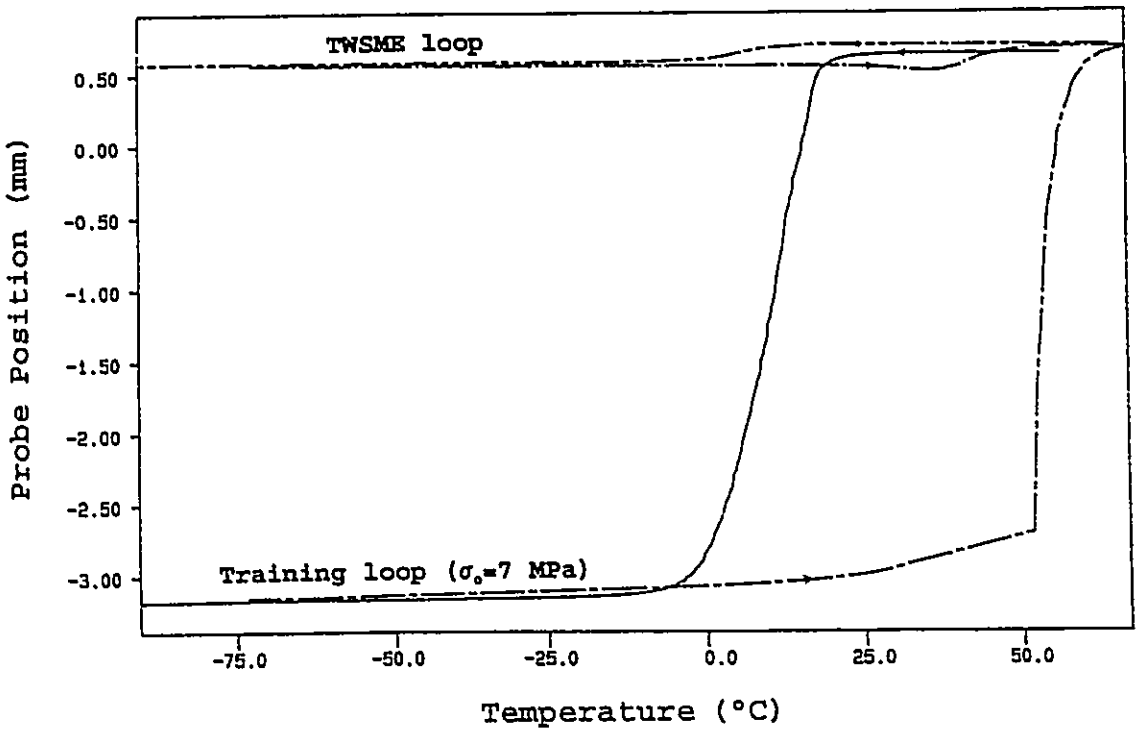

Fig.4.26: Training loop (σ_o=7MPa) and the corresponding TWSME loop of alloy A at a cooling and heating rate of 25°C/min.

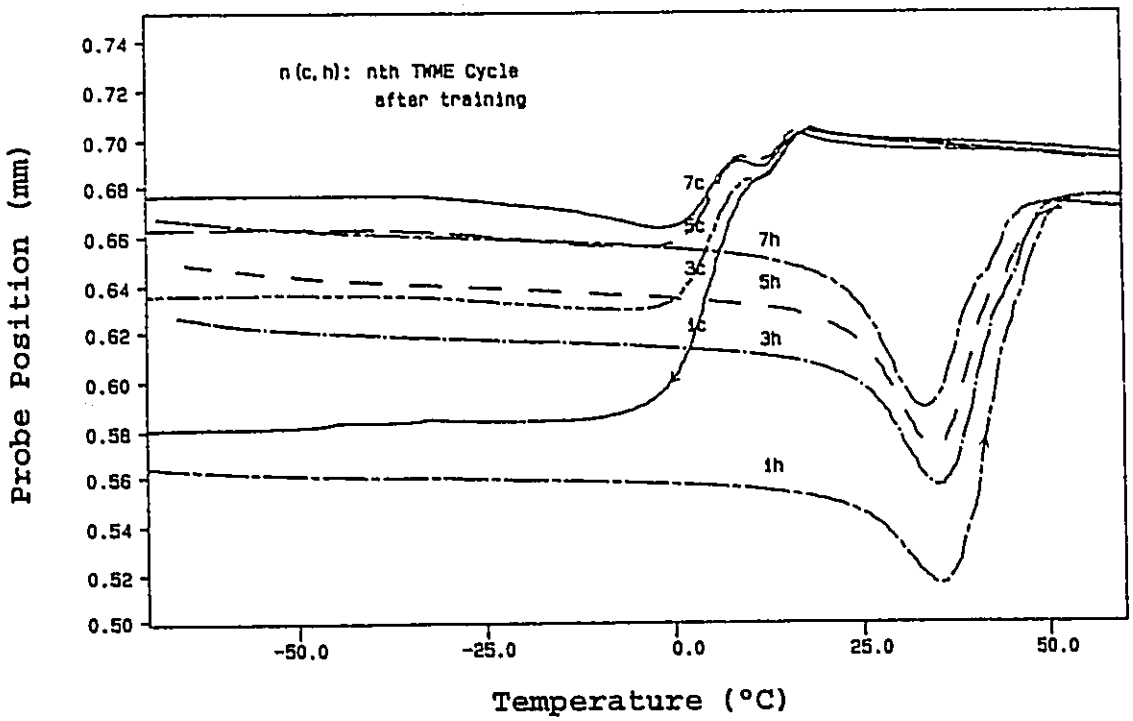

Fig.4.27: Deterioration of TWSME loop developed in Fig.4.26 with the number of thermal cycles. The letters "c" and "h" stand for cooling and heating, respectively.

samples which were not previously trained indicated that certain "residual training" did exist in some samples so that a small shape change (bending) would occur during the transformation, even without prior training. This "residual training" persisted even after 20 minute homogenization treatment at 850°C. Training and TWSME cycles at a lower cooling and heating rate, 5°C/minute, are shown in Fig.4.28, which give a similarly low training efficiency of 5.3%. With the increase of the number of TWSME cycles, the TWSME loop also deteriorates rapidly, as shown in Fig.4.29.

(2).Training with Multiple Thermomechanical Cycles:

The need to overcome the "residual training" and train all martensite variants in alignment with the applied stress suggested that multiple training cycles might be necessary. Fig.4.30 shows the probe position (cooling and heating) and internal friction (cooling only) change during seven consecutive training cycles with a static stress of 3.6MPa and a dynamic stress of 3.0MPa at a cooling and heating rate of 25°C/minute. It is seen that the loop height and the internal friction in the martensite region increase with the number of cycles and reaches saturation at the 7th training cycle, where training is stopped. The fact that the internal friction in the martensite region rises and becomes increasingly jerky suggests that the martensite/martensite interface becomes more

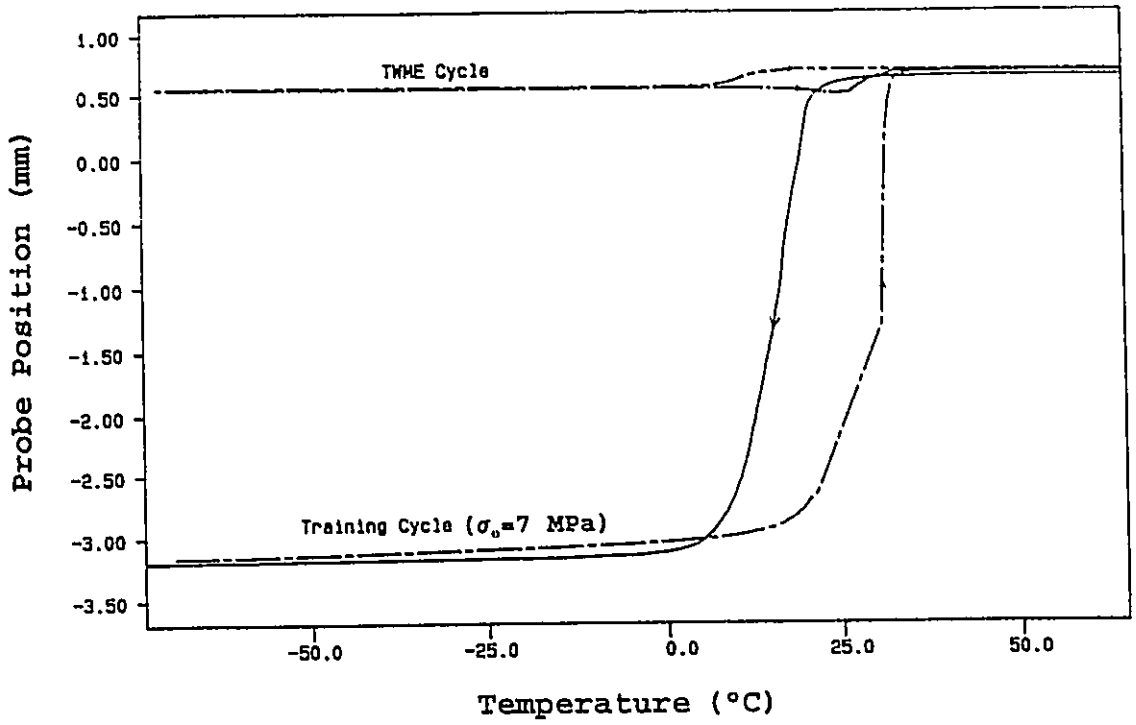

Fig.4.28: Training loop (σ_o=7MPa) and the corresponding TWSME loop of alloy A at a cooling and heating rate of 5°C/min.

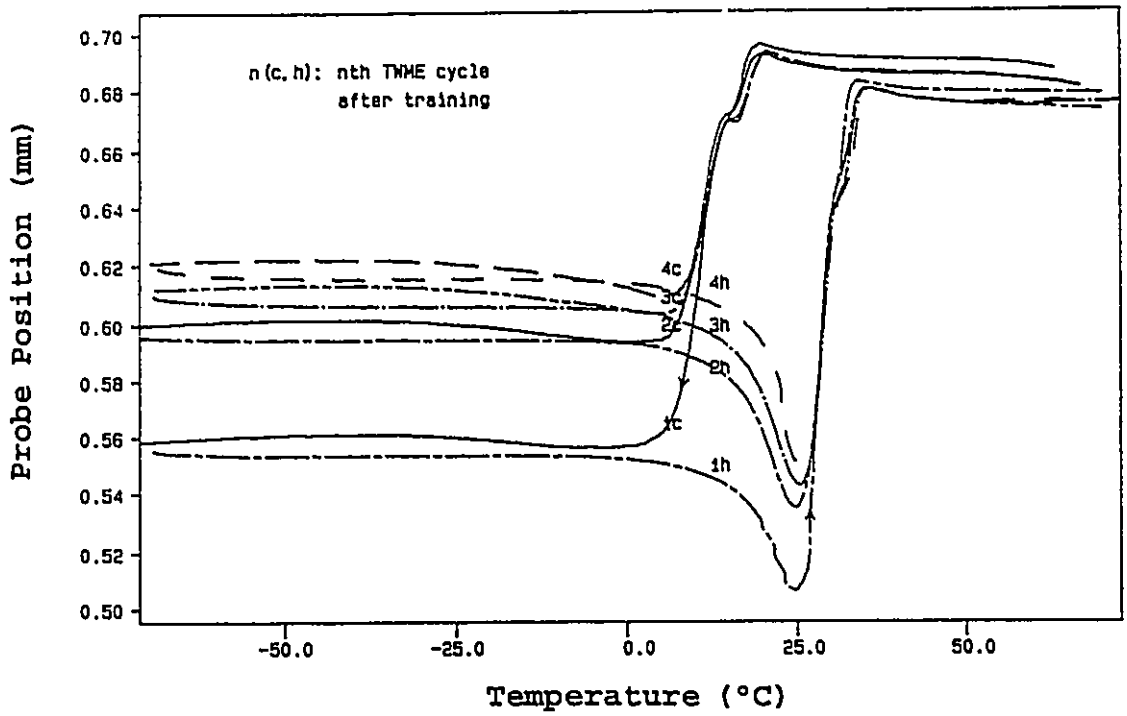

Fig.4.29: Deterioration of TWSME loop developed in Fig.4.28 with the number of thermal cycles.

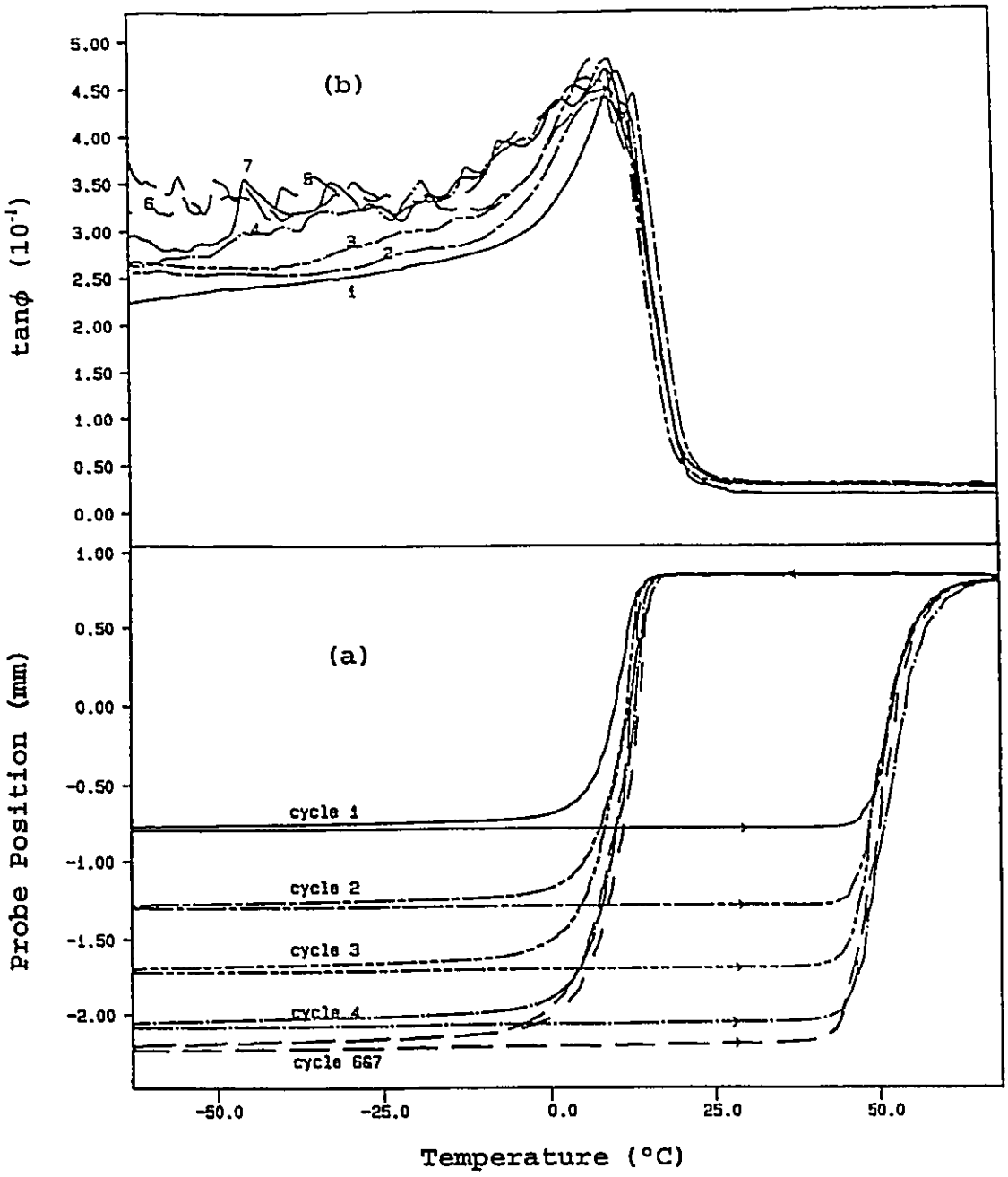

Fig.4.30: Multiple training loops (σ_o=3MPa) and associated internal friction change of alloy A at a cooling and heating rate of 25°C/min. (a) Training loops, (b) Internal friction during cooling.

oriented and mobile with each training cycle. Fig.4.31 shows the subsequent TWSME cycle in comparison with the last training cycle, which gives a much larger training efficiency of 20.7%, about four times that of the first training procedure. Fig.4.32 shows the evolution of TWSME loop with the number of cycles. In the initial five cycles, the TWSME loop height decreases slightly, which could be due to annihilation of the less stable dislocations created by training (Rodriguez and Guenin, 1990). After the 5th TWSME cycle, however, the loop height steadily increases, and finally stabilizes after 30 cycles. This can be explained by the creation of more dislocations during TWSME cycling as a result of so called "self-training" (Rodriguez and Guenin, 1990). The TWSME loop height becomes stabilized when the annihilation and creation of dislocations reaches an equilibrium.

By comparing the two training procedures in (1) and (2), it is concluded that multiple thermomechanical cycling is necessary in order to develop a large and stable TWSME. Single thermomechanical cycling, even at higher stress amplitude, can not achieve the same level of training efficiency, nor can it produce a stable TWSME. It appears that a stable TWSME can only be achieved when the previous training has introduced a high enough density of oriented dislocations (through repeated thermomechanical cycling) so that the subsequent TWSME can be self-sustained by a self-training process which balances the

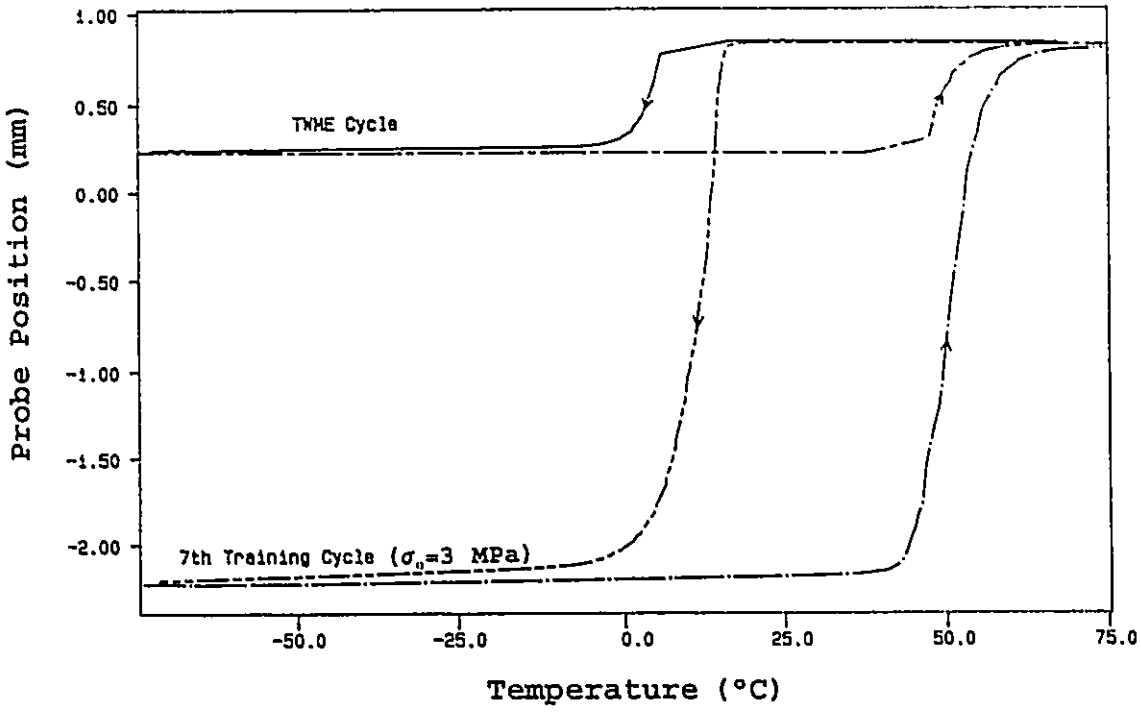

Fig.4.31: Last training cycle in Fig.4.30 in comparison with the subsequent TWSME cycle.

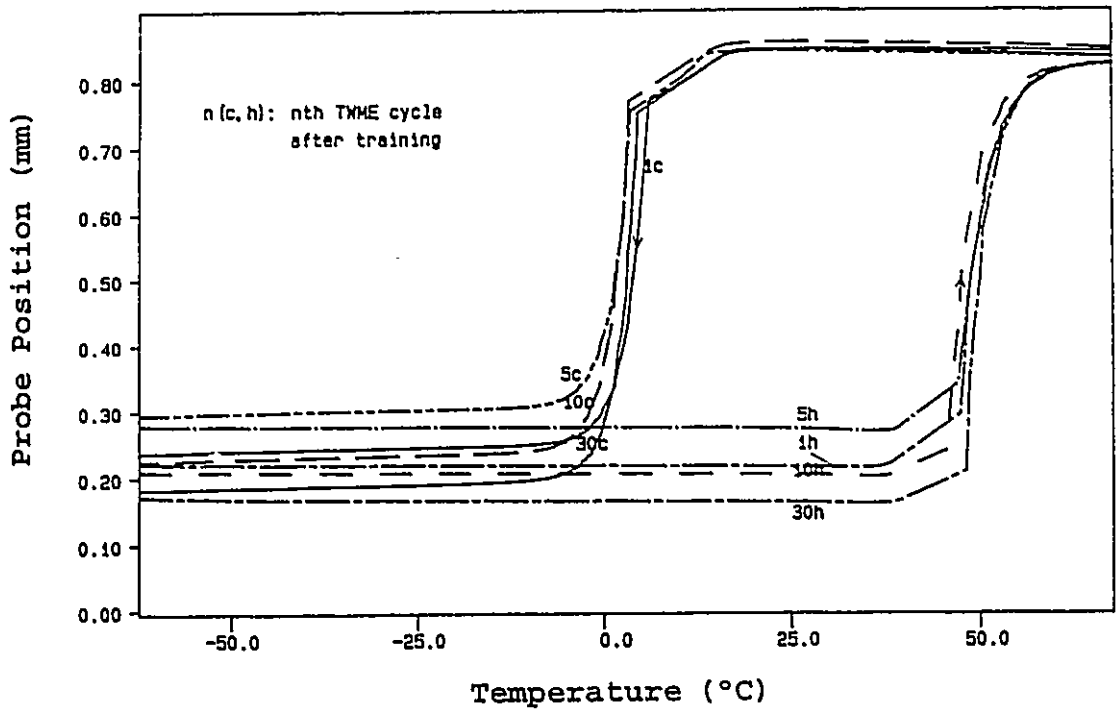

Fig.4.32: Evolution of TWSME loop developed in Fig.4.31 (alloy A) with the number of thermal cycles.

annihilation of dislocations.

4.2.2.2 Dependence of TWSME on the Heating and Cooling Rate

Fig.4.33 shows the effect of heating and cooling rate on the TWSME loop (with no stress) after a stable TWSME loop has been developed by procedure (2) above. The strong dependence of shape change temperatures on the heating and cooling rate, however, is primarily an instrumental effect, and is not due to the time dependence of the transformation, as will be substantiated in Sections 4.3.2, 4.3.3 and 4.4.2 that will follow. The halfway transformation hysteresis of the TWSME loop as a function of heating and cooling rate is plotted in Fig.4.34, and an extrapolated hysteresis of about 3°C is obtained at zero heating and cooling rate. This value reflects the true hysteresis of the transformation and is very close to that determined by DSC (Section 4.3.2) and metallography (Section 4.4.2).

4.2.2.3 Deterioration of TWSME at Higher Temperatures

If the sample is heated to higher temperature after a stable TWSME has been developed, deterioration begins to occur. When the upper temperature limit for thermal cycling is increased from 100°C to 150°C, the TWSME loop shifts approximately 8°C to lower temperature, as observed in Fig.4.35. When the upper temperature increases further to

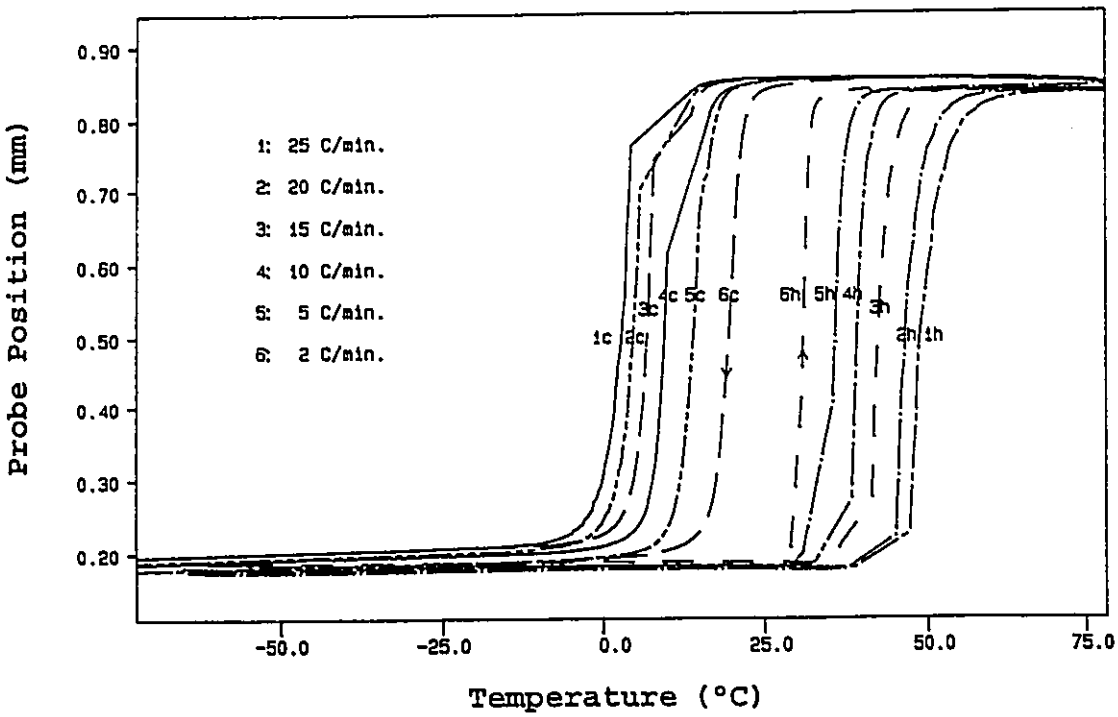

Fig.4.33: Effect of cooling and heating rate on the TWSME loop in alloy A. "c" and "h" stand for cooling and heating respectively.

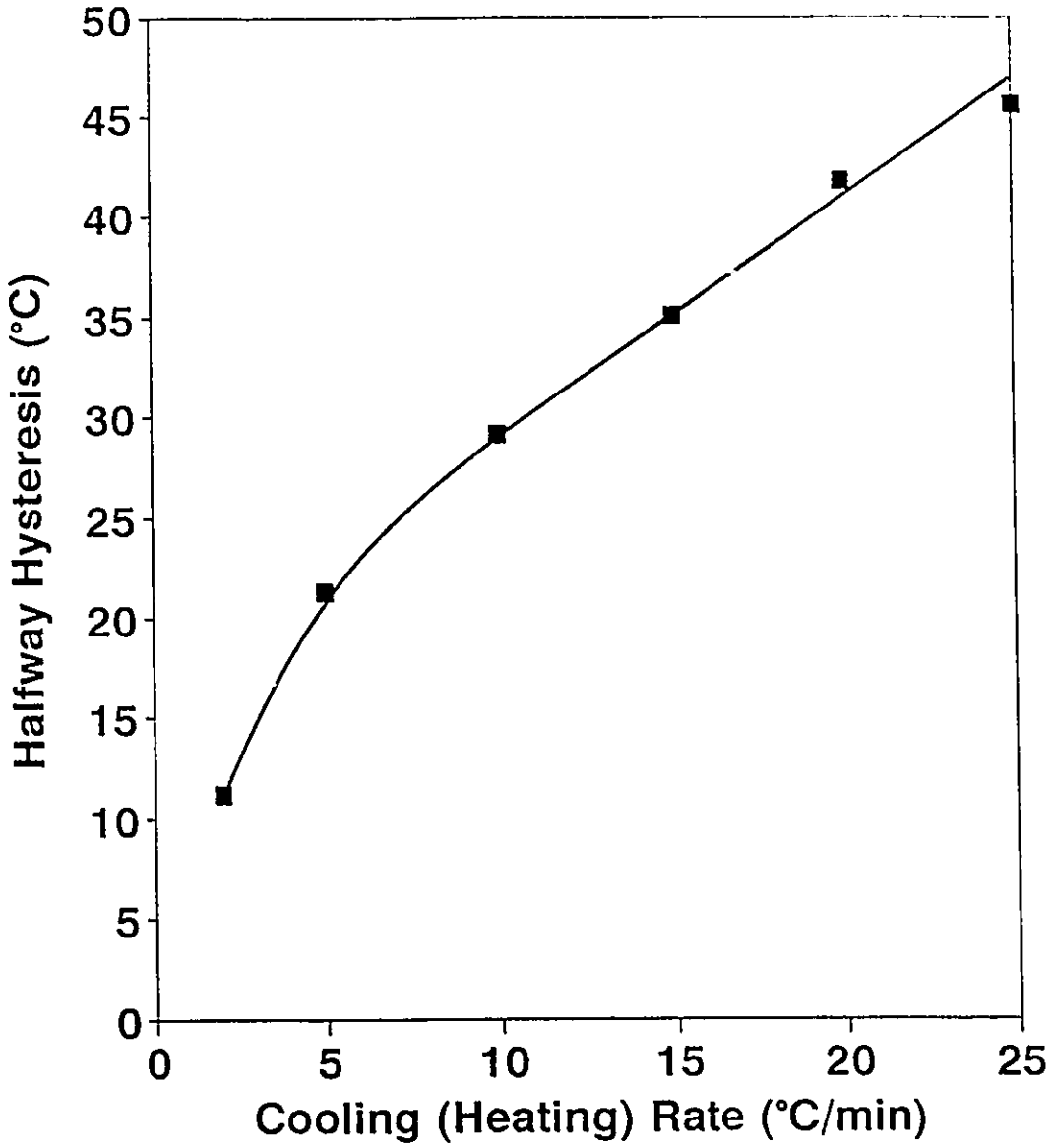

Fig.4.34: TWSME halfway hysteresis as a function of heating and cooling rate.

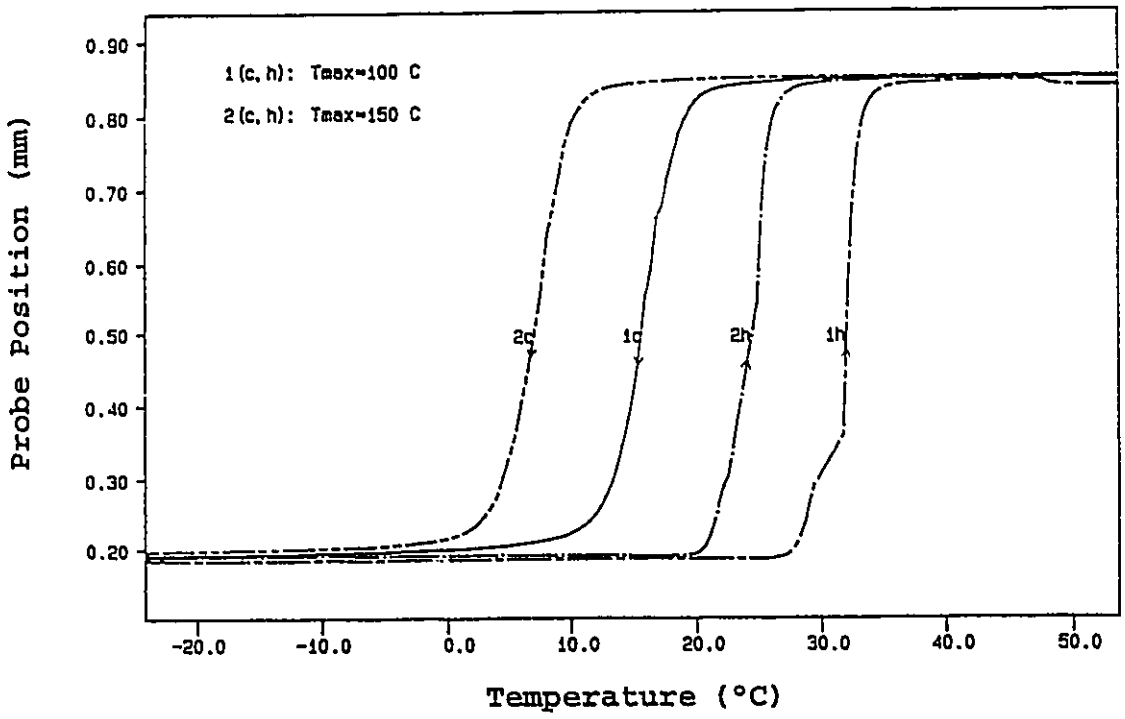

Fig.4.35: Shift of TWSME loop when the upper limit of thermal cycling is raised from 100°C to 150°C.

180°C, 210°C and 240°C, the changes in TWSME loop are shown in Fig.4.36. The initial shift of TWSME loop to lower temperature (Fig.4.35) may be due to a change in the degree of order in β phase, while the decrease of the TWSME loop height (Fig.4.36) is attributed to annihilation of oriented dislocations as well as the precipitation of α phase at higher temperatures.

4.2.3 Study of the Time Dependence of Internal Friction

Studies of the internal friction of martensitic Cu-Zn-Al shape memory alloys since 1981 have shown that they undergo a thermally activated relaxation at low temperatures where martensite phase is stable (Morin et al., 1981, 1985, 1987, Humbeeck and Delaey, 1982, Humbeeck et al., 1984, 1985 and Mantel et al., 1986b). This relaxation process is associated with the migration of vacancies and the pinning of the interfaces. An interesting feature resulting from this process is the time dependence of the internal friction of the alloy sample when it is sinusoidally subjected to a torsional stress at temperatures considerably below the martensitic transformation temperature. At temperatures as low as 100°C below the transformation, Cu-Zn-Al alloys show an internal friction peak when the internal friction is plotted against the number of mechanical oscillations or the total period over which it has been oscillated (Morin et al., 1981, 1985, 1987 and Morin, 1985).

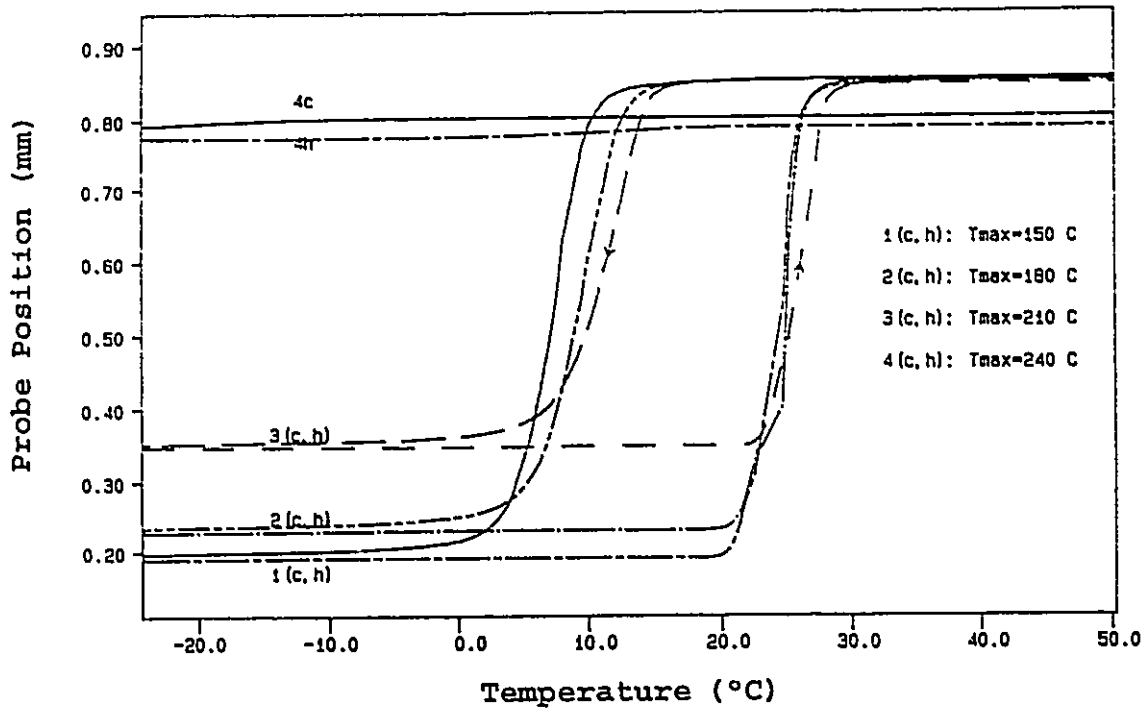

Fig.4.36: Deterioration of the TWSME loop when the upper limit of thermal cycling is progressively raised.

Here a more systematic study of the time dependence of internal friction, modulus and shape change of Cu-Zn-Al alloys A and B has been carried out in their single martensite phase, single parent phase and two-phase microstructural states.

The time dependence of the internal friction, tanϕ, of martensite and parent phases is sensitive to the temperature of measurement relative to the characteristic transformation temperatures. Therefore, it is necessary to determine first these temperatures from measurements of the mechanical properties. For this purpose, measurements were made when the alloy was either being cooled or heated at a rate of 5°C/min, which, as indicated by the calibration with ice in Fig.4.37, is suitable for accurate determination of the martensitic transformation temperatures. Internal friction (tanϕ), elastic modulus (E') and probe position (d) thus obtained are plotted against the temperature in Fig.4.38. These show sharp tanϕ peaks at 43°C on heating and 27°C on cooling for the specimen of alloy A (Cu-13%Zn-9%Al). These peaks correspond to a sharp minimum in E', and a change in the probe position, d, or sample's shape, over a 3°C temperature range. There is a substantial hysteresis in the transformation temperatures indicated by tanϕ, E' and d, as much as 20°C. There is little doubt that the alloy A after quenching in 23°C water is in a two phase region. The same sample was homogenized again in the parent phase region at 850°C for 10 min and quenched to 23°C

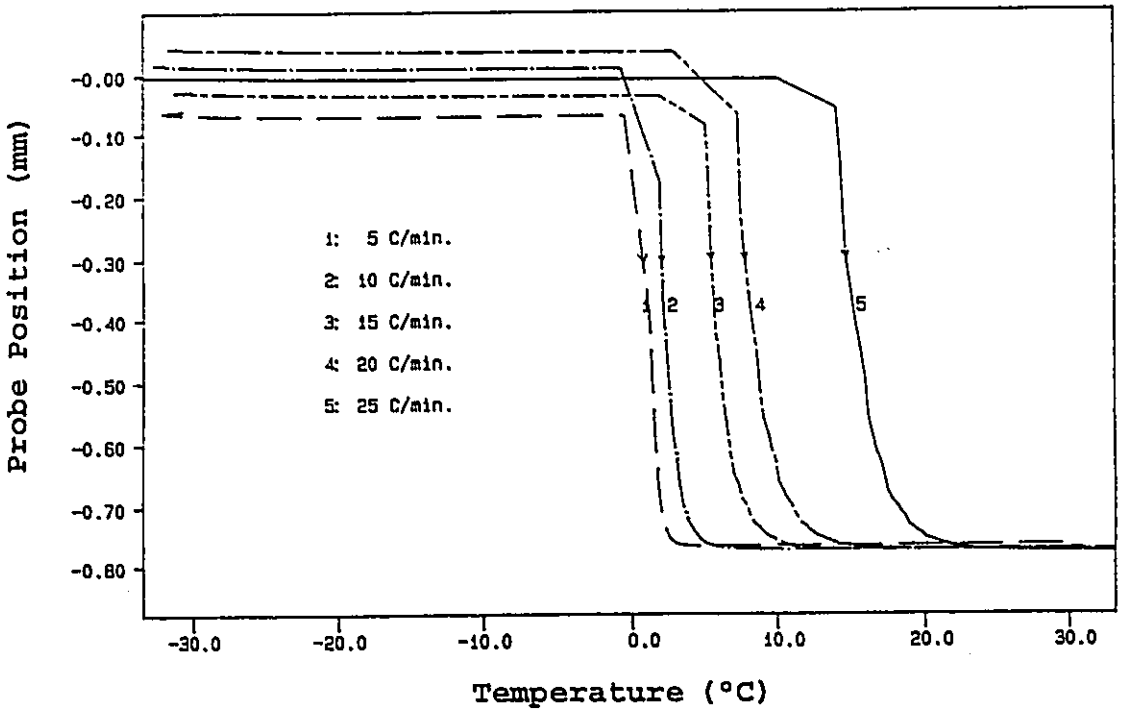

Fig.4.37: Lowering of probe position during melting of ice at various heating rates.

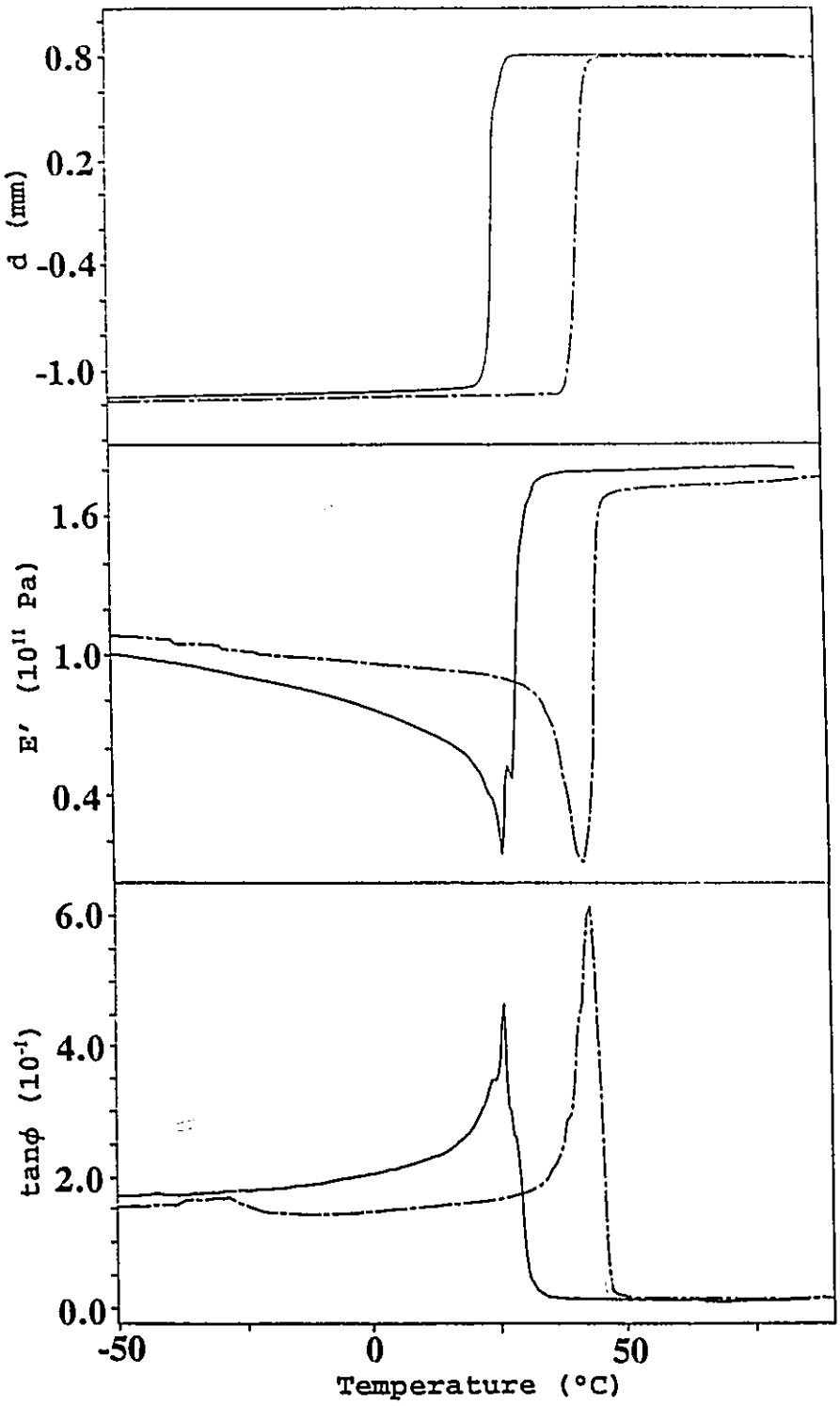

Fig.4.38: The Internal friction (tanϕ), the elastic modulus (E′) and the probe position (d) measured for a frequency of 1Hz are plotted against the temperature during the cooling and heating of a sample of Cu-Zn-Al alloy A at a rate of 5°C/min. Full lines are for cooling and dashed lines for heating.

water and thereafter measured at 23°C while being oscillated at a frequency of 1Hz in a three point bending mode, and the change of its tanϕ, E' and d are plotted against time (or equivalently the number of oscillations, i.e. 60xtime) in Fig.4.39. The simultaneous occurrence of a tanϕ peak, an E' minimum and a step decrease in d in Fig.4.39 bears close resemblance to the features of the stress-oriented martensitic transformation observed during the cooling seen in Fig.4.38. In order to substantiate this observation the time evolution of tanϕ and d was also investigated at other temperatures above and below the transformation temperatures. These are shown in Fig.4.40. Here it is evident that d decreases, or the sample's shape changes only at those temperatures at which the tanϕ peak appears, which are: 23°C, 40°C and 55°C. According to Fig.4.38, the alloy at these temperatures either consists of both martensite and parent phase as at 23°C and 40°C, or has just transformed to the parent phase as at 55°C. At the extreme temperatures of 80°C and -85°C, where the parent phase and martensite, respectively, are stable, both tanϕ and d remain virtually constant with the time. Although more slowly, changes do occur in the martensite phase even at -40°C and -5°C, as the decrease of tanϕ with time in Fig.4.40 shows. But this change in tanϕ is not accompanied by a simultaneous change in d, which is in contrast with the observations at 23°C, 40°C and 55°C. It appears that the internal friction

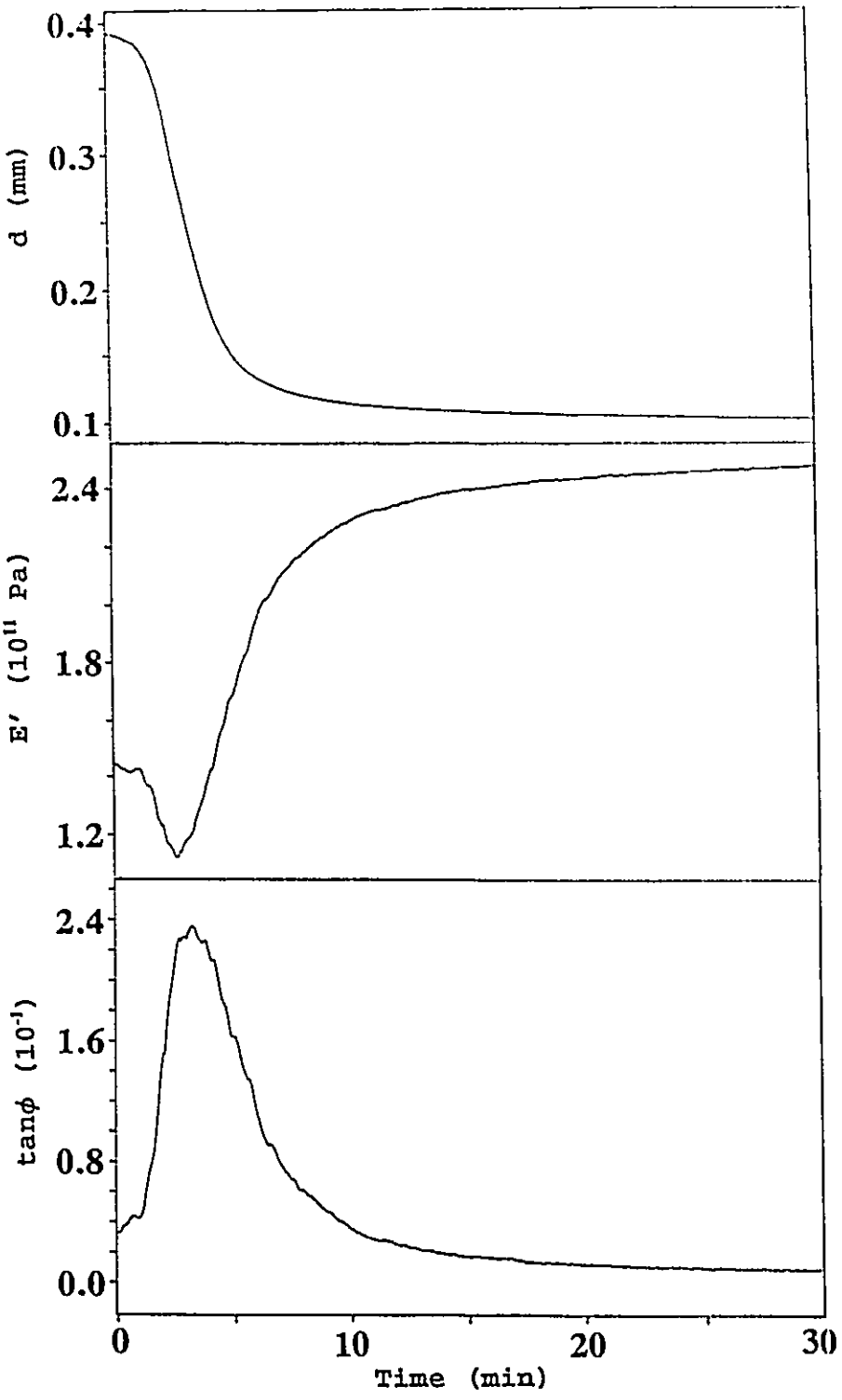

Fig.4.39: The internal friction (tanϕ), the modulus (E′) and the probe position (d), of Cu-Zn-Al alloy A are plotted against time at 23°C as the sample was oscillated at 1Hz frequency.

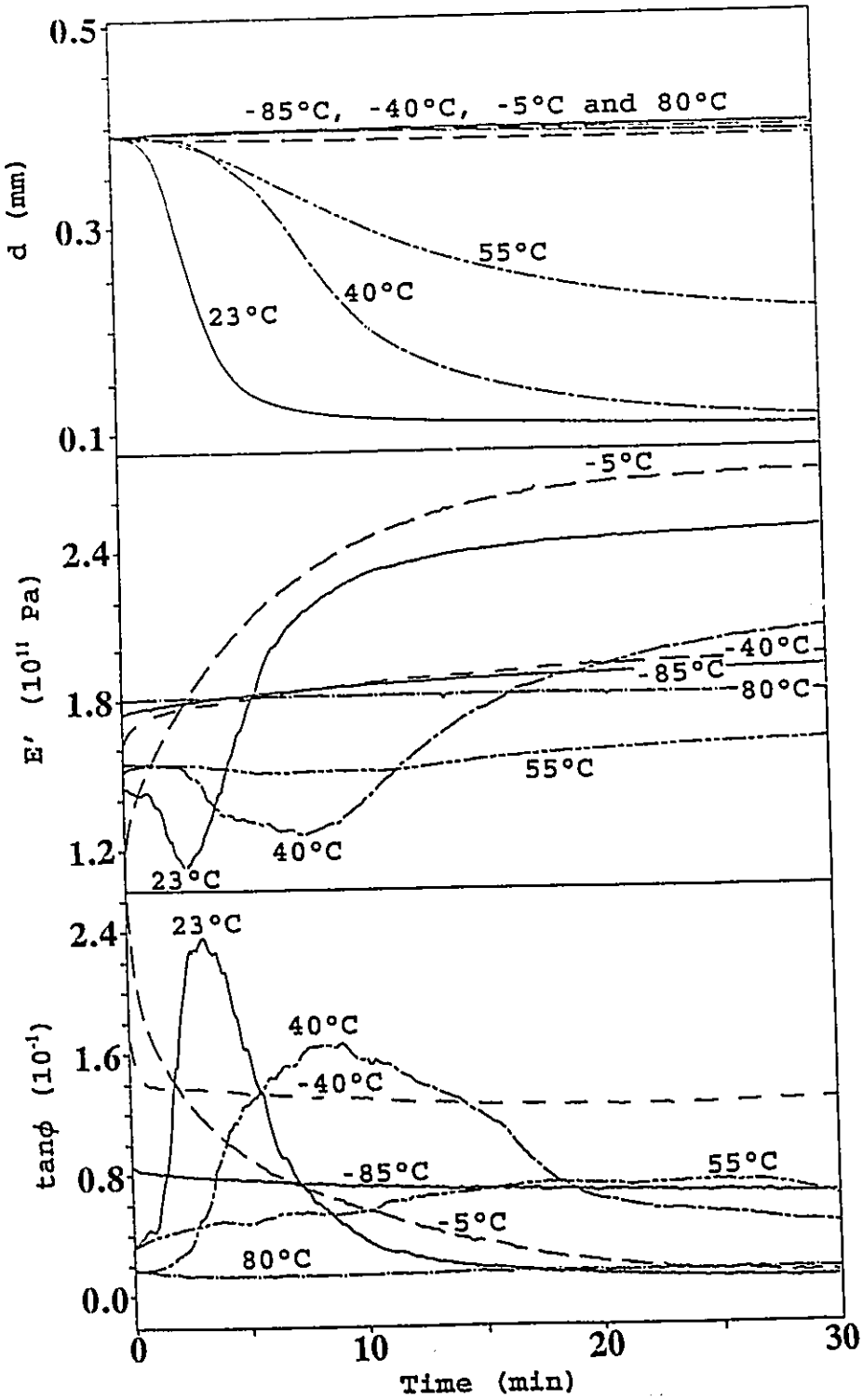

Fig.4.40: The internal friction (tanϕ), the modulus (E′) and the probe position (d), of Cu-Zn-Al alloy A are plotted against the time of oscillation at 1Hz frequency. Samples were isothermally kept at different temperatures as indicated.

peaks observed at 23°C, 40°C and 55°C are caused by the stress-induced martensitic transformation, as these peaks are accompanied by a minimum in E' and a decrease in d as observed in Figs.4.39 and 4.40.

In order to ascertain our explanation for the time-dependence of tanϕ, E' and d, the sample which had been oscillated for 30 minutes at 55°C was then cooled at a rate of 5°C/minute to -50°C, and measurements made at different temperatures. Its tanϕ, E' and d are plotted against the temperature in Fig.4.41. On cooling from 55°C, the remaining parent phase is transformed into martensite, causing further decrease in d, a tanϕ peak and a corresponding minimum in E'. The sample was then heated from -50°C to 100°C and the measured properties are also plotted in Fig.4.41. On heating, both d and tanϕ seem to undergo a two-stage change during transformation to the parent phase. In the first stage, d rises steadily, accompanied by the appearance of an internal friction peak, to the same value as that at the start of cooling from 55°C. Therefore, the first stage indicates the reversal of the partial transformation from parent to martensite phase that had occurred during cooling. In the second stage, d continues to increase after going through a plateau value and ultimately approaches the value as that before the sample was oscillated at 55°C. This is also accompanied by an internal friction peak, as seen in Fig.4.41.

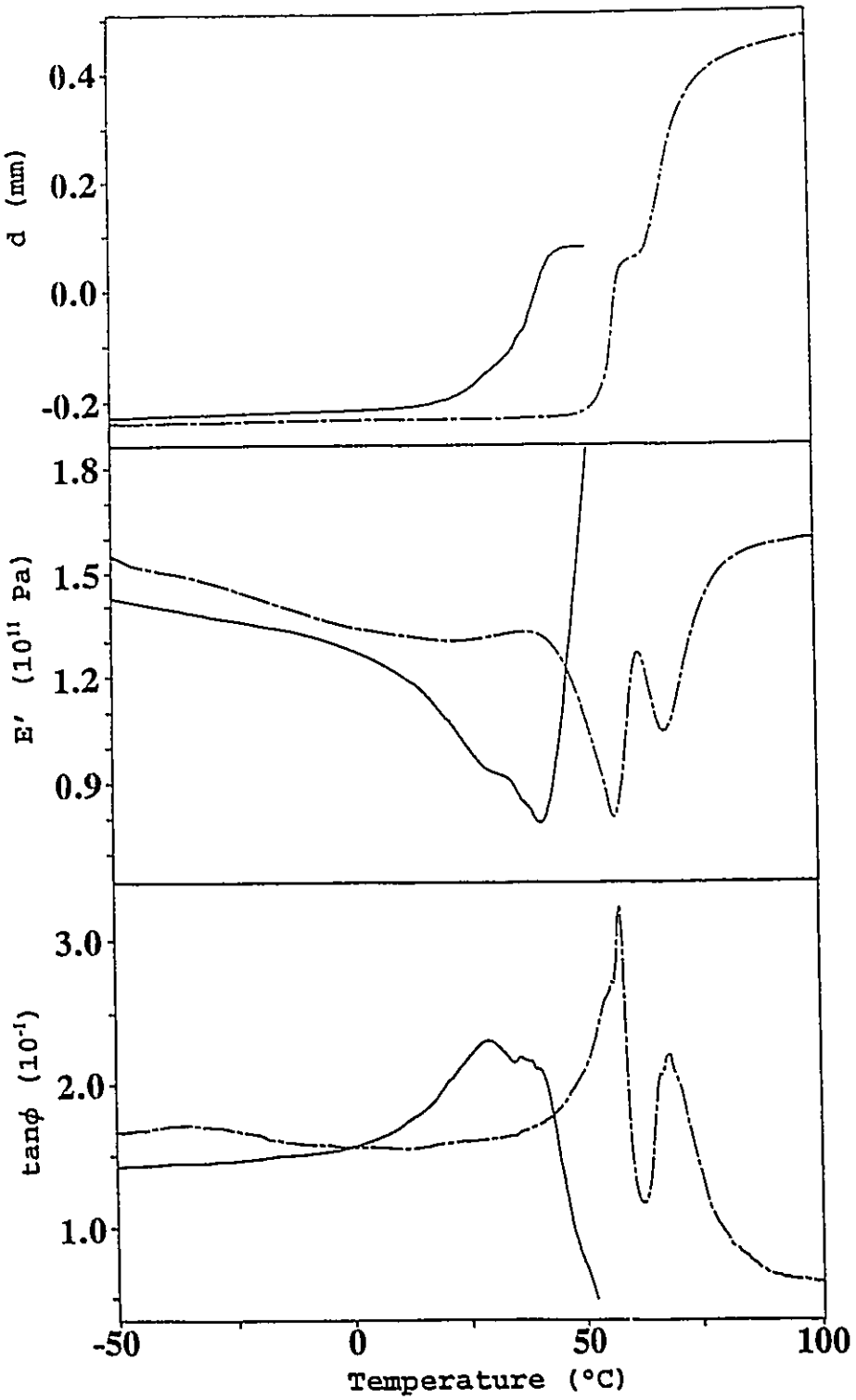

Fig.4.41: The internal friction (tanφ), the modulus (E') and the probe position (d), of Cu-Zn-Al alloy A plotted as a function of temperature during cooling (full lines) to -50°C immediately after oscillation at 1Hz frequency for 30 min at 55°C. The dashed lines are for the data measured on subsequent heating from -50°C to 100°C.

Evidently, this second stage indicates the reversal of the process of phase transformation from parent to martensite phase, which had occurred during the 30 min oscillation of the sample at 55°C. The reversibility of the latter transformation, i.e., that the transformation which was originally induced by the stress during the oscillations under isothermal conditions is recovered by raising the sample's temperature, suggests that the change in internal friction and probe position during the sample's oscillation at 55°C is a reflection of the stress-induced martensitic transformation.

In order to confirm the above-described observations on Cu-Zn-Al shape memory alloy, it was necessary to do a parallel study of another composition of a similar alloy. For this purpose, a Cu-23%Zn-5%Al alloy, labelled B here, was chosen. Its martensitic transformation temperature is about 16°C higher than that of alloy A, as its values of tanϕ, E' and d measured during the cooling and heating part of the cycle plotted against the temperature in Fig.4.42 show. Here also the tanϕ peak measured during the heating is sharper and higher than that measured during the cooling cycle, but except for the transformation temperatures and the magnitude of the change observed, the plots are similar to those for alloy A shown in Fig.4.38.

The tanϕ, E' and d of a sample of alloy B kept at 56°C were then measured as a function of time, as it was

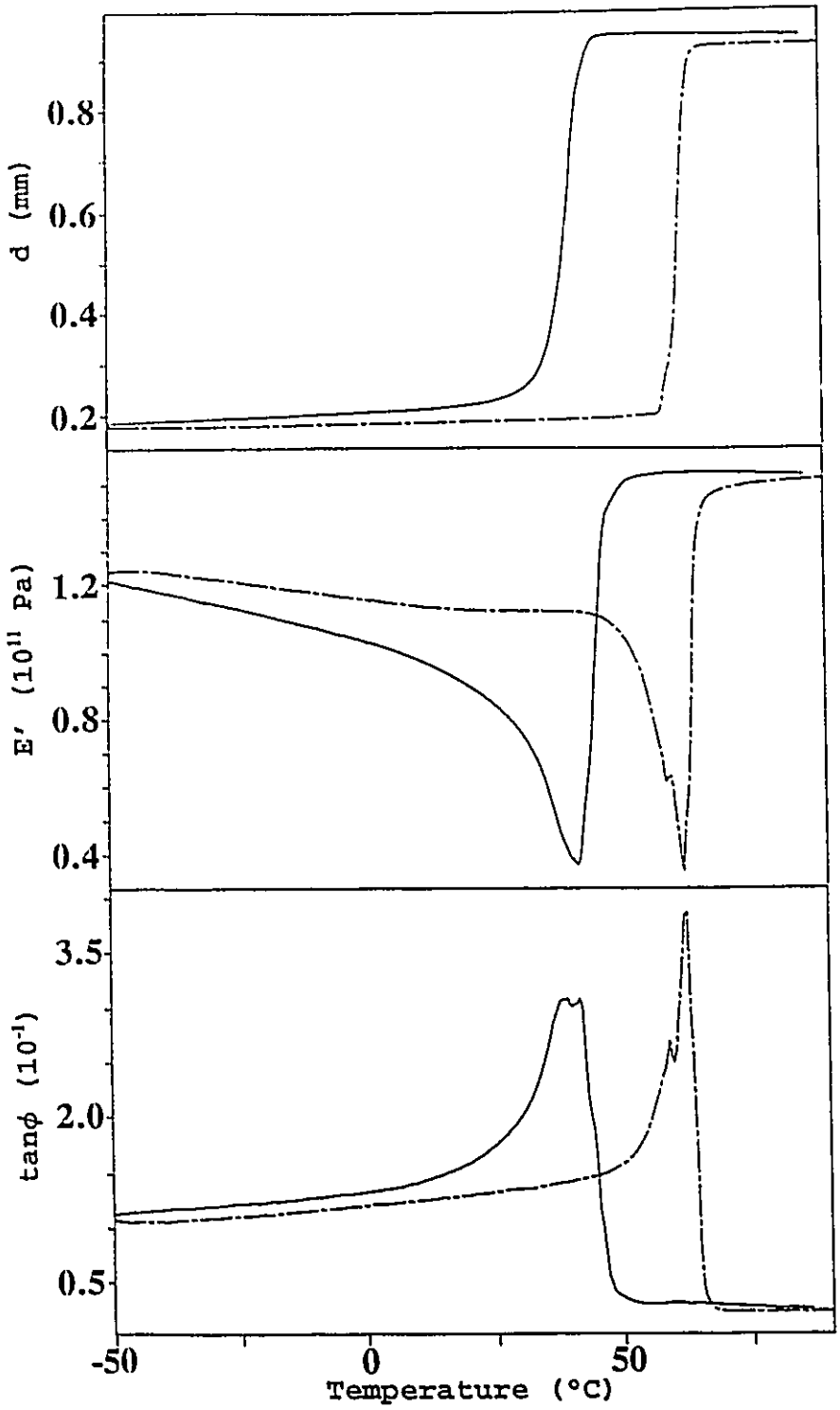

Fig.4.42: The Internal friction (tanϕ), the elastic modulus (E') and the probe position (d) measured for a frequency of 1Hz are plotted against the temperature during the cooling and heating of a sample of Cu-Zn-Al alloy B at a rate of 5°C/min. Full lines are for cooling and dashed lines for heating.

sinusoidally oscillated at 1Hz frequency. Plots of these quantities against the time (number of oscillations=60xtime) are shown in Fig.4.43. Here also tanϕ goes through a peak, E' a minimum and d a step decrease within two min after the beginning of the oscillations. Similar measurements of the internal friction and shape change were made by oscillating the sample isothermally kept at different temperatures from -40°C to 88°C. The corresponding plots of tanϕ, E' and d are shown against time in Fig.4.44. As for the alloy A (Fig.4.40), at the extreme temperatures of -40°C and 88°C, where the martensite and parent phases are respectively stable, the plots are featureless. At other temperatures in or close to phase transition region, they show a tanϕ peak, an E' minimum and a decrease in d, which are indicative of a phase transformation.

The measurements for two alloys of different compositions thus confirm our finding that a stress-induced martensitic transformation takes place during isothermal oscillations at temperatures in or close to phase transition region and that it can be reversed by subsequently raising the sample's temperature.

The time dependence of internal friction at constant temperatures can also be explained by Dejonghe's formulation:

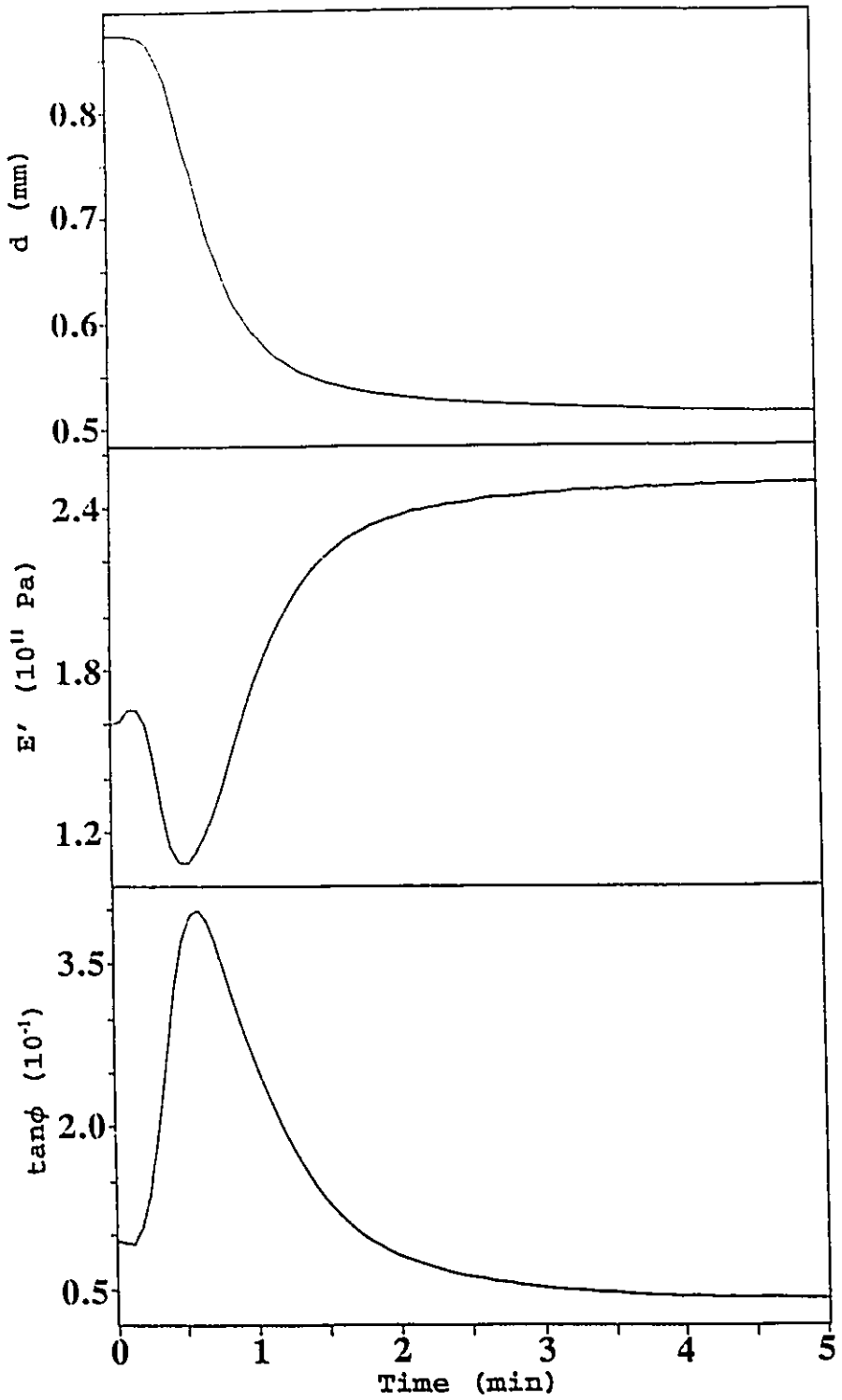

Fig.4.43: The internal friction (tanϕ), the modulus (E′) and the probe position (d), of Cu-Zn-Al alloy B are plotted against time at 56°C as the sample was oscillated at 1Hz frequency.

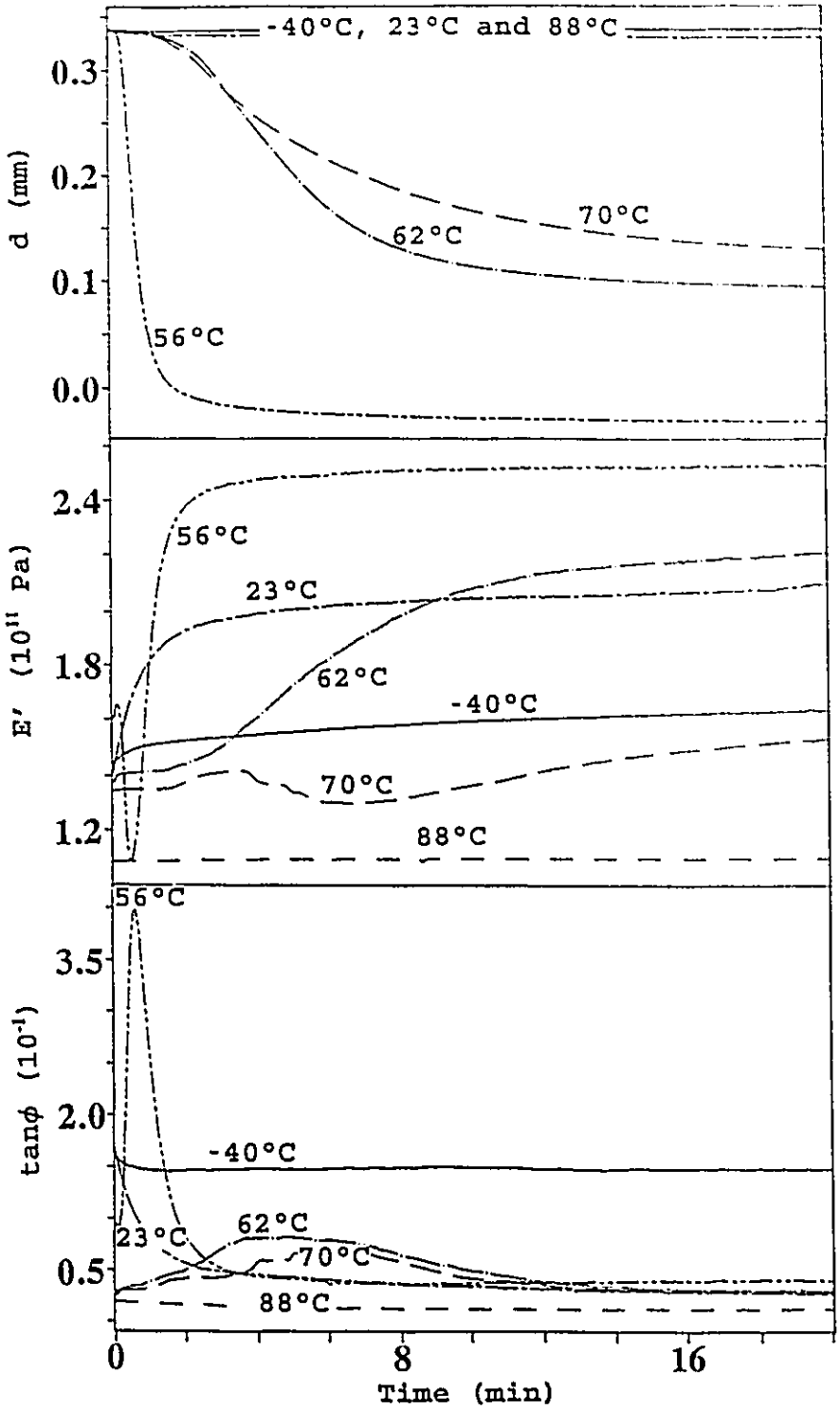

Fig.4.44: The internal friction (tanϕ), the modulus (E') and the probe position (d), of Cu-Zn-Al alloy B are plotted against the time of oscillation at 1Hz frequency. Samples were isothermally kept at different temperatures as indicated.

$$\tan\phi = \frac{A}{2\pi}\{\frac{\partial m}{\partial T}\frac{\partial T}{\partial t}f^{-1}+\frac{4}{3}\sigma_o\frac{\partial m}{\partial \sigma}[1-(\frac{\sigma_c}{\sigma_o})^3]\} \qquad (2.4)$$

Since $\partial T/\partial t=0$ at constant temperature, the first term in equation (2.4) vanishes. As σ_o is maintained constant during the isothermal measurement with time, the change in $\tan\phi$ with time is attributable only to a change in $(\partial m/\partial \sigma)$. With increase in the number of stress cycles during the isothermal measurement with time, increase in the stress-induced martensite production creates more interfaces between the martensite and the parent phase. This results in an increase of $\partial m/\partial \sigma$, and thus $\tan\phi$ increases according to equation (2.4). Subsequent decrease of $\tan\phi$ can arise from the progressive pinning of the martensite/parent interfaces by the large concentration of vacancies in the sample retained by quenching, as has been suggested by Morin et al.(1987). To test this hypothesis, samples of alloy A and B, after isothermally oscillating for 30 minutes, as shown in Figs.4.40 and 4.44, were heated to 70°C and 80°C, respectively, and their $\tan\phi$, E' and d measured on cooling to -50°C and -40°C, respectively, at a rate of 5°C/min. The results of $\tan\phi$, E' and d are plotted in Figs.4.45 and 4.46. These figures show that, where a $\tan\phi$ peak has appeared during the previous isothermal measurements with time, the $\tan\phi$ peak on subsequent

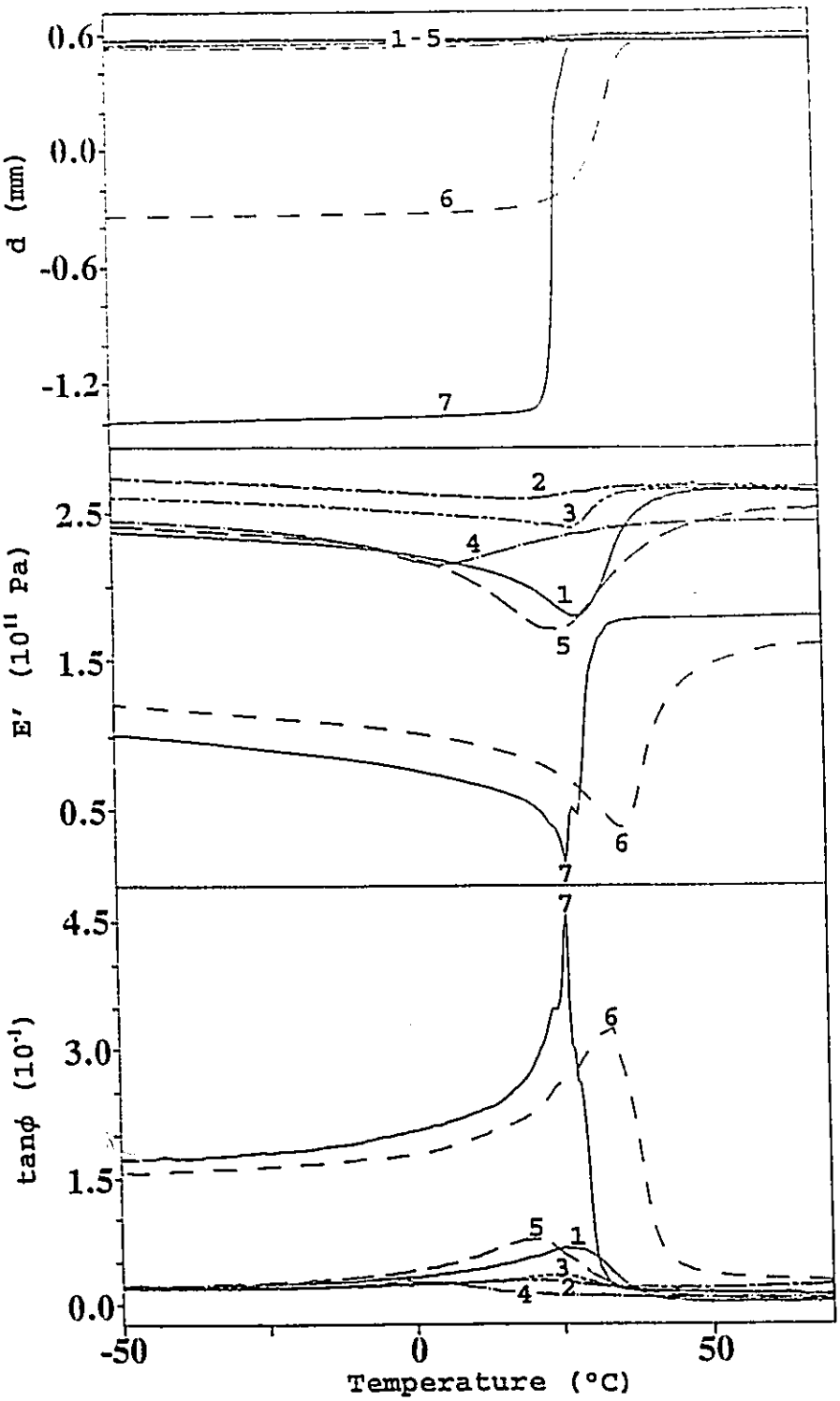

Fig.4.45: The internal friction (tanϕ), the modulus (E') and the probe position (d), of Cu-Zn-Al alloy A measured during the cooling from 70°C following oscillation at 1Hz frequency for 30 min at various temperatures as indicated, 1: -85°C, 2: -40°C, 3: -5°C, 4: 23°C, 5: 40°C, 6: 55°C and 7: 80°C.

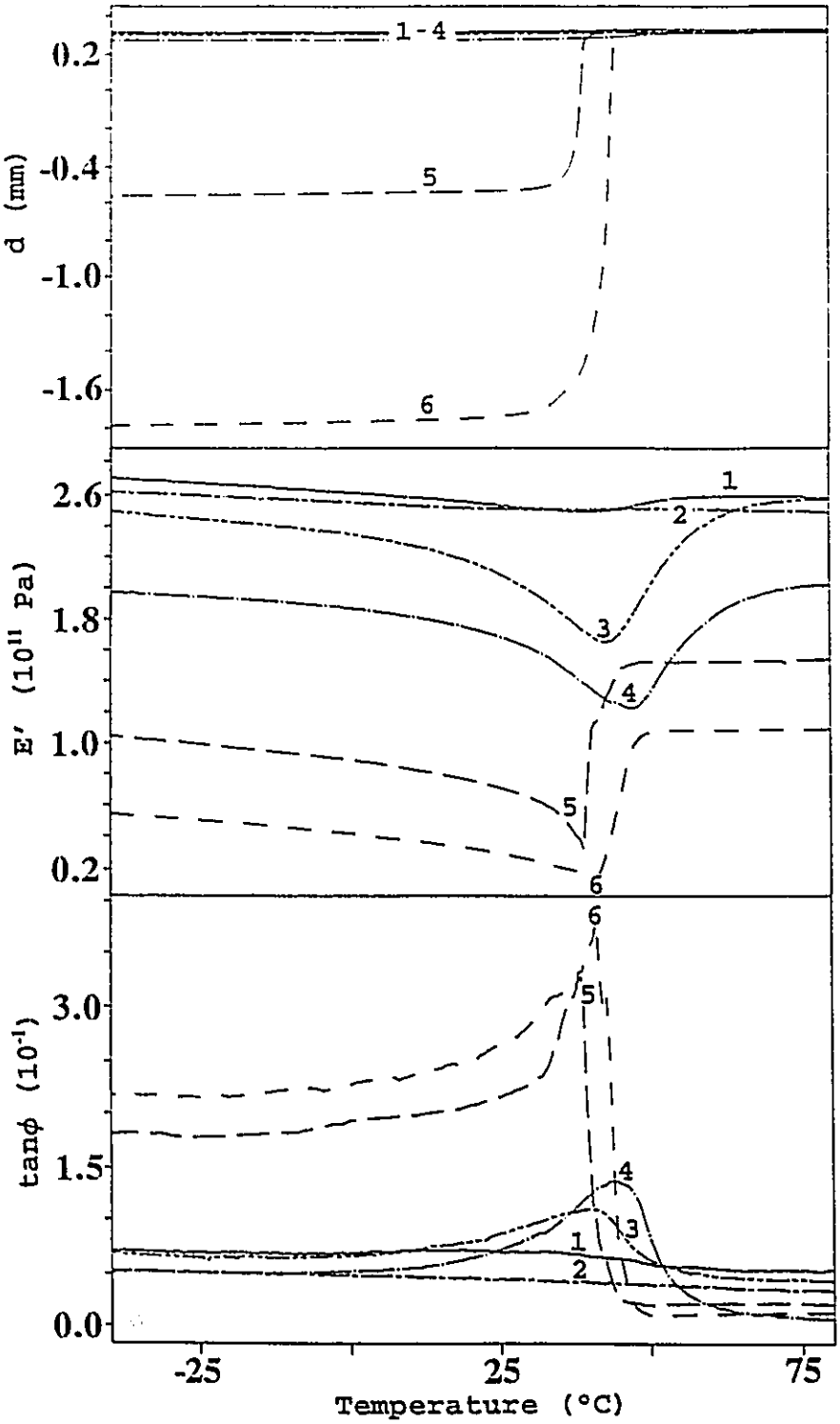

Fig.4.46: The internal friction (tanϕ), the modulus (E′) and the probe position (d), of Cu-Zn-Al alloy B measured during the cooling from 80°C following oscillation at 1Hz frequency for 30 min at various temperatures as indicated, 1: -40°C, 2: 23°C, 3: 56°C, 4: 62°C, 5: 70°C and 6: 88°C.

cooling is significantly suppressed, and that the stronger the peak observed during the isothermal measurements, the weaker the peak measured during subsequent cooling. This becomes more clear from comparisons of Fig.4.45 with Fig.4.40 and Fig.4.46 with Fig.4.44.

The monotonic decrease of tanϕ with time at low temperatures where the sample is completely martensitic (Figs.4.40 and 4.44), may be understood in terms of the occurrence of only one process, namely, the progressive increase in the pinning of the existing martensite/martensite interfaces (Morin, 1985 and Morin et al., 1987). As this does not produce a shape change similar to the stress-induced martensitic transformation, no change in probe position accompanying the decrease in tanϕ is observed. It is noteworthy that the decrease in tanϕ with time is less at lower temperatures mainly because the pinning of martensite/martensite interfaces depends on the diffusion of vacancies, which, being a thermally activated process, is much slower at lower temperatures. This suggestion is consistent with the observation that the tanϕ peak of curve 1 in Figs.4.45 is higher than that of curves 2 and 3, and supports Morin et al's conclusions.

Decrease of tanϕ with time in the martensite phase of a Cu-Zn-Al alloy has also been reported by Morin et al. (1985), who found a less significant decrease of internal

friction with time at lower temperature. They too attributed the observed time dependence of the internal friction to the interaction of martensite/martensite interfaces with point defects.

The results of this study suggest that in order to avoid the deterioration of shape memory effect with time due to the pinning of martensite/martensite or martensite/parent interfaces, the sample should, upon quenching from high temperature, be immediately heated to the region of stability of single parent phase, which would allow the population of quenched-in vacancies to decrease. This is clearly seen from Figs.4.45 and 4.46, where the sample which is immediately heated to and oscillated at 80°C and 88°C after quenching (curve 7 and 6, respectively) exhibits during cooling the highest tanϕ peak and the maximum shape change. This treatment therefore has the potential for providing more stable shape memory effect in Cu-Zn-Al alloys.

The studies of the time dependence of internal friction in the Cu-Zn-Al shape memory alloys have shown that:

(i). The evolution of internal friction with time during the application of a sinusoidal and static stress depends on both the microstructural state and the holding temperature.

(ii). In the single martensite state, the monotonic decrease of internal friction with time is due to the

progressive pinning of martensite/martensite interfaces by vacancies, whose diffusion is thermally activated.

(iii). When the parent and martensite phases are present together, an internal friction peak appears. This peak is due to the stress-induced martensitic transformation and the subsequent pinning of the martensite/parent as well as the martensite/martensite interfaces.

4.3 DSC Studies

4.3.1 Effect of Heat Treatment on the Transformation

Since Cu-Zn-Al alloy undergoes B2 and DO_3 ordering (Rapacioli and Ahlers, 1977, Singh et al., 1978) before transforming to martensite, different heat treatments have a strong influence on the atomic ordering and hence the subsequent martensitic transformation (Tong and Wayman, 1975, Rapacioli et al., 1975, Cook and Brown, 1978).

In this study, after homogenization at 850°C for 10 minutes, the sample was either quenched in water maintained at different temperatures or in liquid nitrogen, and then immediately transferred to DSC at -100°C. The first two heating curves for each case are shown in Figs.4.47-4.49. In all three cases, the peak position becomes stabilized after the appearance of an "abnormal" peak during the first heating run. The position of this "abnormal" peak, relative to the

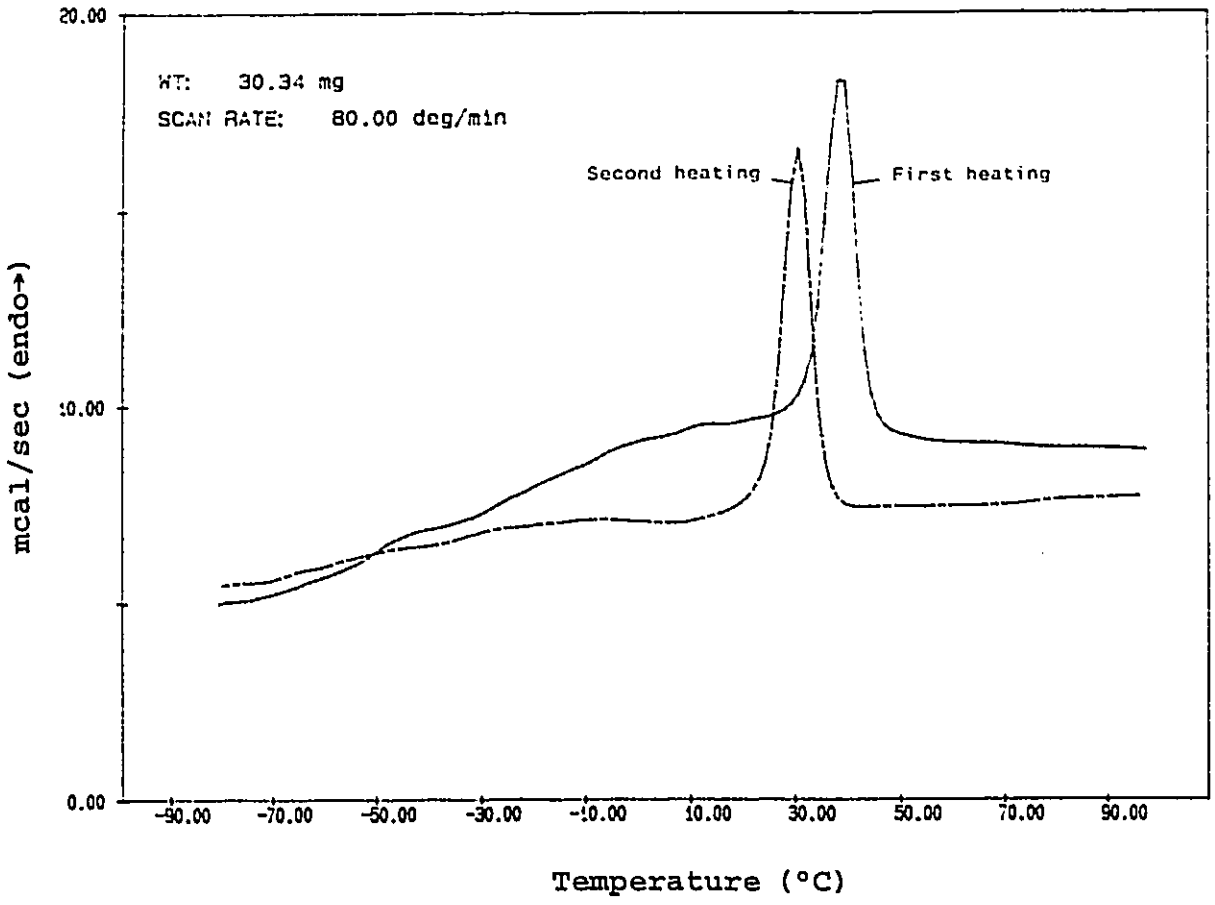

Fig.4.47: First and second DSC heating runs after the sample of alloy A is quenched and kept in 60°C water for 5 min.

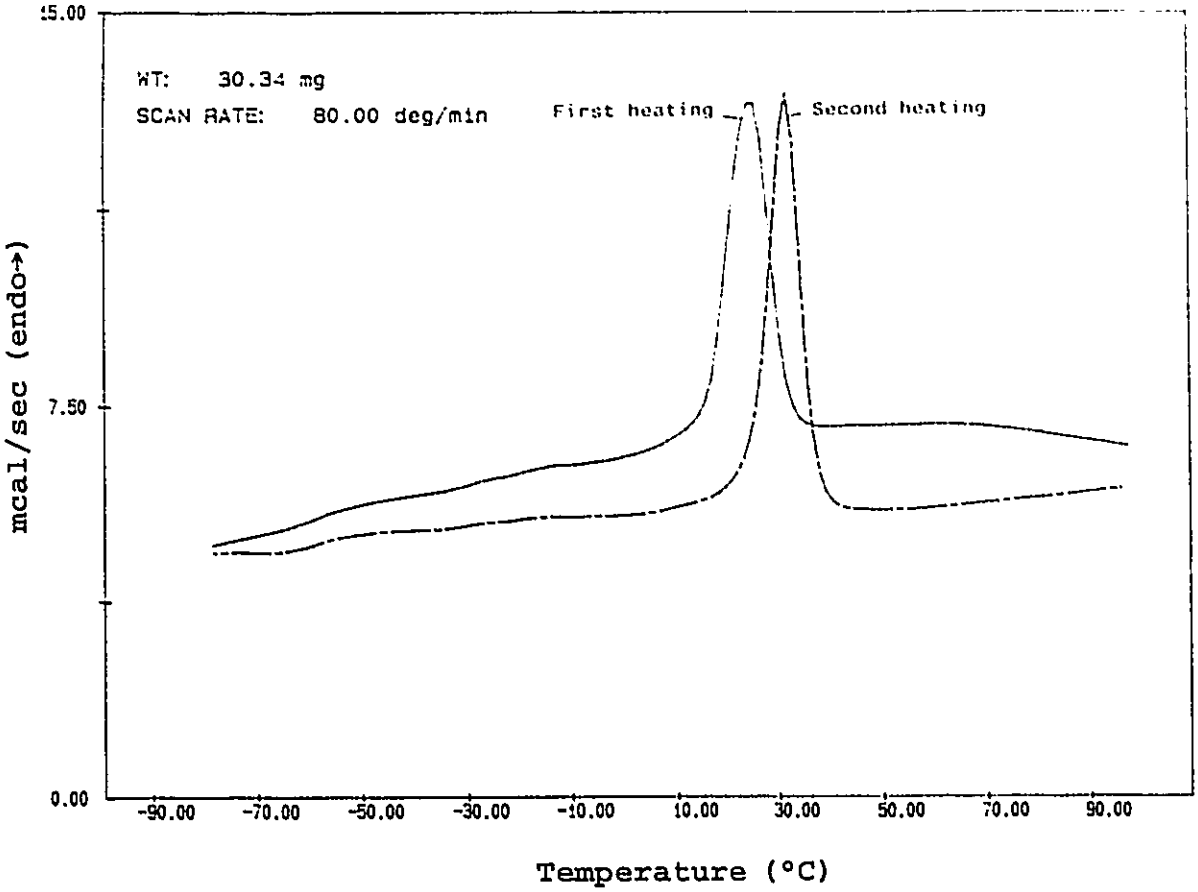

Fig.4.48: First and second DSC heating runs after the sample is quenched and kept in 18°C water for 5 min.

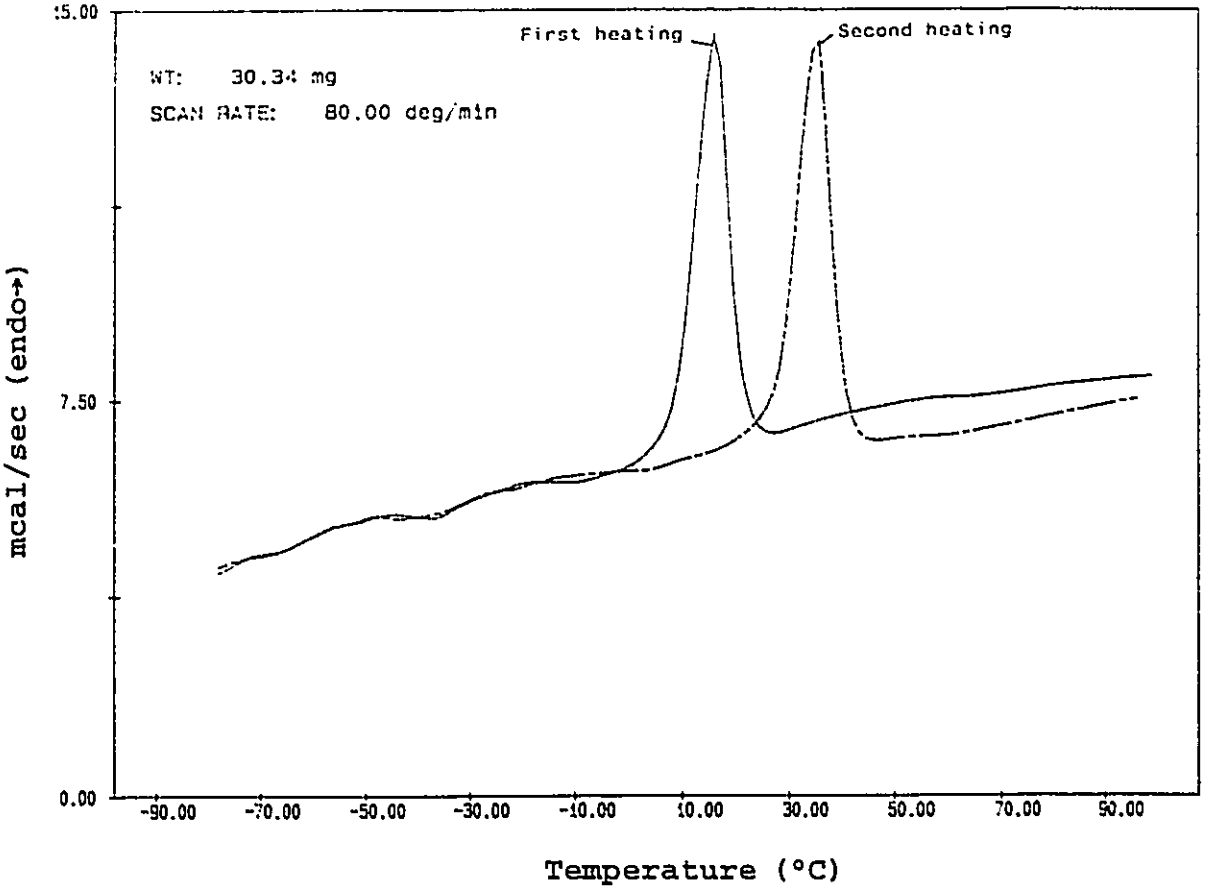

Fig.4.49: First and second DSC heating runs after the sample is quenched and kept in liquid nitrogen for 5 min.

subsequent "normal" peaks, is sensitive to the heat treatment and seems to be related to the degree of order in the martensite phase. When the sample was quenched from 850°C to above its M_s temperature (Fig.4.47) and maintained for 5 minutes, a DO_3 order was developed in the parent phase. Accordingly, the martensite formed during subsequent cooling had a 18R order. But when the sample was directly quenched from 850°C to below its M_s temperature (Figs.4.48 & 4.49), the martensite formed might inherit certain degree of disorder from the high temperature β phase, tending it to be less stable and to transform to parent phase at a lower temperature. After one cycle of heating and cooling in the DSC, the martensite was able to develop an equilibrium degree of order, and would thus transform at the same temperature at each subsequent cycles. This observation is in agreement with the findings by Rapacioli and Ahlers (1979) and Schofield and Miodownik (1980) who also found a depression of the martensitic transformation temperature in the directly-quenched sample. Planes et al.(1981) suggested that the transformation temperature in the directly-quenched sample was decreased because certain degree of disorder was introduced by quenching. When the sample was held at around M_s temperature for certain time, the degree of DO_3 order improved and the martensitic transformation temperatures increased. Their

explanation is also in agreement with our observations here.

4.3.2 Effect of Cooling and Heating Rate on the Transformation

Typical reproducible DSC cooling and heating curves for the Cu-Zn-Al alloy A under the standard heat treatment (18°C water quench) condition are shown in Fig.4.50. From these, the fraction of martensite transformed is calculated from the heat evolved at any temperature divided by the total heat of transformation. To eliminate any instrumental effects, distilled water was chosen as a calibration standard and its freezing and melting peaks were measured at the same cooling and heating rates. The transformation temperatures, hysteresis (between cooling and heating) and transition range (transition temperature spread), as defined in Fig.4.50, for Cu-Zn-Al alloy A and the water standard, are plotted against cooling and heating rate in Fig.4.51 & 4.52, respectively. Using water as calibration standard, the corrected curves are shown in Fig.4.53. It is found that Tonset (cooling & heating) increases only slightly with cooling and heating rate, while transition range and halfway hysteresis decreases with cooling and heating rate. Moreover, the onset hysteresis remains almost independent of cooling and heating rate. These results suggest that the onset temperature of the martensitic transformation is hardly affected by the rate of cooling or

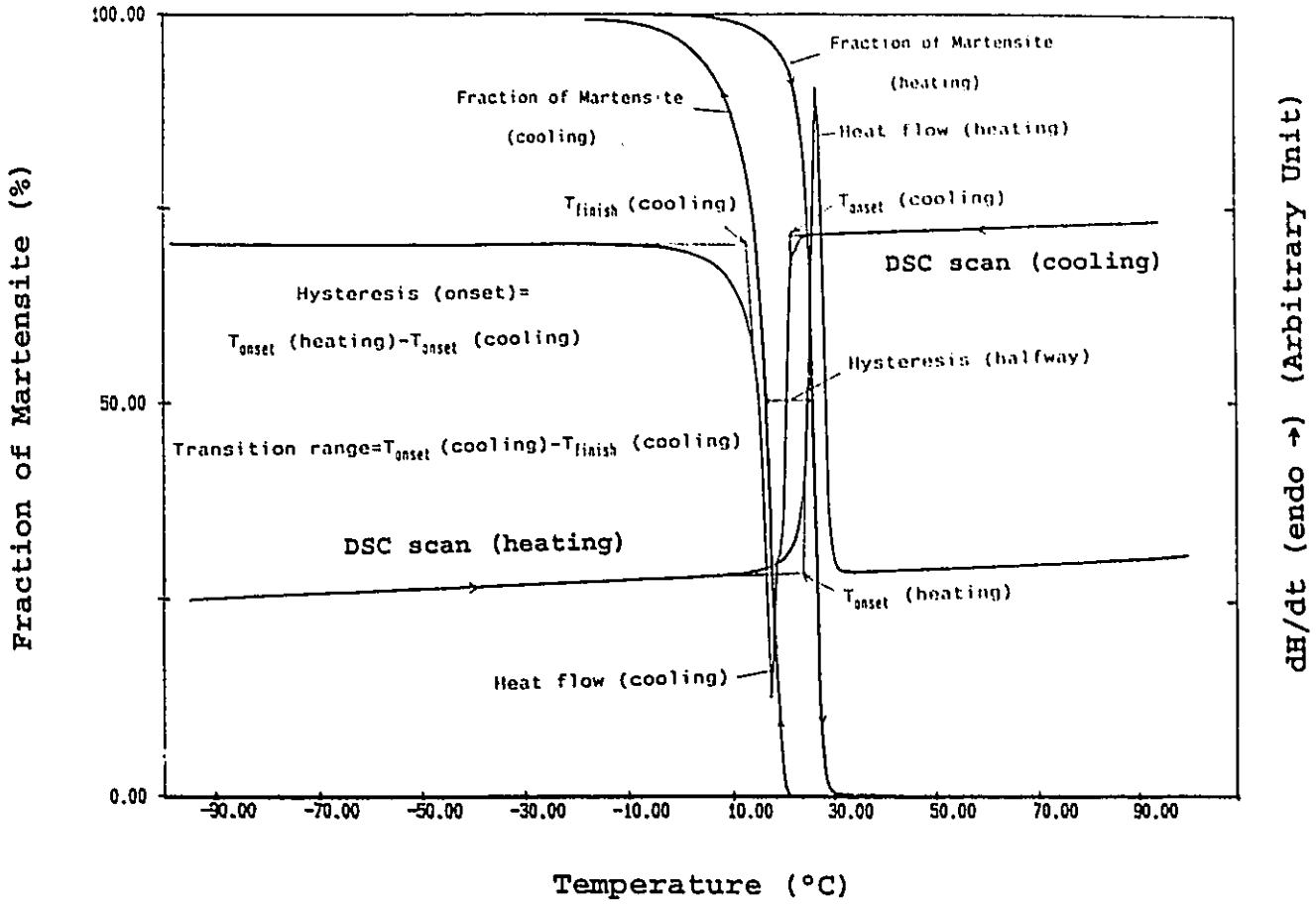

Fig.4.50: DSC heat flow and fraction of martensite as a function of temperature obtained at a cooling and heating rate of 20°C/min.

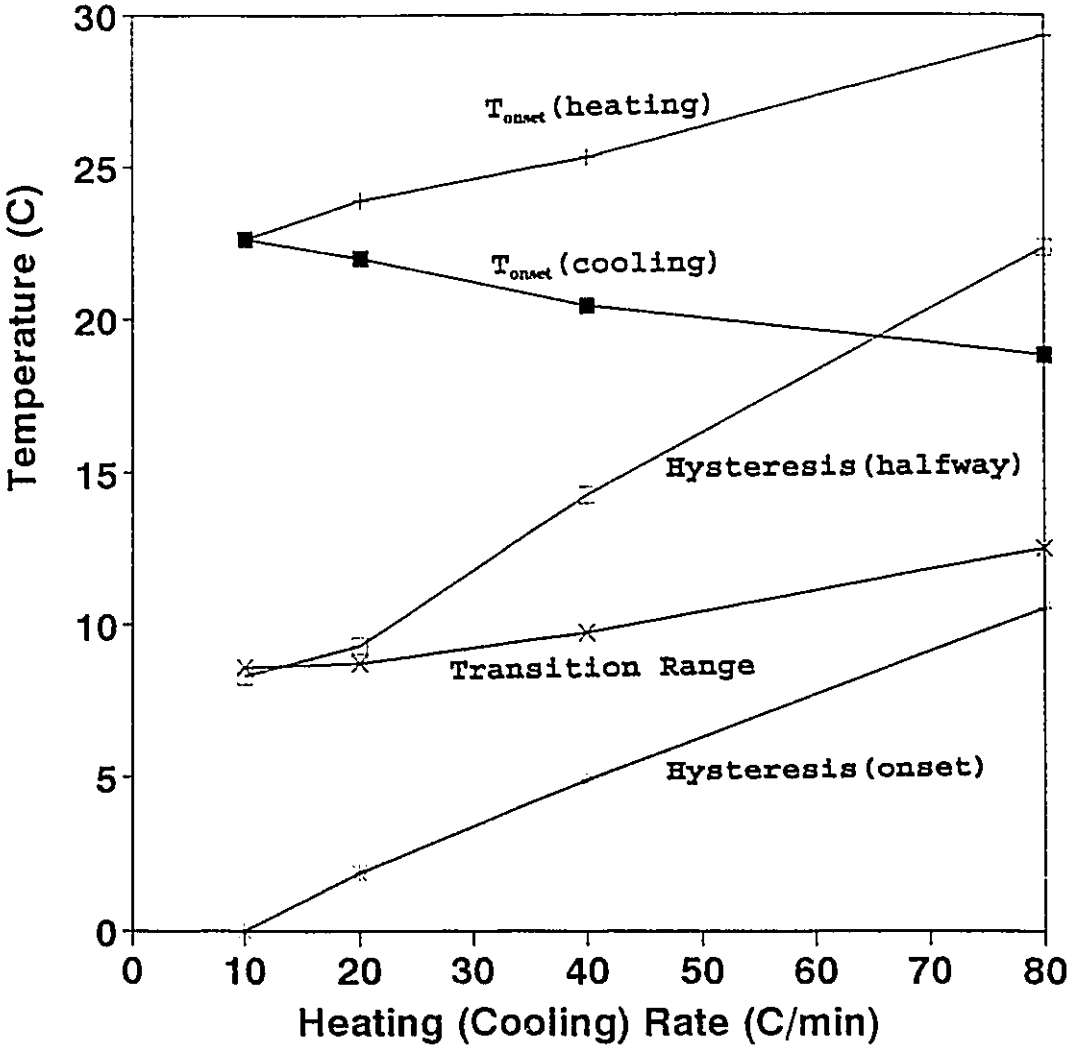

Fig.4.51: T_{onset} (cooling and heating), hysteresis (onset and halfway) and transition range as a function of cooling and heating rate for Cu-Zn-Al alloy A.

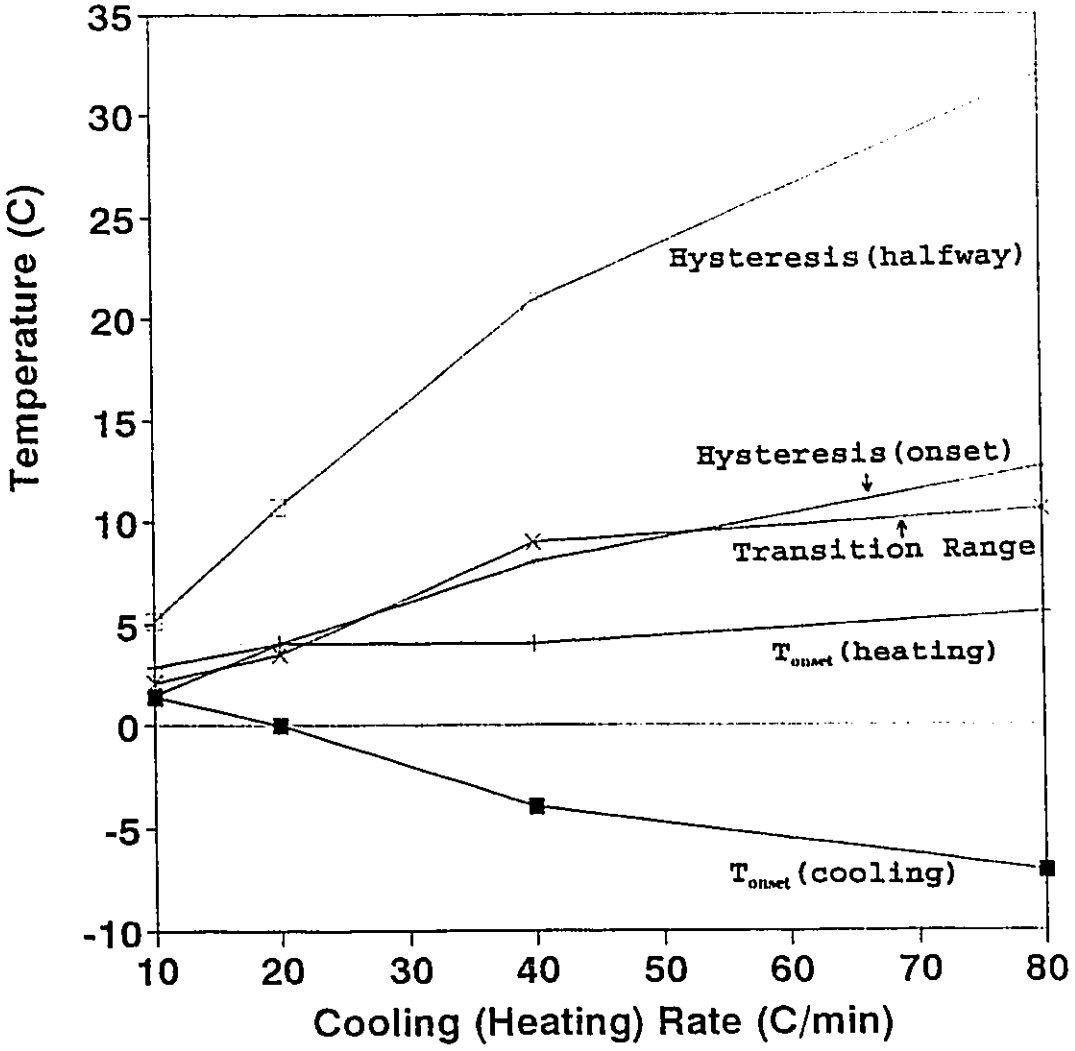

Fig.4.52: T_{onset} (cooling and heating), hysteresis (onset and halfway) and transition range as a function of cooling and heating rate for distilled water.

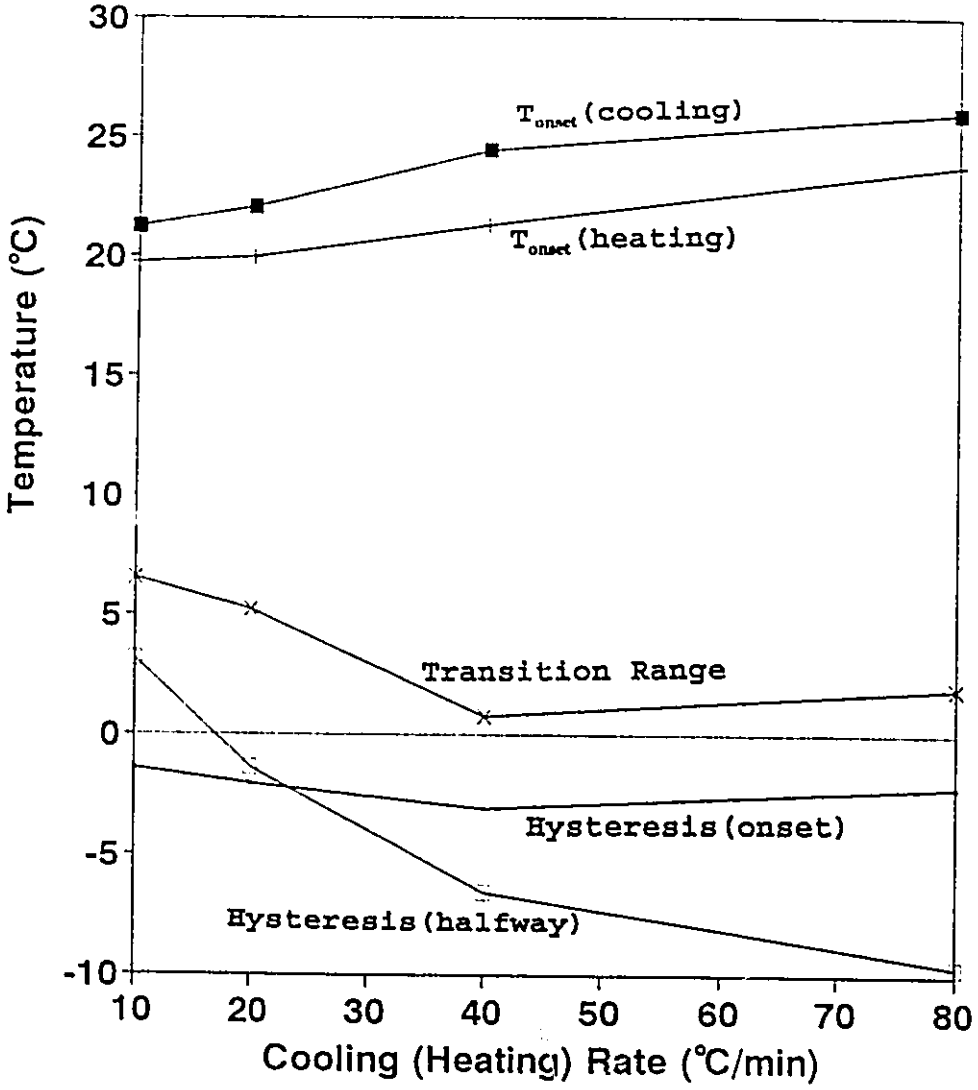

Fig.4.53: Corrected values of T_{onset} (cooling and heating), hysteresis (onset and halfway) and transition range as a function of cooling and heating rate.

heating. The apparent change in the halfway hysteresis and transition range with cooling and heating rate, however, may not reflect the true change in the shape memory alloy since the difference in thermal conductivity between the shape memory alloy and water necessarily causes a different dependence of thermal lag on the cooling and heating rate. Because the onset of the transformation is relatively less dependent on the thermal conductivity of the sample, it is believed that the calibrated values of T_{onset} (cooling and heating) and the onset hysteresis are more reliable than those of halfway hysteresis and transition range in Fig.4.53. In order to further study the dependence of the halfway hysteresis on the heating and cooling rate, indium, another metal standard which had a closer thermal conductivity to that of the shape memory alloy, was also used to study its hysteresis between melting and solidification. Fig.4.54 shows the halfway hysteresis of the shape memory alloy, the indium standard, as well as their difference, as a function of the heating and cooling rate. The difference in halfway hysteresis between the shape memory alloy and the indium standard represents a value closer to the true transformation hysteresis of the shape memory alloy, after eliminating (at least partially) the instrumental effects. Extrapolating the difference curve to zero heating and cooling rate yields a

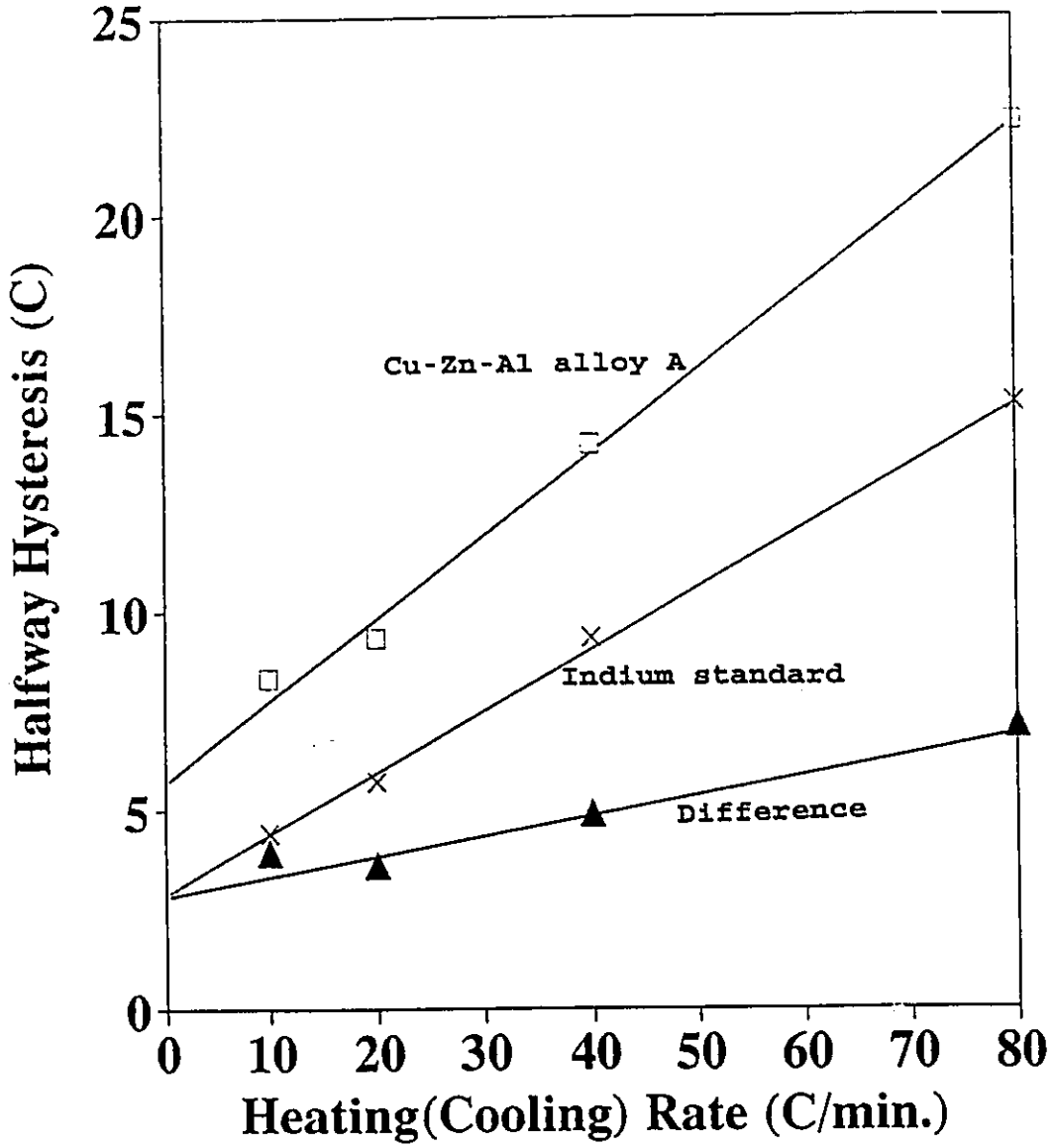

Fig.4.54: Halfway hysteresis of Cu-Zn-Al alloy A (martensitic transformation), indium standard (melting and solidification), and their difference, as a function of heating and cooling rate.

value of about 2.5-3°C, in agreement with the hysteresis obtained metallographically at a heating and cooling rate of 0.5°C/minute (section 4.4.2).

4.3.3 Isothermal DSC Experiments

In section 4.3.2, a weak heating and cooling rate dependence of the halfway hysteresis of the memory alloy (after indium calibration) was observed. If this was real and not due to experimental errors, this effect, i.e., the time dependence of the transformation, should be observable in an isothermal DSC experiments in the temperature range of the transformation. For this purpose, isothermal experiments were carried out for both Cu-Zn-Al alloys A and B.

Fig.4.55 shows the isothermal DSC curves for alloy A measured at two constant temperatures between the onset and the maximum of the cooling peak after the sample was quickly cooled (80°C/minute) from 50°C to the holding temperatures. The cooling and heating curves are also shown for comparison. Obviously there is no sign of any isothermal martensitic transformation taking place. The small bump in the cooling curve of Fig.4.55(a), as is occasionally observed, suggests that thermoelastic martensitic transformation proceeds by a sequence of local transformations, which may not always be continuous.

The cooling and heating curves in comparison with the

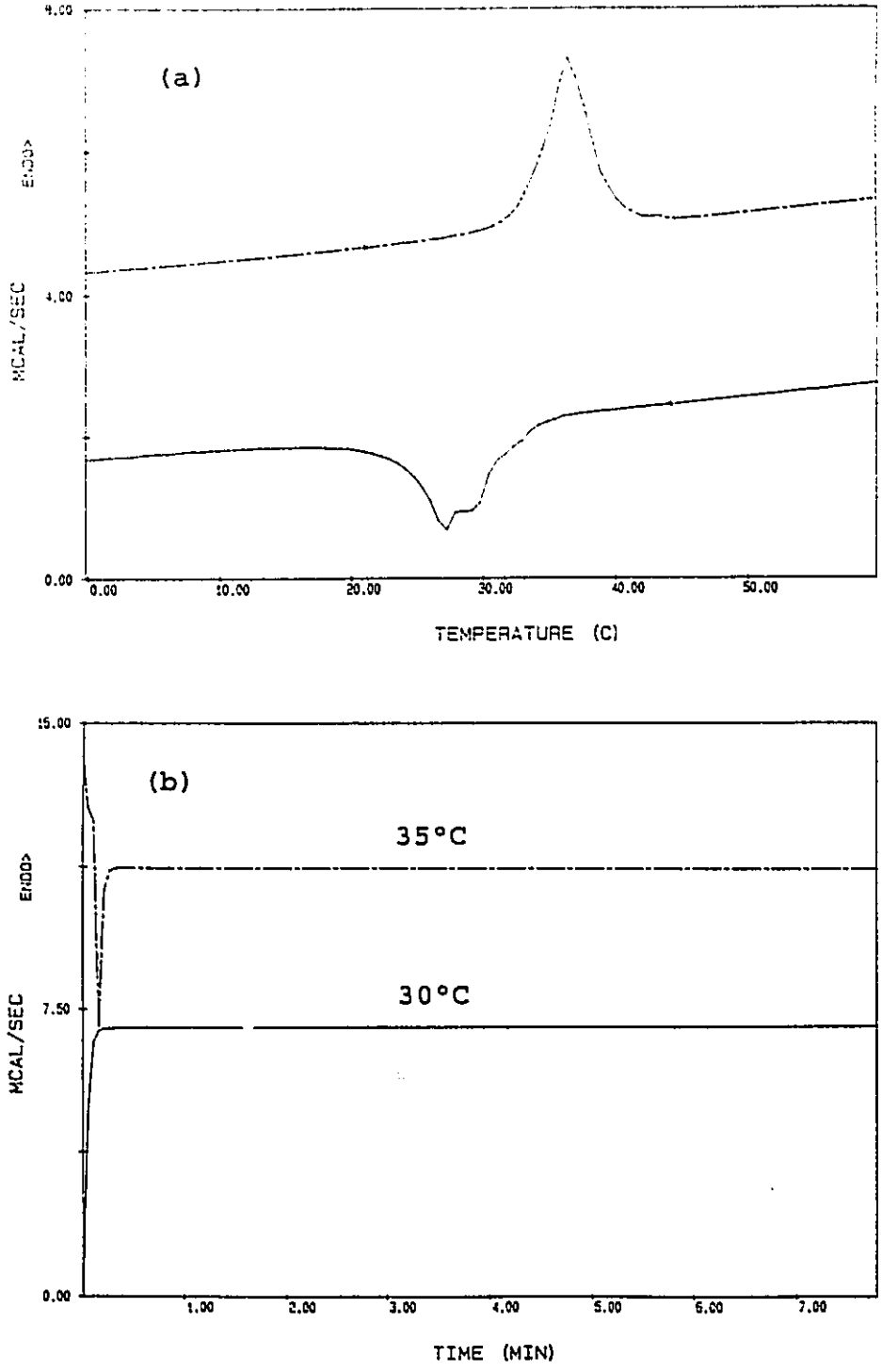

Fig.4.55: (a) DSC heating and cooling scans, and (b) isothermal scans in the temperature range of martensitic transformation for Cu-Zn-Al alloy A.

isothermal curves were also obtained for alloy B, as shown in Fig.4.56. Similarly, no sign of isothermal martensitic transformation is observed in the temperature range where athermal transformation takes place.

4.3.4 Study of the Interface/Defect Interactions

Equation (2.2) in section 2.1.3 of Chapter 2 is particularly useful in studying the interaction of interfaces with vacancies and precipitates by means of DSC.

Fig.4.57 shows the frictional energy, calculated from Equation (2.2) using the transformation heats measured by DSC, as a function of the number of thermal cycles between -100°C and 100°C, for Cu-Zn-Al alloy A. At the first thermal cycle following the standard heat treatment, the large number of vacancies retained in the quenched martensite interfered with the interfacial motion during the (reverse) martensitic transformation, giving rise to a higher frictional energy. With each additional thermal cycle, the vacancies were gradually annealed out, leading to a decrease in the frictional resistance to the interfacial motion and hence a smaller frictional energy.

Fig.4.58 shows the deterioration in the shape and reversibility of the transformation peak as the sample was slowly heated (2°C/minute) to 180°C and then cooled at the same rate. A frictional energy as large as 0.145 cal/gram.,

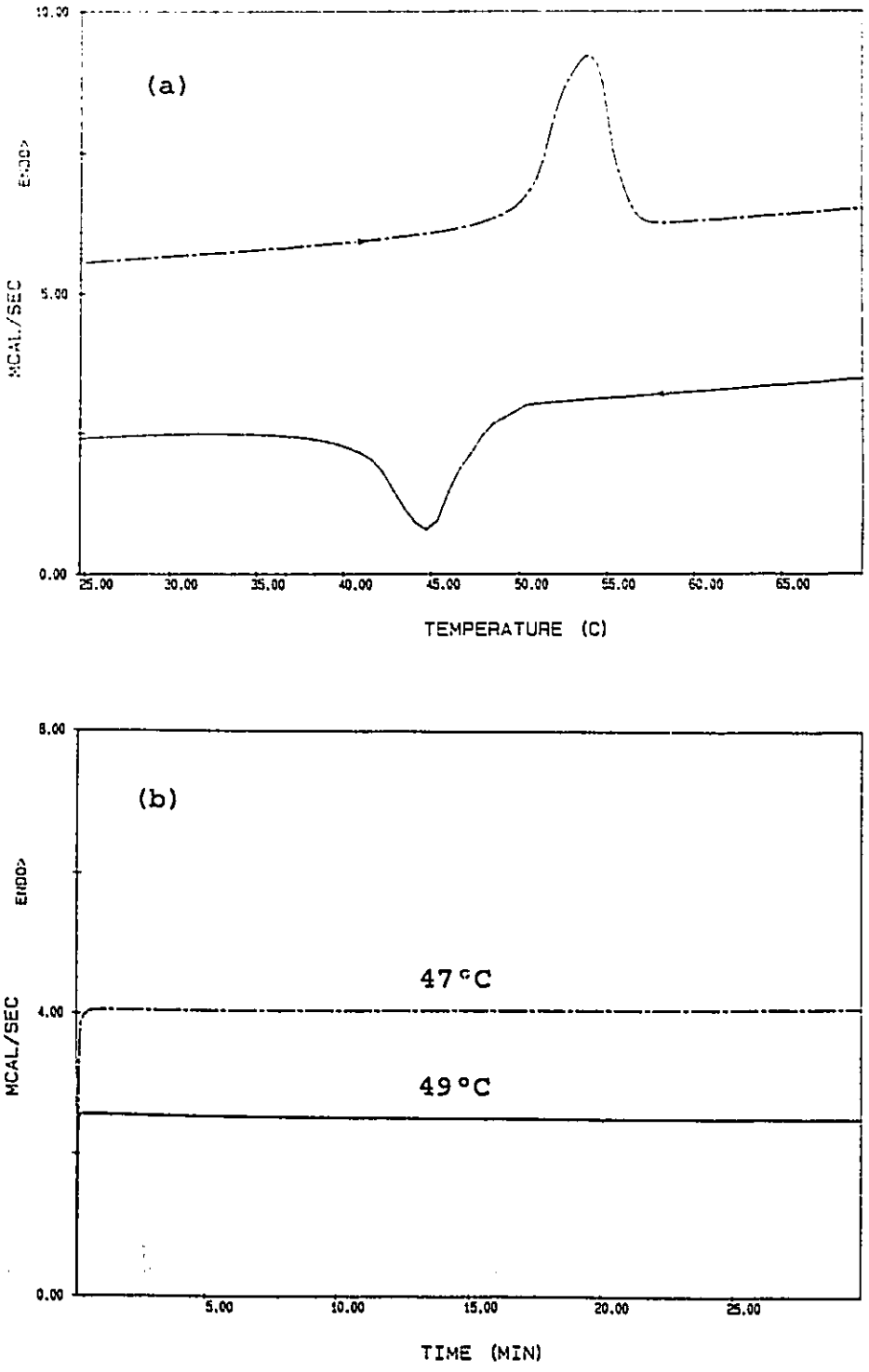

Fig.4.56: (a) DSC heating and cooling scans, and (b) isothermal scans in the temperature range of martensitic transformation for Cu-Zn-Al alloy B.

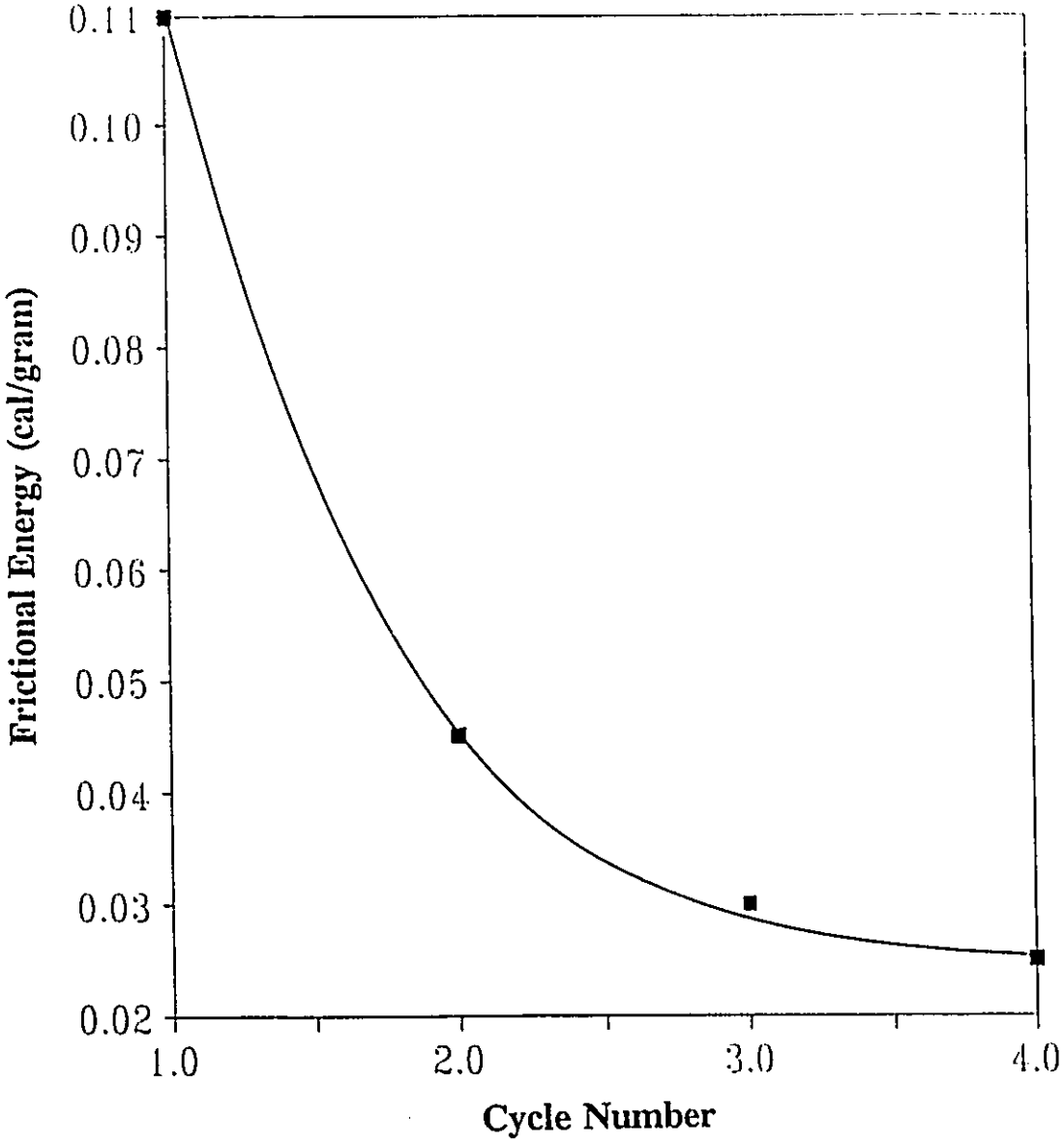

Fig.4.57: Frictional energy as a function of the number of thermal cycle for a Cu-Zn-Al alloy A sample quenched to 18°C water.

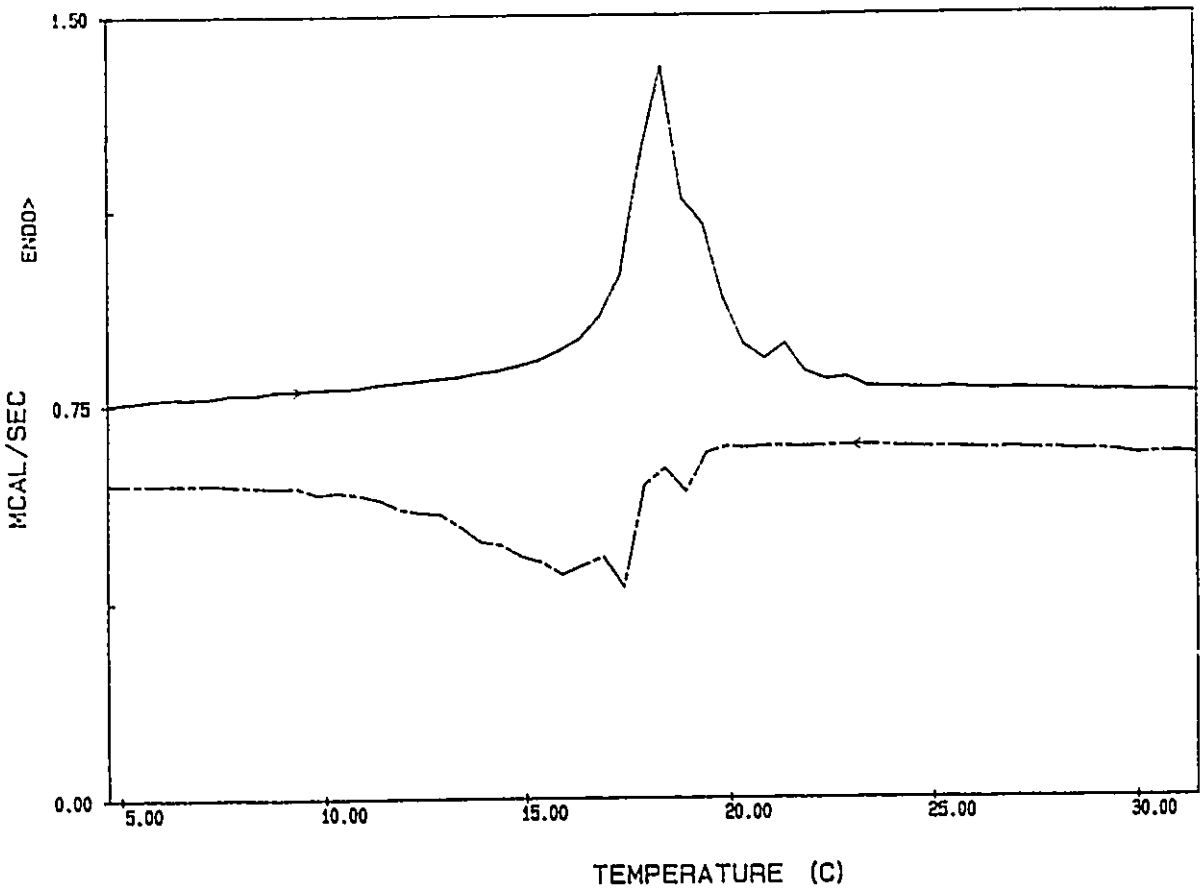

Fig.4.58: Deterioration of the shape and reversibility of DSC heat flow peak as the sample was heated at 2°C/min. to 180°C and then cooled at the same rate.

i.e., about 9% the transformation heat, has been calculated, suggesting a serious hindrance of interfacial motion by the precipitation of the α-phase. This is in agreement with the earlier torsional pendulum results (section 4.2.1.1) which showed a decrease in the height of the internal friction peak associated with the martensitic transformation after thermal cycling at 2°C/minute to 177°C.

Aging in the martensite state causes the martensite to stabilize. This stabilization effect, noted by a decrease in the mobility of martensite/martensite interface, can also be studied by DSC. Fig.4.59 shows the change of transformation heat and frictional energy with aging time at 24°C for a sample of alloy B immediately following quenching from 850°C. It is seen that martensite stabilization is fastest between 10 and 20 minutes after quenching, with a rapid decrease in the transformation heat and sharp rise in the frictional energy with aging time. It should be noted that during aging at 24°C the alloy B sample was completely in the martensitic state, according to Fig.4.56. However, after the alloy A sample (partially martensitic at 24°C, according to Fig.4.55) was aged at 24°C for a period of up to 60min, its transformation heat decreased by a much smaller amount, as is shown in Fig.4.60. Obviously the existence of parent phase effectively reduced the tendency of stabilization in the martensite. It appears that the β parent phase, whose structure is less

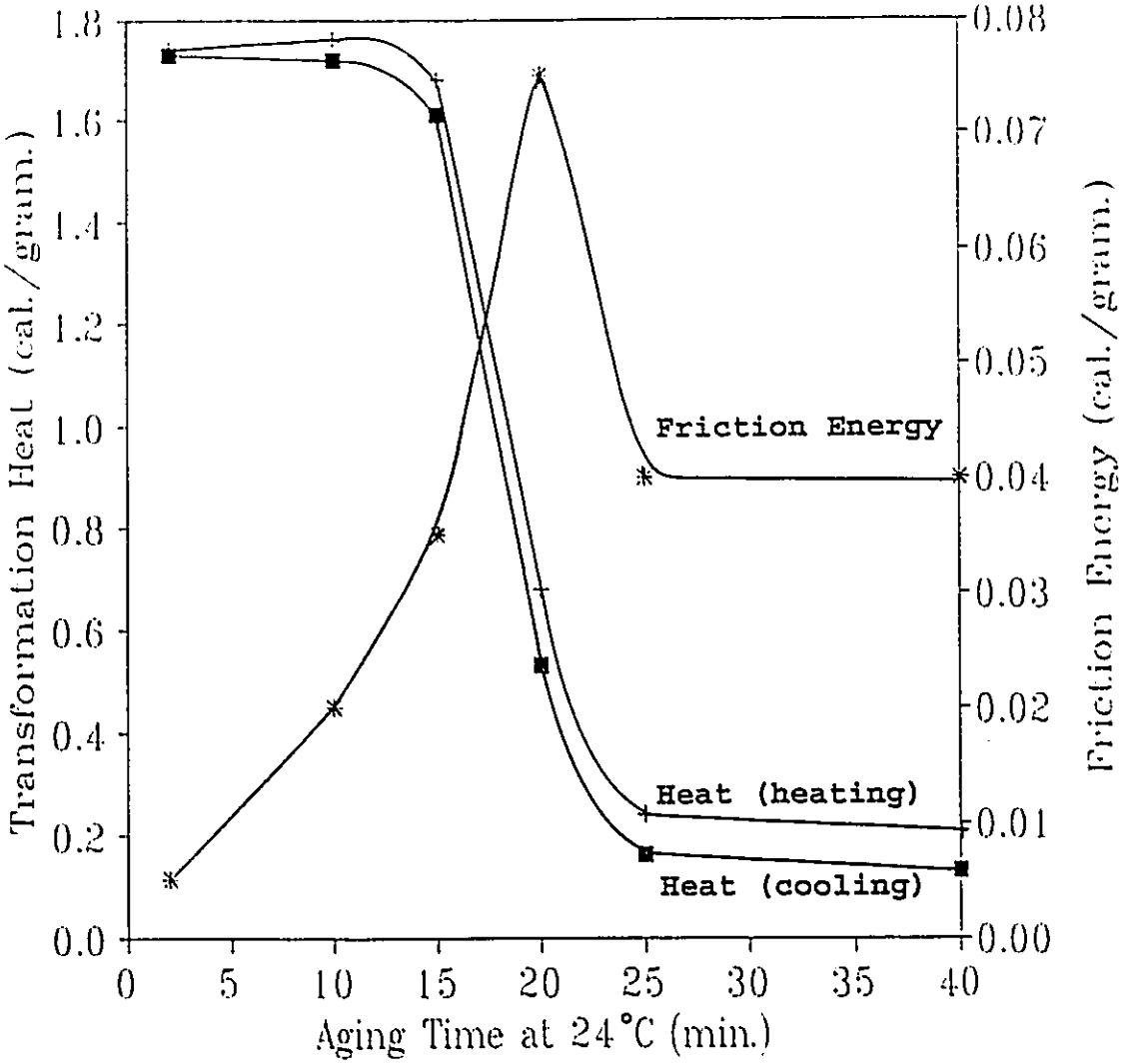

Fig.4.59: Transformation heats during cooling and heating and frictional energy as a function of aging time at 24°C for Cu-Zn-Al alloy B.

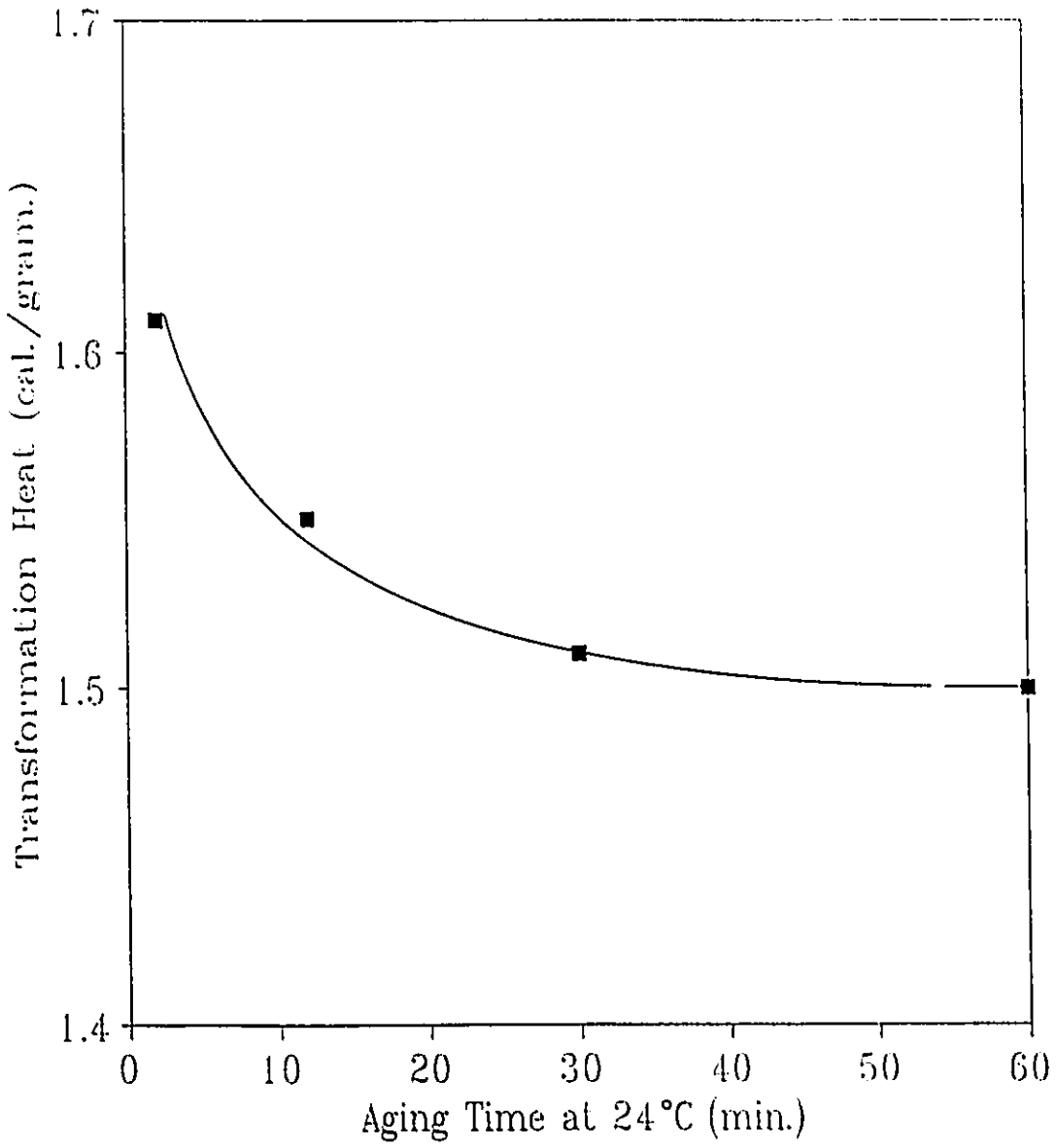

Fig.4.60: Transformation heat (during cooling) as a function of aging time at 24°C for Cu-Zn-Al alloy A.

complex and less densely packed (Funakubo, 1987), may serve as a sink through which most of the vacancies retained from quenching may annihilate and therefore may not contribute to the stabilization effect arising from the pinning of the interfaces by vacancies.

4.4 Metallographic Studies

4.4.1 Static Observation of Etched Microstructures

Metallographic examination was first made on an as-quenched sample (15mmx2mmx0.5mm) of alloy A, as shown in Fig.4.61(a). Here, V-shaped, self-accommodating martensite plates in the parent phase matrix are clearly observed. The same sample was then thermally cycled to 180°C and 280°C and re-examined, as shown in Fig.4.61(b)&(c). Compared to the as-quenched condition, no significant changes were observed after six thermal cycles to 180°C. However, thermal cycling to 280°C resulted in noticeable precipitation of the α-phase between martensite plates, as can be clearly seen as the white specks in the dark regions in Fig.4.61(c). This observation supports the claim in section 4.2.1.1 that the α-phase precipitation is responsible for the suppression of the internal friction peak associated with the martensitic transformation.

(a)

(b)

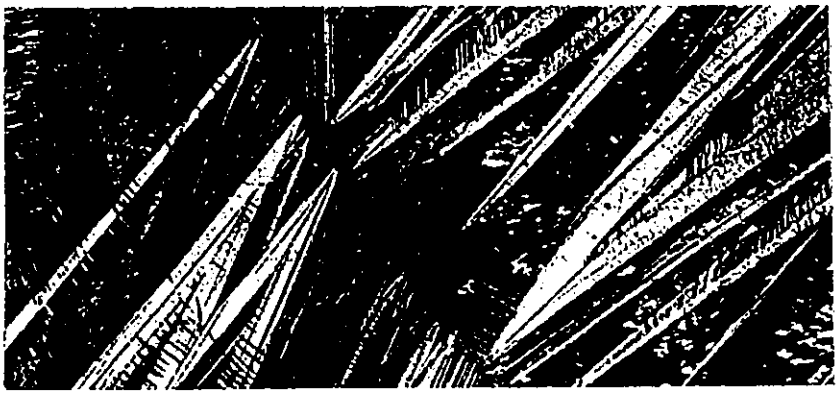

(c)

Fig.4.61: Optical photomicrographs of Cu-Zn-Al alloy A. (a) as quenched condition, (b) after six thermal cycles between room temperature and 180°C at 2°C/min., (c) after another thermal cycle to 280°C at 2°C/min.

4.4.2 In Situ Observation of Surface Relief Variation During Martensitic Transformation

Fig.4.62 shows the gradual development of the surface relief in a heat-treated and polished sample of alloy A during cooling (left) and heating (right) at a rate of 0.5°C/minute. The series of micrographs show a number of important features of the thermoelastic martensitic transformation. Upon cooling to 25°C some martensite variants appeared first in certain regions and gradually thickened on further cooling. Large plates appeared to evolve from the coalescence of parallel variants. Further, the plates which grew by joining up on cooling transformed back on heating by the formation of parallel segments, i.e., the inverse of the cooling process. The formation and reversal sequences were virtually identical in subsequent thermal cycles, when the cooling and heating rates were constant. This coalescence of plates to form larger ones and its reversal is a rather common characteristic of thermoelastic martensitic transformation and has also been observed by Wayman (1975) in a Cu-Zn alloy. The fact that the position and formation sequence of the martensite plates on cooling are repeated almost precisely in the next cooling cycle (after complete reversal by heating) suggests that preferred nucleation sites necessarily exist in the parent phase. By comparing the left and right columns of Fig.4.62 at a fixed amount of transformation, a thermal hysteresis of

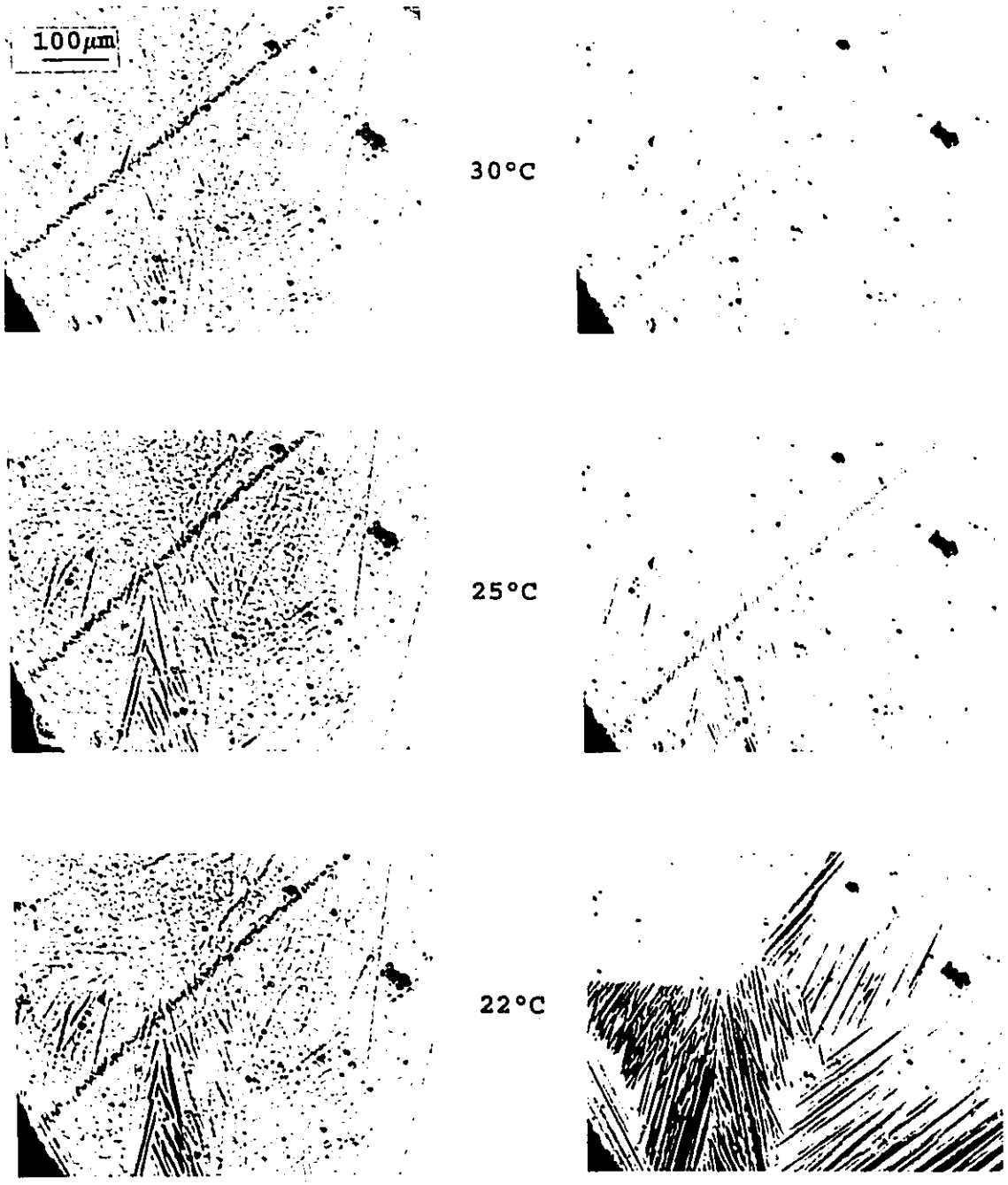

Fig.4.62: Development of the surface relief in an as-quenched and polished sample of alloy A during cooling (left column) and heating (right column) at a rate of 0.5°C/min. Continued in the following two pages.

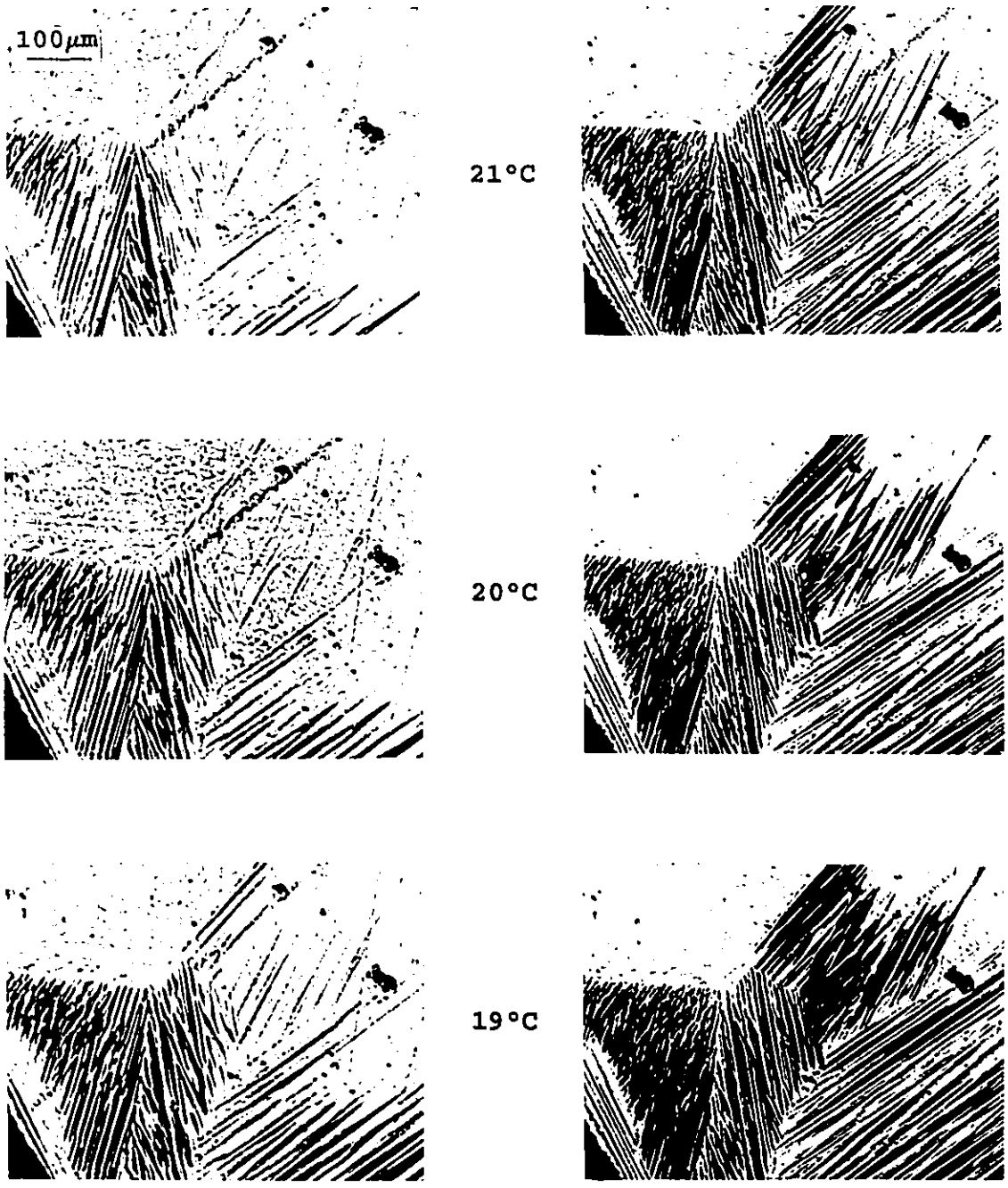

Fig.4.62: Continues from the previous page.

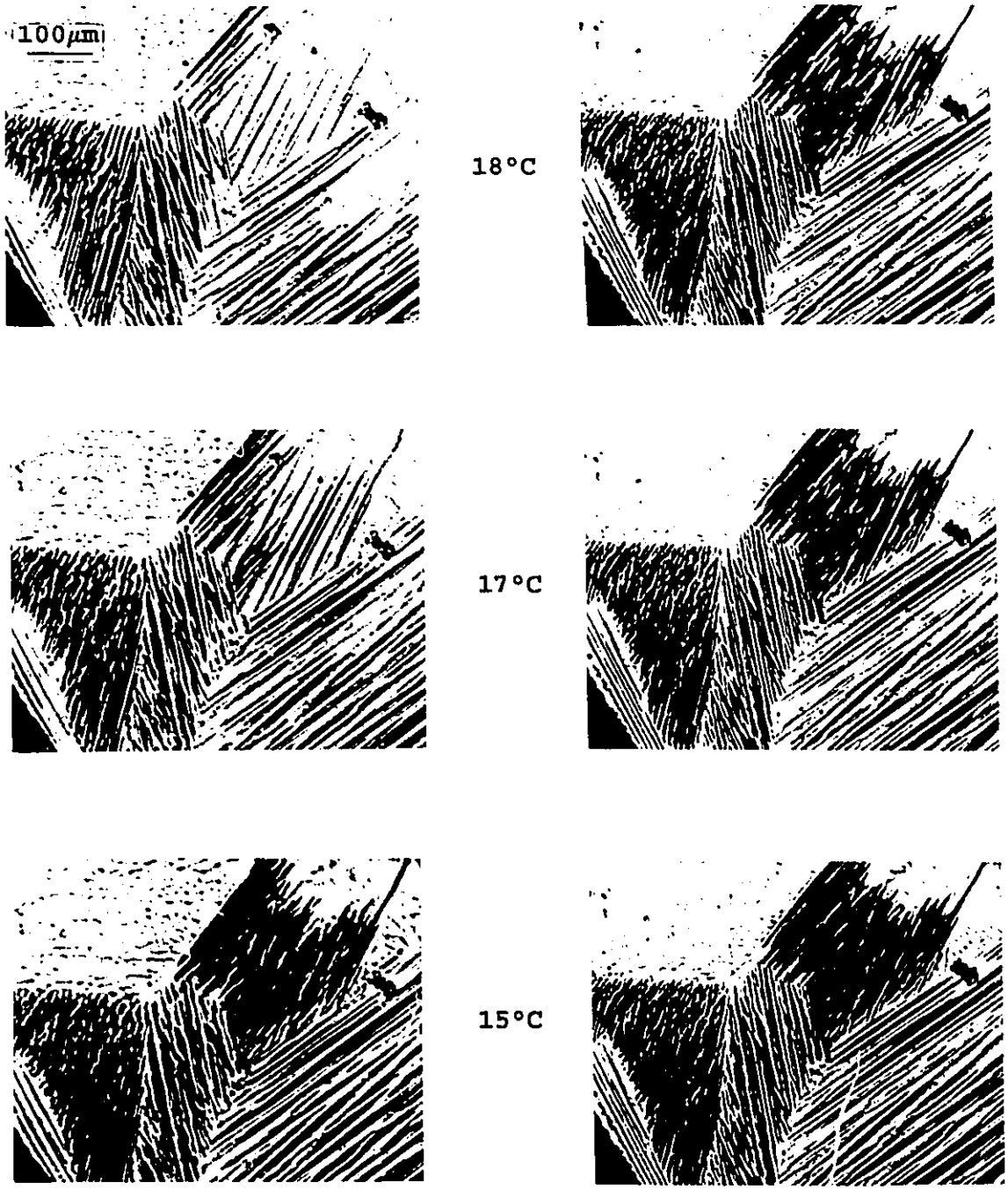

Fig.4.62: Continues from the previous page.

about 3-4°C can be estimated.

In order to check if martensitic transformation could take place isothermally, the sample was isothermally held for 15 minutes, upon cooling or heating to various temperatures in the range of the transformation, and photomicrographs were taken at the beginning and end of the isothermal holding, as shown in Figs.4.63 & 4.64. In either case, no obvious change was observed before and after the isothermal holding. In conclusion, the growth or shrinkage of martensite plates occurs only when the temperature decreases or increases, but not at a constant temperature. This indicates that a thermoelastic equilibrium exists at a given temperature.

The effect of aging in the parent phase on the martensitic transformation was also studied by metallography. Fig.4.65 shows a series of micrographs taken during cooling and heating a sample of alloy A aged for 87.5 hours at 107°C. By comparing Fig.4.62 with Fig.4.65, it is evident that, after the aging treatment, the extent of the variation of surface relief with temperature is greatly reduced suggesting a decrease in the amount of parent phase going through the martensitic transformation. This observation is in agreement with the earlier internal friction results shown in Fig.4.5 (Section 4.2.1.1) where a significant decrease in the transformation peak height was observed after aging for 87.5 hours at 107°C. It appears that a lower internal friction peak

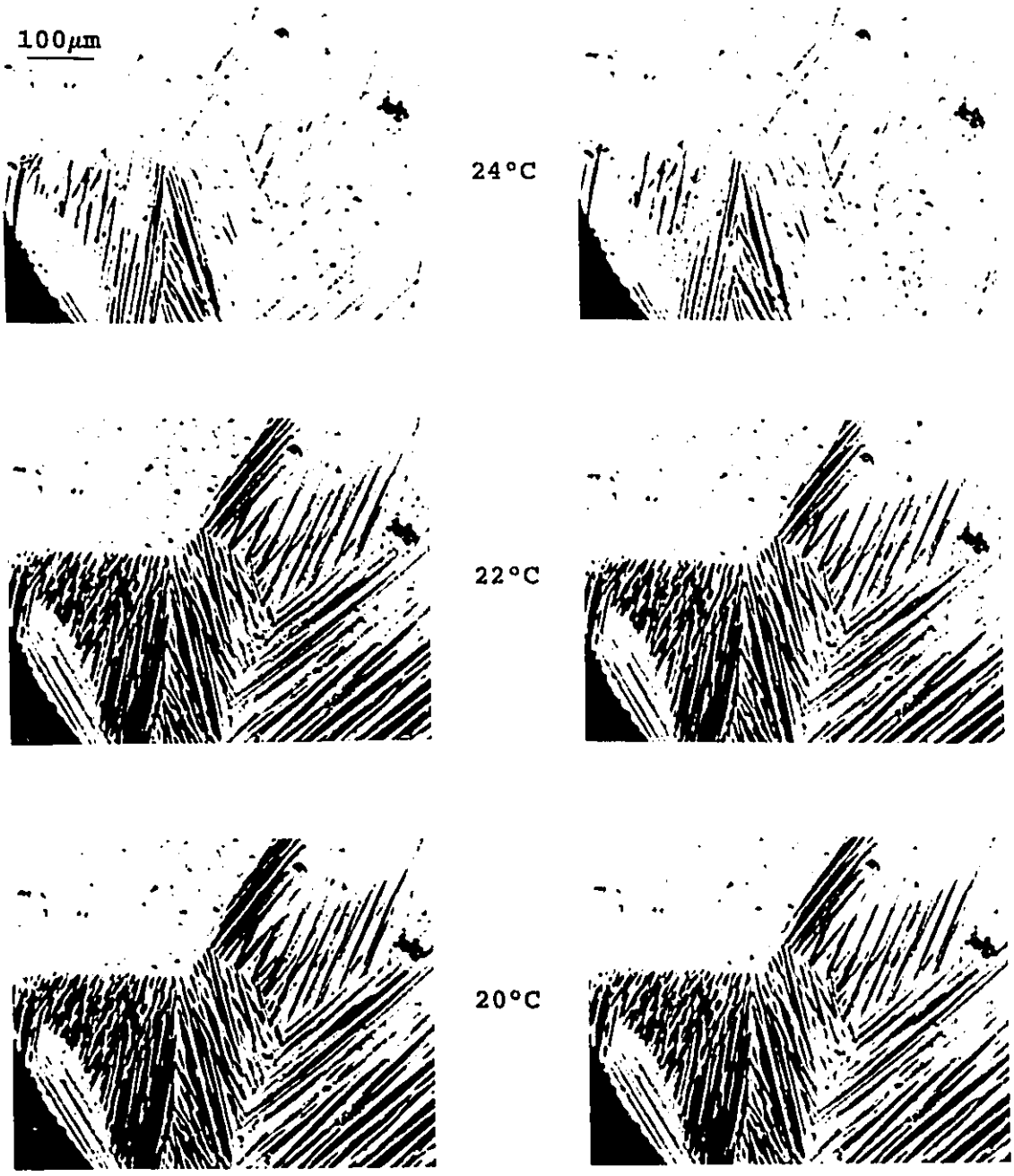

Fig.4.63: Photomicrographs taken at the beginning (left column) and the end (right column) of the isothermal holding (15 min) at progressively lower temperatures during cooling.

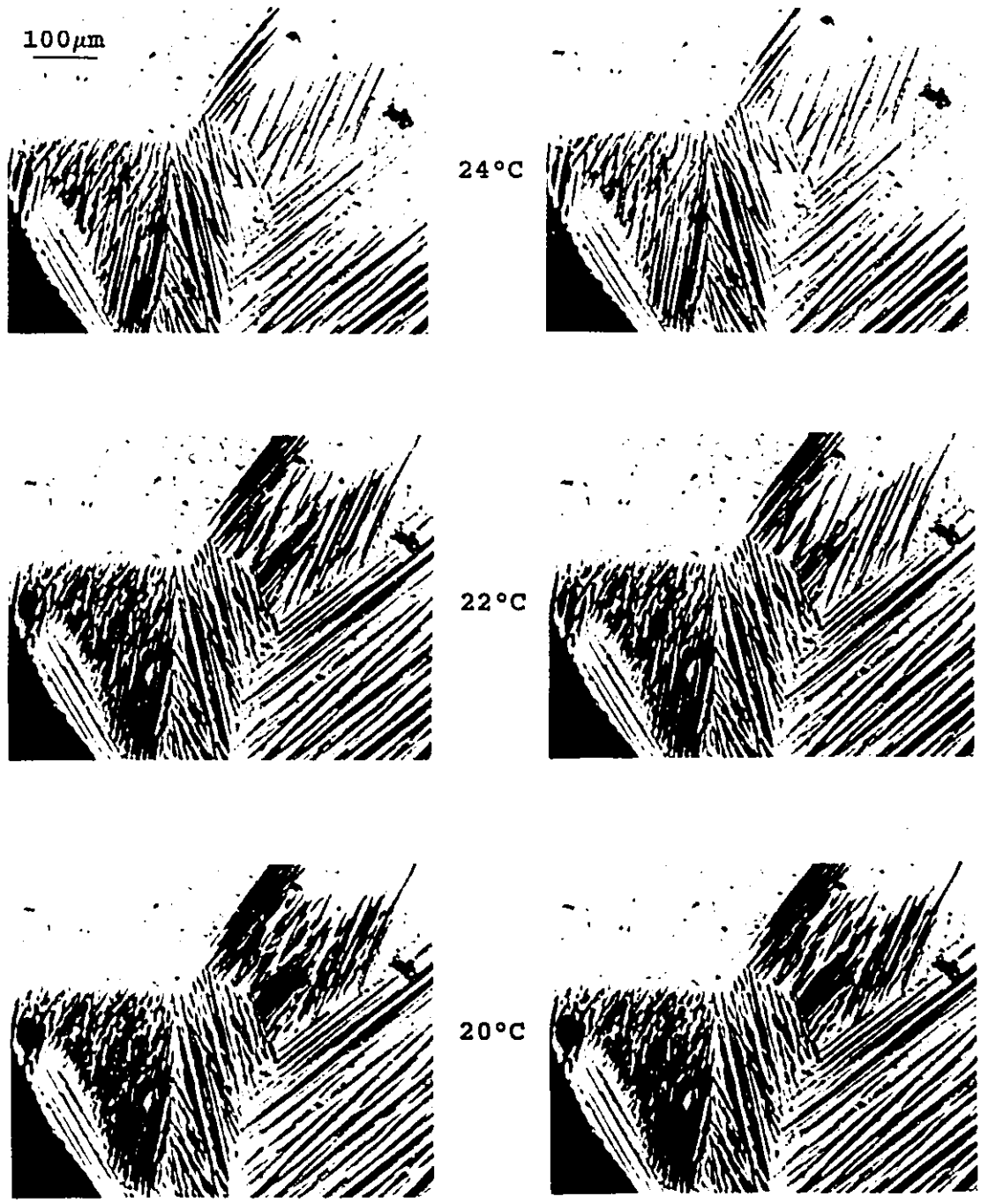

Fig.4.64: Photomicrographs taken at the beginning (left column) and the end (right column) of the isothermal holding (15 min) at progressively higher temperatures during heating.

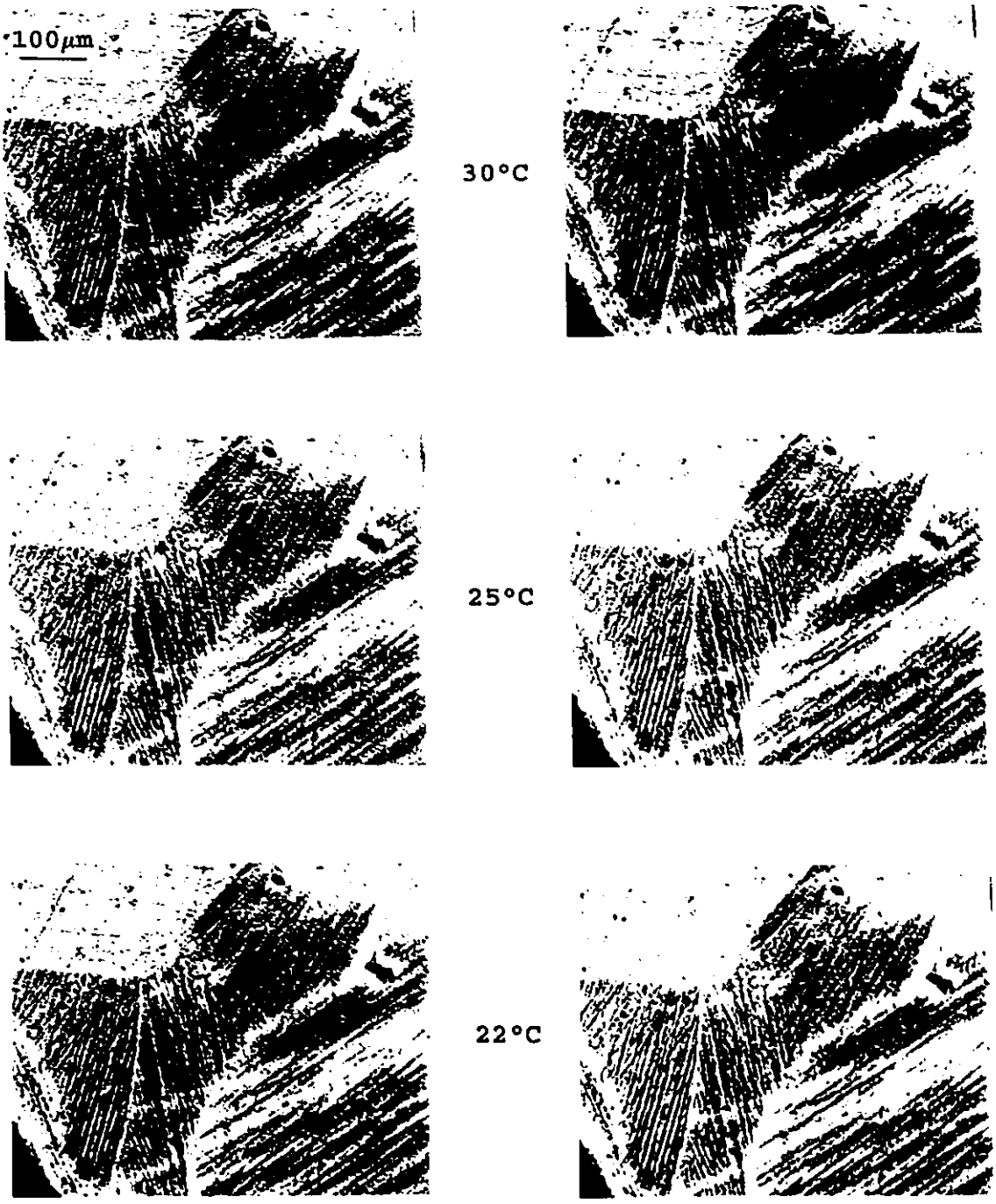

Fig.4.65: Development of the surface relief during cooling (left column) and heating (right column) at 0.5°C/min in the same sample as Fig.4.62, but aged for 87.5 hours at 107°C. Continued in the following two pages.

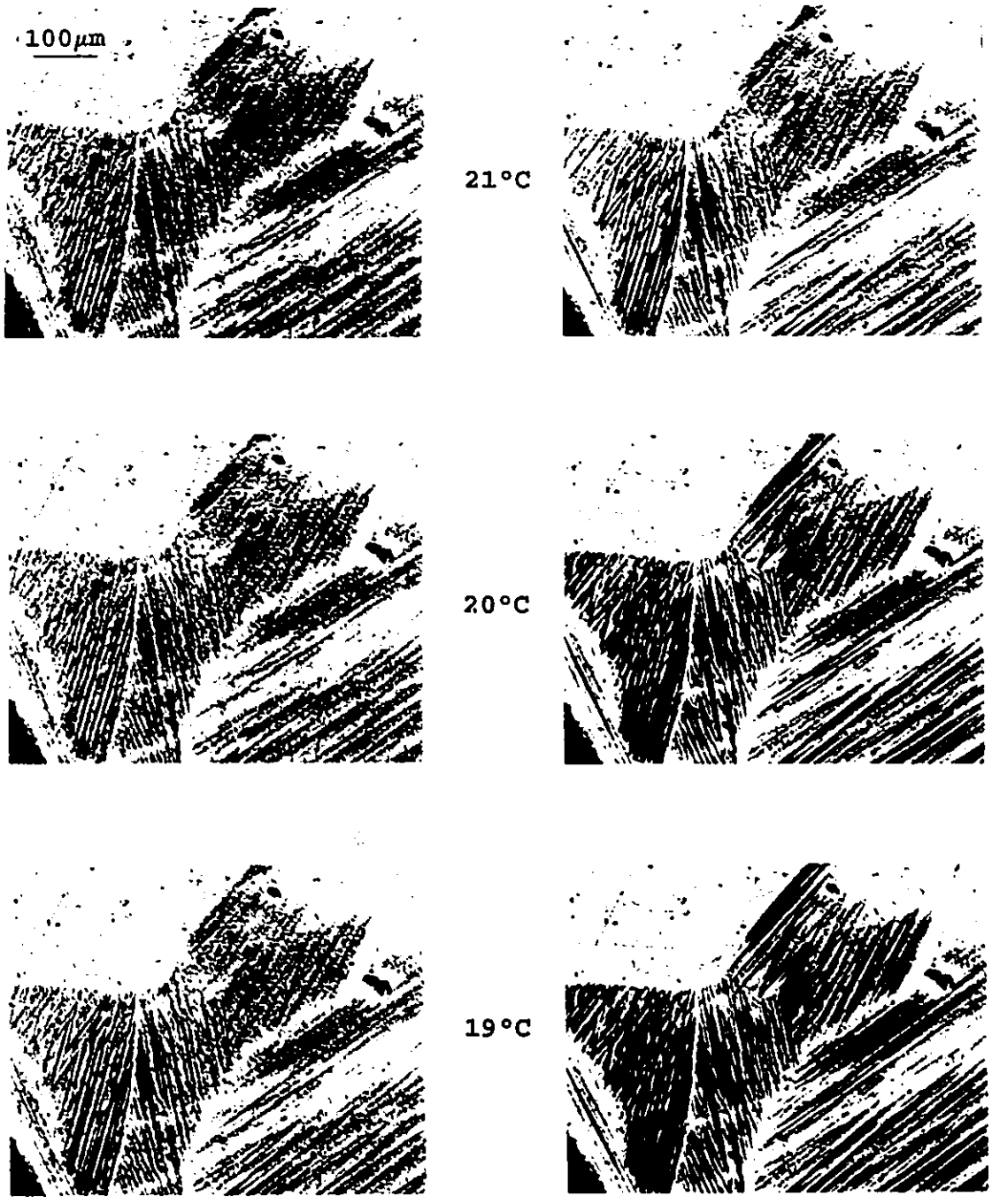

Fig.4.65: Continues from previous page.

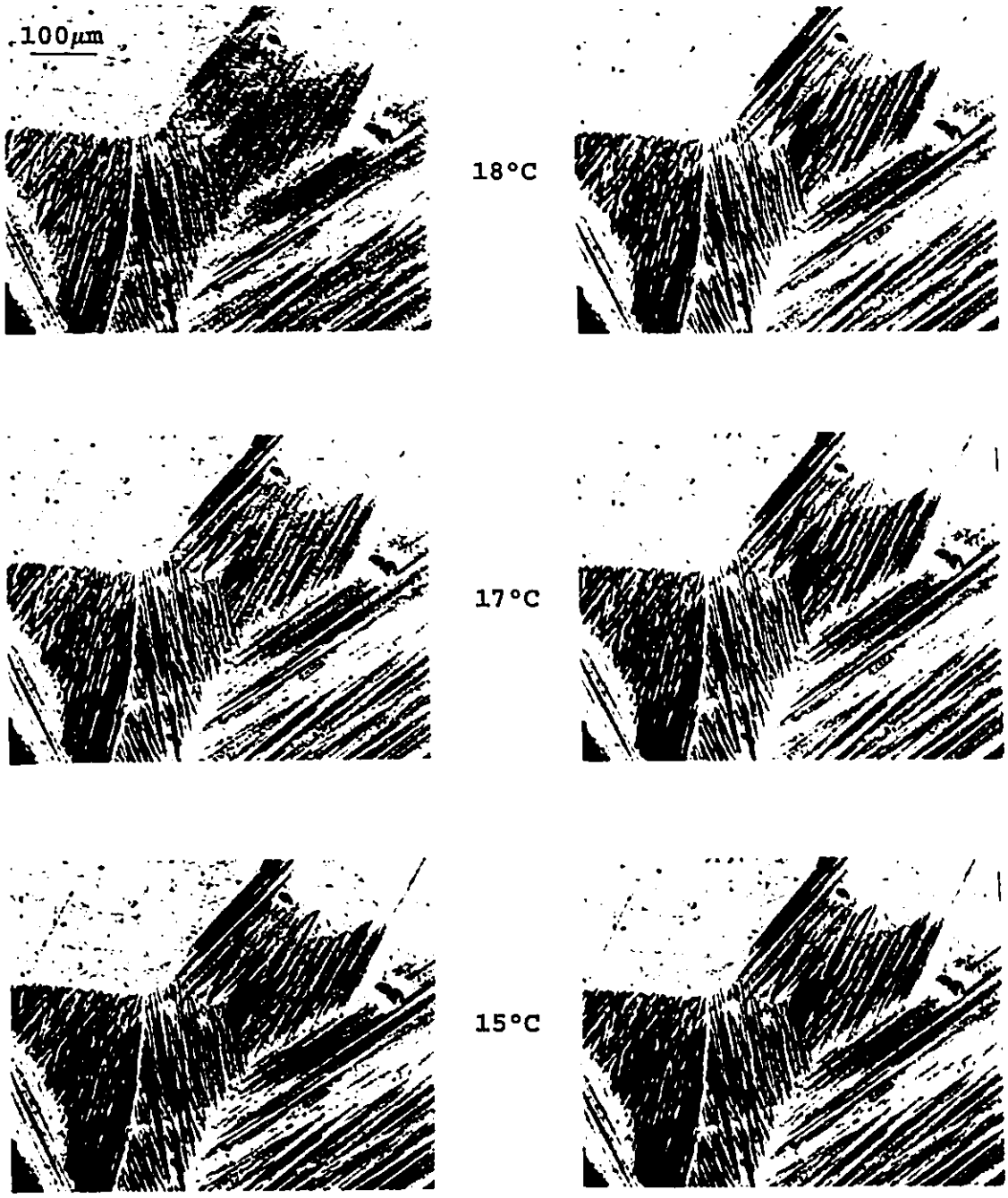

Fig.4.65: Continues from previous page.

is related to a reduced mobility of the martensite/parent interfaces due to their pinning by the fine α-precipitates.

4.5 X-ray Diffraction Analysis

4.5.1 Determination of the Structure

The sample of alloy A (15mmx2mmx0.5mm) which was previously examined by metallography was also used for X-ray diffraction analysis and the result is shown in Fig.4.66. The diffraction peaks have been identified by comparing and matching the pattern with that given by Suzuki (1989) for a Cu-12%Zn-9%Al alloy (composition of alloy A is Cu-13%Zn-9%Al). Suzuki identified the alloy as having a 18R martensite phase in the as-quenched condition. Their results clearly showed the existence of the 111 peak associated with DO_3 type of order in the β phase transformed from the quenched martensite. It is therefore assumed that the as-quenched alloy A consists of a mixture of 18R martensite and DO_3 ordered β phase, despite the fact that the β phase superlattice reflections are too weak to be directly observable. Tadaki et al.(1987) have also identified the parent phase of an as-quenched Cu-14%Zn-9%Al alloy as having a DO_3 type of order. Due to the relatively high Al content in alloy A, the B2→DO_3 transition is expected to occur at a temperature as high as 420°C, according to Singh et al.(1978), and the parent phase is therefore expected to be

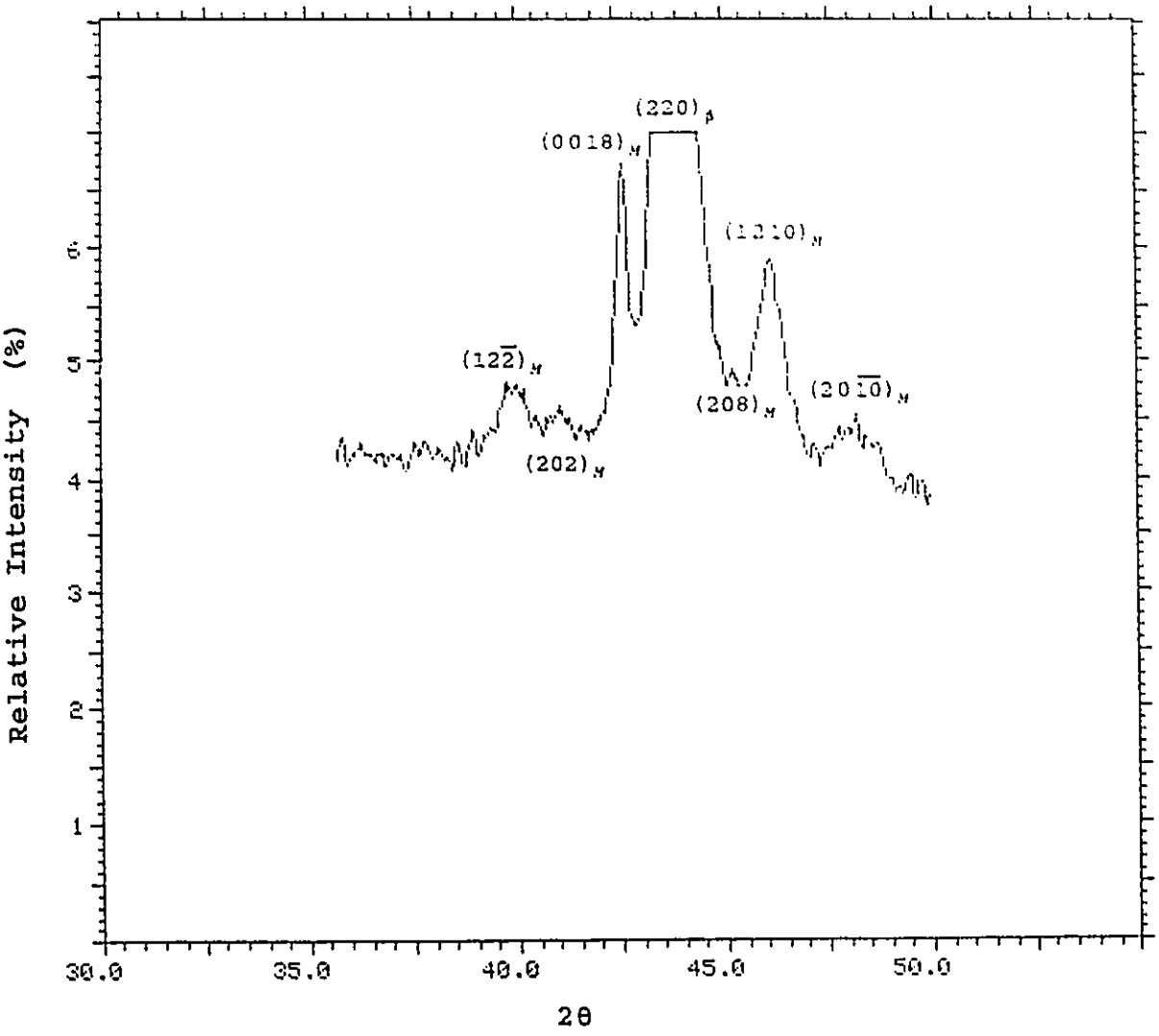

Fig.4.66: X-ray diffraction pattern of an as-quenched Cu-Zn-Al alloy A sample.

in DO_3 order before transforming to martensite during quenching.

4.5.2 Study of Stress-induced Martensite

A flat plate specimen (25mmx2.5mmx0.5mm) of alloy A was first heat-treated and analyzed in the stress-free as-quenched condition, as shown in Fig.4.67(a). The same specimen was then bent into a half circle and examined again at the same central spot. The diffraction pattern of the bent (and therefore stressed) specimen is shown in Fig.4.67(b). Evidently, the most significant change is the dramatic increase of one specific [i.e.,(1210)] martensite peak intensity, which suggests the formation of stress-induced, and therefore preferentially oriented martensite variants. If martensite variants had formed in a random manner, the intensities of all martensite peaks would have increased proportionately. The small shift of the peak positions may be due to the slight difference in the positioning of the sample.

4.5.3 Study of the Aging Effects

To further study the microstructural changes responsible for the decrease in the extent of surface relief variation (section 4.4.2), and deterioration of internal friction (section 4.2.1.1) and DSC peak (section 4.3.4)

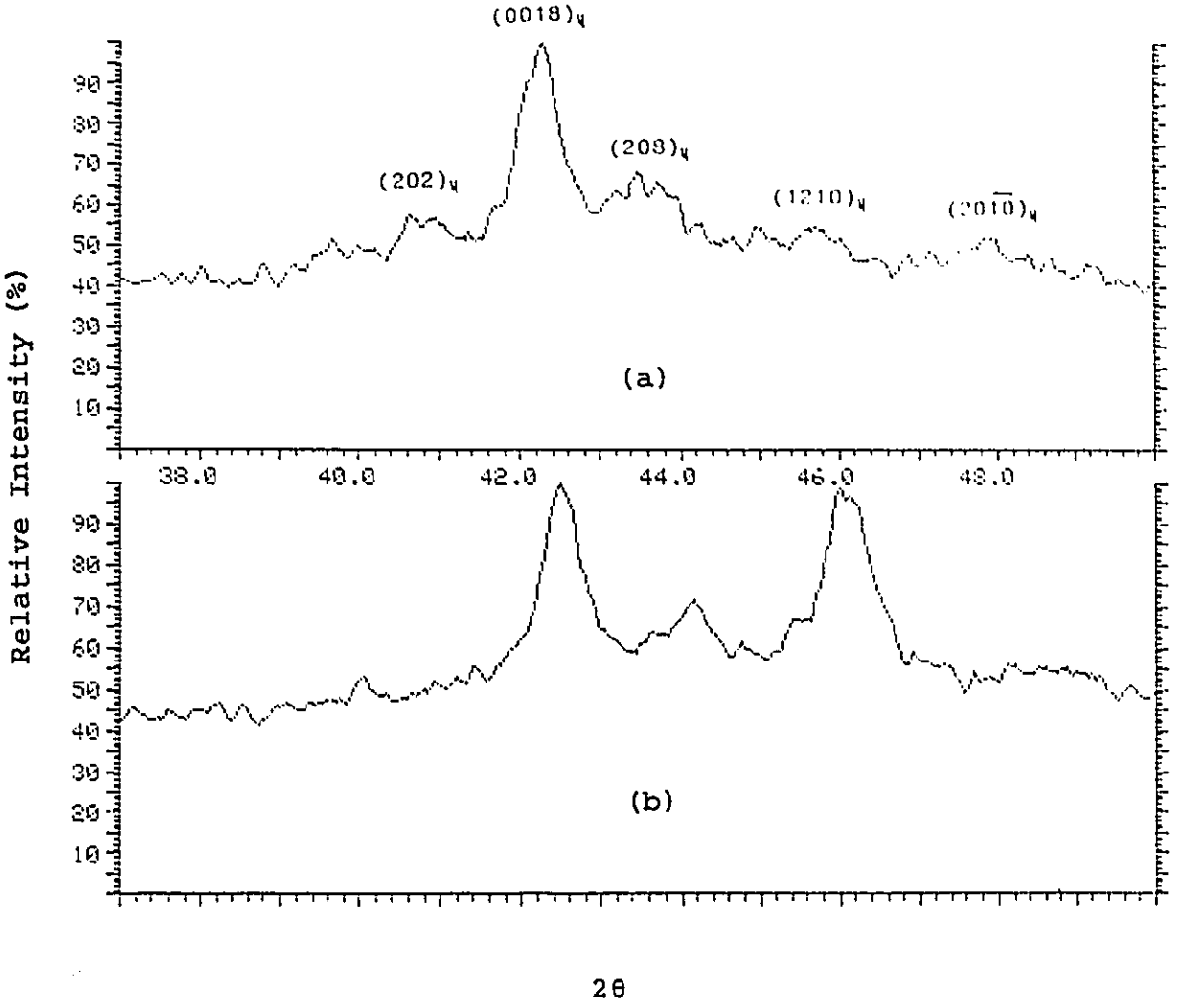

Fig.4.67: Comparison of the X-ray diffraction pattern of an as-quenched Cu-Zn-Al alloy A sample (a) with that of the same sample after being subject to bending (b).

associated with the martensitic transformation, X-ray diffraction analysis was carried out after the sample had been thermally cycled to different upper temperature limits. Fig.4.68 compares the diffraction peaks observed in the as-quenched condition with those obtained after six thermal cycles to 180°C at 2°C/minute. No significant changes are observed. Fig.4.69 further compares the as-quenched case to that obtained after another thermal cycle to 280°C following the treatment in Fig.4.68(b). It is seen that after thermal cycling to 280°C, the only peak of interest appears at 49.3°, which according to Suzuki (1989) is (200) peak of the α-phase. This, together with the metallographic observation in section 4.4.1, suggests the formation of the α-phase precipitate when the sample is thermally cycled to higher temperatures.

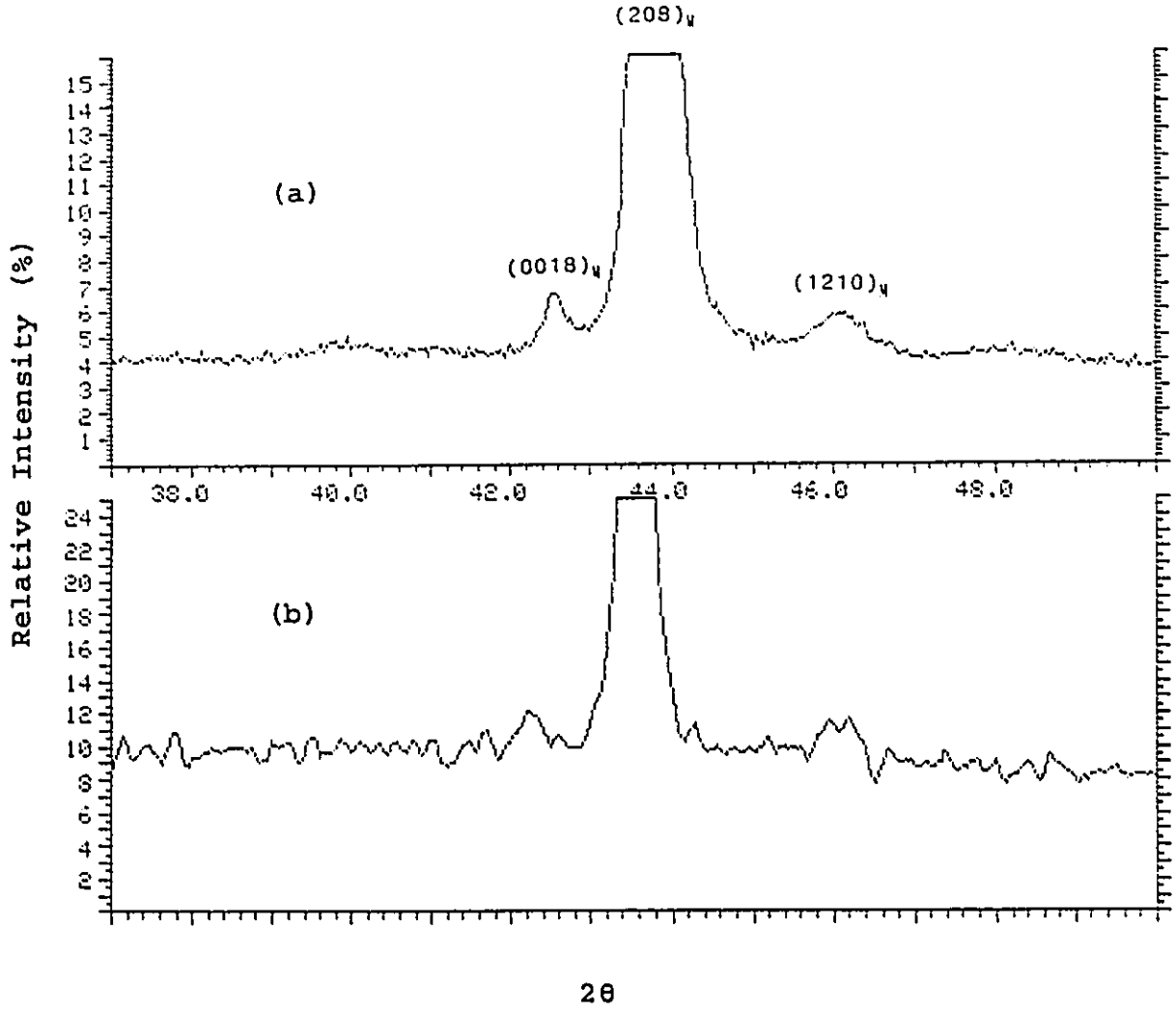

Fig.4.68: Comparison of the X-ray diffraction pattern of an as-quenched Cu-Zn-Al alloy A sample (a) with that of the same sample after 6 thermal cycles from room temperature to 180°C at 2°C/min (b).

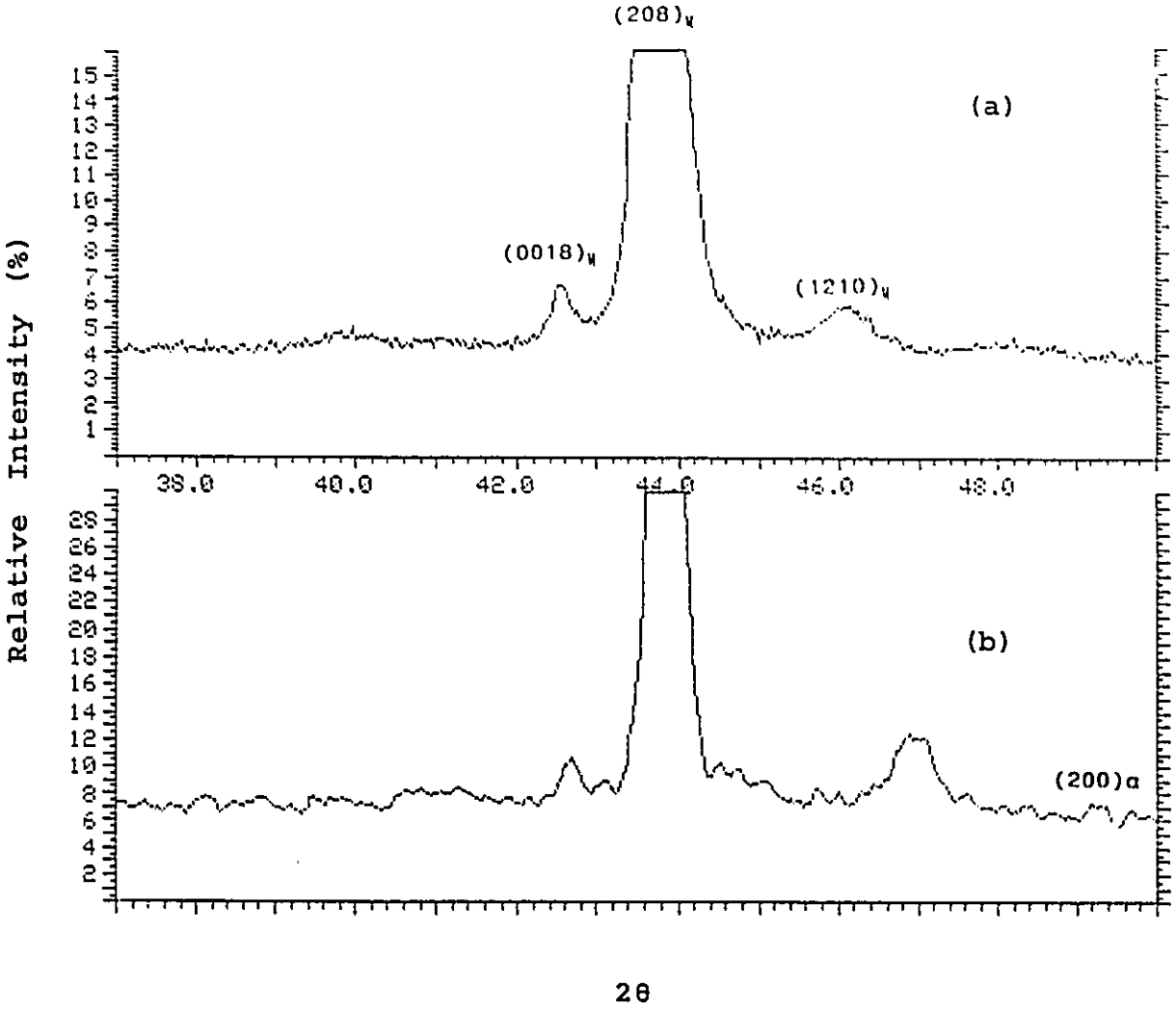

Fig.4.69: Comparison of the X-ray diffraction pattern of the as-quenched Cu-Zn-Al alloy A sample (a) with that of the same sample after 6 thermal cycles to 180°C and then 1 thermal cycle to 280°C at 2°C/min (b).

CHAPTER 5

A NEW FORMULATION OF INTERNAL FRICTION DUE TO THERMOELASTIC MARTENSITIC TRANSFORMATION

5.1 The Need for a New Formulation

The limitations of the existing formulations of internal friction due to martensitic transformation, including the widely accepted formulation (equation 2.4) by Dejonghe, have already been discussed in section 2.3.2. Among the several variables which can affect the internal friction of martensitic transformation, the effects of the oscillation or stress amplitude seem to be the most controversial, as discussed below. While some have found that internal friction increases as the oscillation amplitude increases (Dejonghe et al., 1975 and 1977, Koshimizu and Benoit, 1982), others have found it to increase with decreasing amplitude (Gremaud et al., 1987 and Bidaux et al., 1989 & 1993), and still others have found it to be independent of amplitude (Delorme et al., 1971, Mercier and Melton, 1976, and Evsyukov, 1991). In this study, as reported in section 4.2.1.2, a monotonic increase in internal friction with the decrease in stress amplitude occurred when the sample was initially "trained" by the applied stress. However, when the applied stress was initially low and then gradually increased to "train" the sample, a

three-stage change of internal friction with the increasing stress amplitude was observed. Unfortunately, none of the existing formulations are able to explain the above results and therefore the development of a new and more general formulation is necessary.

5.2 Development of the New Formulation

To interpret the observed amplitude dependence of the internal friction due to martensitic transformation, a physical model and mathematical treatment is now developed and explicit relations between the internal friction and the applied stress amplitude are derived. Part of this derivation has been published (Xiao, 1993). For doing so, we consider a bar specimen undergoing a dynamic tensile stress of $\sigma=\sigma_0(1+\sin\omega t)/2$ at a temperature above M_s (i.e., in β phase). The pseudoelastic behaviour during loading and unloading, with a hysteresis h, is represented by Fig.5.1(a). Note that since static stress does not contribute to the internal friction, only dynamic stress is considered in this treatment.

The pseudoelastic transformation strain (ϵ_p) as a function of time, can now be illustrated by Fig.5.2, where σ_{c1} and σ_{c2} are defined in Fig.5.1(a).

According to Dejonghe et al.(1976), the change in the pseudoelastic strain ($d\epsilon_p$) is related to the amount of

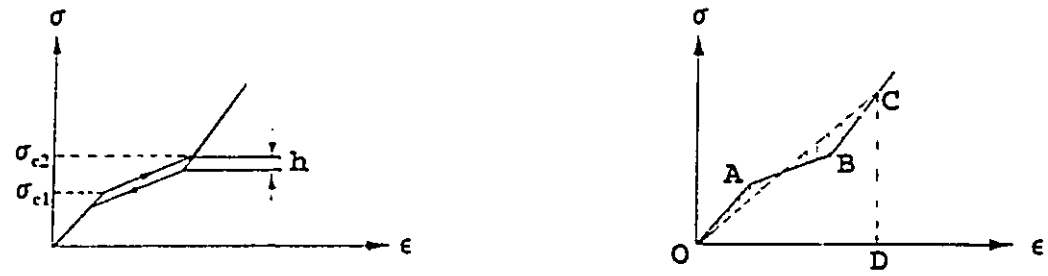

Fig.5.1: Simplified pseudoelastic behaviour in β phase (a) and maximum stored energy represented by the area under curve OABC (b).

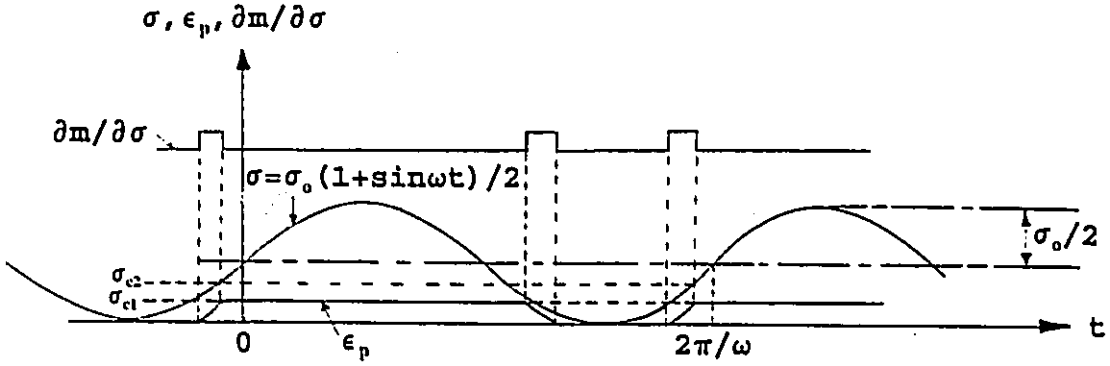

Fig.5.2: Stress (σ), pseudoelastic transformation strain (ϵ_p) and $\partial m/\partial \sigma$ as a function of time (t).

martensite transformed (dm) by:

$$d\epsilon_p = A\sigma E^{-1} dm \tag{5.1}$$

where E is the Young's modulus and A a material constant with a unit of $(mass)^{-1}$ or $(volume)^{-1}$.

From the general definition of internal friction,

$$\tan\phi = \frac{1}{2\pi}\frac{\Delta W}{W} \tag{5.2}$$

where W is the maximum potential energy stored in the material during a stress cycle, and ΔW is the energy dissipated in a full cycle:

$$\Delta W = \oint \sigma d\epsilon_p \tag{5.3}$$

substituting (5.1) into (5.3):

$$\Delta W = \oint \sigma A \sigma E^{-1} dm = \oint A E^{-1} \sigma^2 \left(\frac{dm}{dt}\right) dt \tag{5.4}$$

Since martensitic transformation can be caused either by a change in temperature, or by an applied stress, thus:

$$\frac{dm}{dt} = \frac{\partial m}{\partial T}\frac{\partial T}{\partial t} + \frac{\partial m}{\partial \sigma}\frac{\partial \sigma}{\partial t} \tag{5.5}$$

Substituting equation (5.5) into equation (5.4) yields:

$$\Delta W = \oint A E^{-1} \sigma^2 \left(\frac{\partial m}{\partial T}\frac{\partial T}{\partial t} + \frac{\partial m}{\partial \sigma}\frac{\partial \sigma}{\partial t}\right) dt \tag{5.6}$$

Integrating equation (5.6) over the cycle (0, $2\pi/\omega$), and noting that $h/(\sigma_{c1}+\sigma_{c2}) \ll 1$, one obtains**:

$$\Delta W = AE^{-1}\left(\frac{\partial m}{\partial T}\frac{\partial T}{\partial t}\int_0^{(\frac{2\pi}{\omega})}\sigma^2 dt+\frac{\partial m}{\partial \sigma}\int_{\sigma_{c1}}^{\sigma_{c2}}\sigma^2 d\sigma+\frac{\partial m}{\partial \sigma}\int_{(\sigma_{c2}-h)}^{(\sigma_{c1}-h)}\sigma^2 d\sigma\right) \qquad (5.7)$$

$$= \frac{AE^{-1}(\sigma_o)^2}{2}\left\{\frac{3}{4}\frac{\partial m}{\partial T}\frac{\partial T}{\partial t}f^{-1}+2h\left(\frac{\sigma_{c2}}{\sigma_o}\right)^2\frac{\partial m}{\partial \sigma}\left[1-\left(\frac{\sigma_{c1}}{\sigma_{c2}}\right)^2\right]\right\}$$

Substituting equation (5.7) into equation (5.2) and noting that $W=(\sigma_o)^2/2E$ [assuming that Area(OABCD) =Area(OCD) in Fig.5.1(b) provided that the two shaded areas are relatively small and approximately compensate for each other], one obtains:

$$\tan\phi = \left(\frac{A}{2\pi}\right)\left\{\frac{3}{4}\frac{\partial m}{\partial T}\frac{\partial T}{\partial t}f^{-1}+2h\left(\frac{\sigma_{c2}}{\sigma_o}\right)^2\frac{\partial m}{\partial \sigma}\left[1-\left(\frac{\sigma_{c1}}{\sigma_{c2}}\right)^2\right]\right\} \qquad (5.8)$$

By using this equation, we now discuss the following three situations:

(a) $\sigma_o > \sigma_{c2} > \sigma_{c1}$

In this case, the stress amplitude (σ_o) is higher than the critical stresses (σ_{c1}, σ_{c2}) and equation (5.8) applies effectively and can be further expressed as:

** To ensure that σ_{c1} and σ_{c2} are constant, the temperature is fixed at where the internl friction peak occurs.

$$\tan\phi = C+B(\sigma_o)^{-2} \qquad (5.9)$$

$$where \quad C=\frac{3A}{8\pi}\frac{\partial m}{\partial T}\frac{\partial T}{\partial t}f^{-1} \qquad (5.10a)$$

$$and \quad B=\frac{Ah}{\pi}\frac{\partial m}{\partial \sigma}(\sigma_{c2})^2\left[1-\left(\frac{\sigma_{c1}}{\sigma_{c2}}\right)^2\right] \qquad (5.10b)$$

Note that C and B are constants independent of σ_o. Equation (5.9) shows that internal friction increases rapidly with decreasing stress amplitude σ_o.

(b) $\sigma_{c2}>\sigma_o>\sigma_{c1}$

In this case the stress amplitude (σ_o) is between the upper (σ_{c2}) and lower (σ_{c1}) critical stresses. It is obvious from Fig.5.2 that the upper limit of integration σ_{c2} should now be replaced by σ_o, thus equation (5.8) should be rewritten as:

$$\tan\phi = \frac{A}{2\pi}\left\{\frac{3}{4}\frac{\partial m}{\partial T}\frac{\partial T}{\partial t}f^{-1}+2h\frac{\partial m}{\partial \sigma}\left[1-\left(\frac{\sigma_{c1}}{\sigma_o}\right)^2\right]\right\} \qquad (5.11)$$

Equation (5.11) bears resemblance to the expression (equation 2.4) derived by Dejonghe et al.(1976) and shows that under certain circumstances the internal friction could increase with increasing stress amplitude σ_o.

(c) $\sigma_{c1}>\sigma_o$

In this case, the stress amplitude (σ_o) is lower than the lower critical stress (σ_{c1}) and thus no stress-induced martensite would occur and therefore $\partial m/\partial\sigma=0$ at any time, so that the second term in the brackets of equation (5.6) vanishes, and equation (5.8) becomes:

$$\tan\phi = \frac{3A}{8\pi}\frac{\partial m}{\partial T}\frac{\partial T}{\partial t}f^{-1} \qquad (5.12)$$

Equation (5.12) resembles the expression derived by Delorme et al.(1971), and can be used to explain the amplitude independence of the internal friction observed under certain circumstances.

It is therefore believed that the seemingly conflicting results of the amplitude dependence of the internal friction due to martensitic transformation reported by different investigators are in fact not contradictory, but rather complementary to each other. All of them can be explained by one of the three special cases discussed above.

We now proceed to apply the results of equation (5.9) (when $\sigma_o>\sigma_{c2}>\sigma_{c1}$) to the specific specimen geometry and loading condition for which the internal friction measurements were carried out in this study. For a three point bending loading condition, the tensile or compressive stress (σ) at any point

in the central cross section is linearly proportional to the distance (x) from the neutral axis (x-axis points vertically downwards in the DMA), as shown in Fig.5.3, where

$$\sigma(x) = \left(\frac{\sigma_o}{R}\right)x \qquad (5.13)$$

$$\text{and at } \sigma=\sigma_{c2}, \quad x=x_o=\left(\frac{\sigma_{c2}}{\sigma_o}\right)R \qquad (5.14)$$

Substituting $\sigma(x)=(\sigma_o/R)x$ for σ_o in equation (5.9), $\tan\phi$ can now be expressed as a function of x:

$$\tan\phi(x) = C+B\left(\frac{\sigma_o}{R}\right)^{-2}x^{-2} \qquad (5.15)$$

Averaging along the cross section yields:

$$\langle\tan\phi\rangle = \frac{\int_{x_o}^{R}\tan\delta(x)\cdot(2y)\,dx}{\int_{x_o}^{R}2y\,dx} \qquad (5.16)$$

Substituting $x_o=(\sigma_{c2}/\sigma_o)R$ and $y=(R^2-x^2)^{1/2}$ into equation (5.16), one obtains:

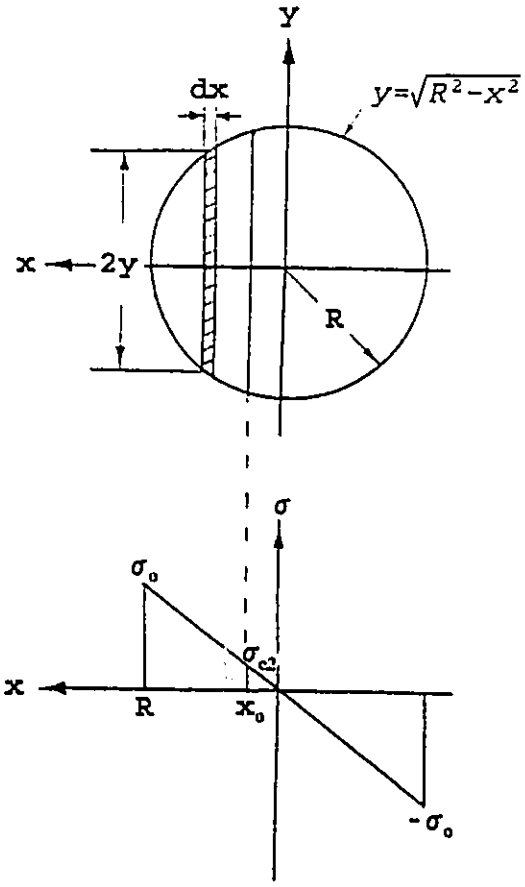

Fig.5.3: Stress distribution in the sample cross section.

$$\langle \tan\phi \rangle = C + 2B\sigma_o^{-2} \frac{\left(\frac{\sigma_o}{\sigma_{c2}}\right)\sqrt{1-\left(\frac{\sigma_{c2}}{\sigma_o}\right)^2} + \arcsin\left(\frac{\sigma_{c2}}{\sigma_o}\right)}{\frac{\pi}{2} - \left(\frac{\sigma_{c2}}{\sigma_o}\right)\sqrt{1-\left(\frac{\sigma_{c2}}{\sigma_o}\right)^2} - \arcsin\left(\frac{\sigma_{c2}}{\sigma_o}\right)} \qquad (5.17)$$

If $\sigma_o \gg \sigma_{c2}$, equation (5.17) can be simplified as:

$$\langle \tan\phi \rangle = C + 2B(\sigma_o)^{-2} \frac{\left(\frac{\sigma_o}{\sigma_{c2}} + \frac{\sigma_{c2}}{\sigma_o}\right)}{\frac{\pi}{2} - \frac{\sigma_{c2}}{\sigma_o} - \frac{\sigma_{c2}}{\sigma_o}} \qquad (5.18)$$

$$= C + \left(\frac{4B}{\sigma_{c2}}\right)(\sigma_o)^{-1} \frac{1+\left(\frac{\sigma_{c2}}{\sigma_o}\right)^2}{\pi - 4\left(\frac{\sigma_{c2}}{\sigma_o}\right)}$$

If the term (σ_{c2}/σ_o) is neglected, the above becomes:

$$\langle \tan\phi \rangle = C + \left(\frac{4B}{\pi\sigma_{c2}}\right)(\sigma_o)^{-1} = C + D(\sigma_o)^{-1} \qquad (5.19)$$

$$where \quad D = \frac{4B}{\pi\sigma_{c2}} = \frac{4Ah}{\pi^2}\frac{\partial m}{\partial \sigma}\sigma_{c2}\left[1-\left(\frac{\sigma_{c1}}{\sigma_{c2}}\right)^2\right] \qquad (5.20)$$

and C is defined earlier in Equation (5.10a). Note that equation (5.19) is valid only when $\sigma_o \gg \sigma_{c2}$.

The inverse relation between the internal friction and the stress amplitude, suggested in equation (5.19), can be physically understood by looking at Fig.5.2. Evidently, at a fixed frequency (or period) of oscillation, a larger stress amplitude (σ_o) means that the dynamic stress reaches the σ_{cl} faster and therefore a smaller phase lag of pseudoelastic strain (ϵ_p) behind the dynamic stress occurs, resulting in smaller internal friction.

Equation (5.19) can now be used to interpret the observed stress amplitude dependence reported in section 4.2.1.2, and will be discussed in detail in Section 5.3.

5.3 Interpretation of the Observed Stress Amplitude Dependence in Terms of the Derived Formulation

(1) Decreasing Stress Amplitude

If the experimental results presented in Fig.4.12 are re-plotted in the form of $\tan\phi$ versus $(\sigma_o)^{-1}$, as shown in Fig.5.4, one observes that at higher level of stress amplitude (10^6-10^7 Pa), there is a relatively good linear relation between $\tan\phi$ and $(\sigma_o)^{-1}$. However, as the stress amplitude becomes too small, the linearity becomes rather poor (Fig.5.5). Therefore, the experimental results seem to be in good agreement with the theoretical prediction only at higher stress amplitude according to equation (5.19).

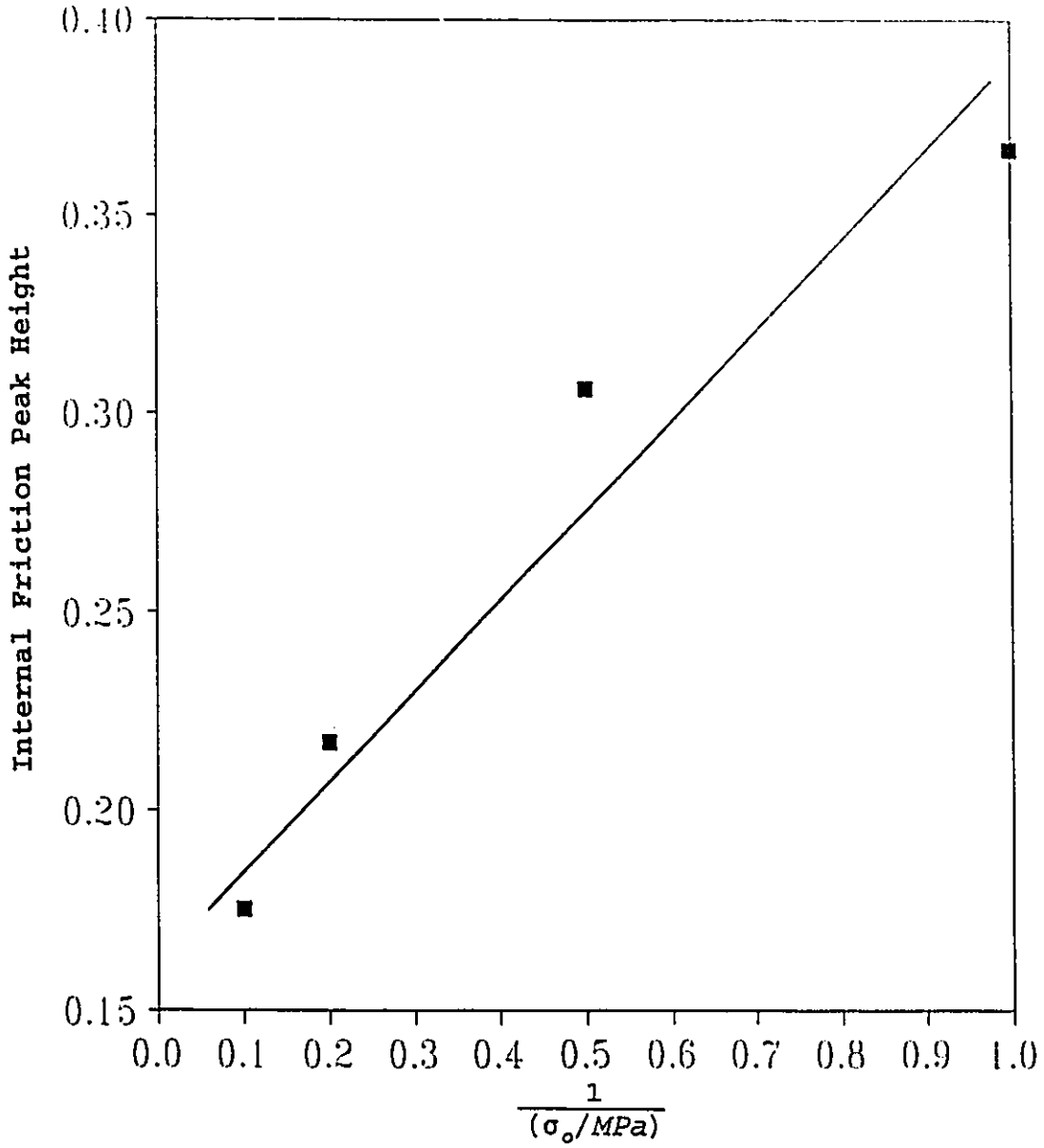

Fig.5.4: Internal friction peak height versus reciprocal of stress amplitude.

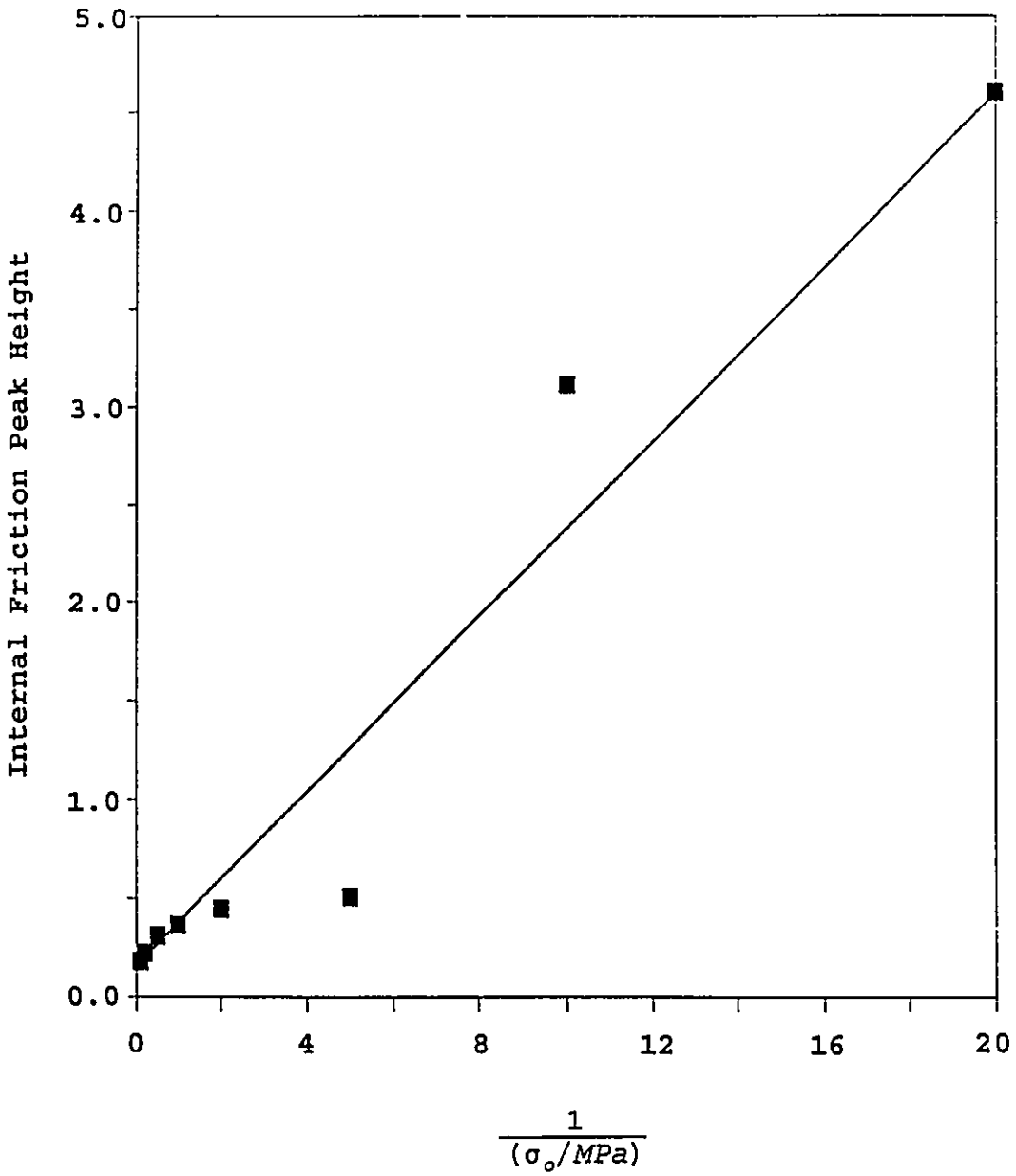

Fig.5.5: Internal friction peak height versus reciprocal of stress amplitude for a wider range.

As for the shift of peak temperature (M_p) with applied stress observed in Fig.4.14, the initial decrease of M_p with decrease in stress is in qualitative agreement with the relation between M_p and σ_o predicted by the Clausius-Clapeyron Equation. The sudden reversal of the trend below a stress amplitude of $5x10^5$ Pa, accompanied by a drastic increase in internal friction, is explained as follows. Contardo and Guenin (1990) have recently observed that repeated stress cycling causes σ_{c1} to decrease while σ_{c2} remains relatively constant. Therefore, it is assumed that in this case the σ_{c1} begins to decrease significantly after prolonged stress and temperature cycling, at which point the stress-induced martensite is able to form at a higher temperature. From equation (5.20), it is evident that if σ_{c2} remains constant and σ_{c1} decreases, D would increase significantly, giving rise to a much more drastic increase in the internal friction than would be expected from the decrease of σ_o alone from equation (5.19).

(2) Increasing Stress Amplitude

The features of the three-stage amplitude dependence of the internal friction due to martensitic transformation reported earlier in section 4.2.1.2 can be further understood in terms of the formulations developed in section 5.2.

In Fig.4.19, one notices that in the early part of stage I there is little amplitude dependence of the internal friction peak height as well as negligible bending deflexion. This suggests that only thermally-induced martensitic transformation (which results in zero net shape change) is taking place below certain critical stress amplitude, and thus the internal friction peak is independent of the stress amplitude, in agreement with the prediction by equation (5.12). In the later part of stage I, there is a noticeable increase of internal friction peak height with stress amplitude, suggesting that the maximum applied stress may now fall between σ_{c1} and σ_{c2} so that equation (5.11) applies, resulting in an increase in the internal friction with increasing stress amplitude.

In stage II, the rapid rise in the bending deflexion, coupled with the simultaneous decrease in internal friction peak height, suggests that the maximum applied stress is now higher than σ_{c2} in the bulk of the sample and the amplitude dependence of the internal friction shifts away from equation (5.11) towards equation (5.9). In the latter part of stage II, where equation (5.9) becomes fully effective, the average internal friction exhibited by the sample should be predicted by equation (5.19). This is verified by a linear plot of internal friction peak height versus $(\sigma_o)^{-1}$ for the last three

data points in stage II, as shown in Fig.5.6.

In stage III, the stress amplitude is so high that the maximum applied stress is able to activate the movement of interfaces between different martensite variants. Thus the martensite variants are further oriented into favourable orientation under the application of stress. The movement of martensite/martensite interfaces is evidenced by a sudden jump of the martensitic internal friction above a certain stress amplitude (Fig.4.19) as well as the jerky appearance of the martensitic internal friction shown in Fig.4.17. Therefore, the rise of internal friction peak height with stress amplitude in stage III is primarily attributed to the increased internal friction in the martensite phase.

To summarize, the equations developed here relating $\tan\phi$ and σ_o are able to explain the amplitude dependence of the internal friction due to martensitic transformation when the stress is either progressively increased or decreased. In the case where the stress amplitude (σ_o) is much higher than the critical stress for inducing the martensitic transformation (σ_{c2}, σ_{c1}), the derived inverse relation between $\tan\phi$ and σ_o is in good agreement with the experimental results.

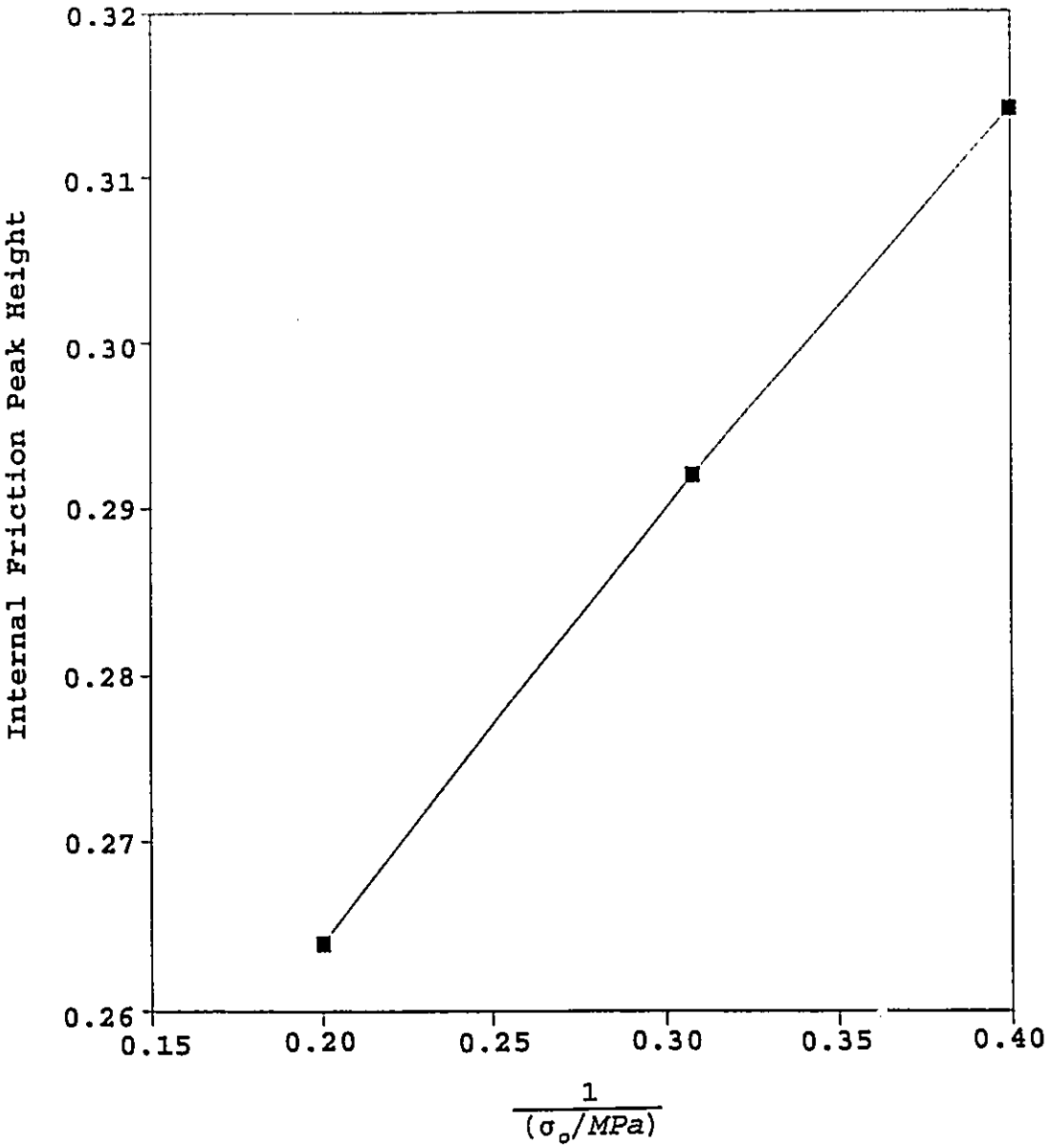

Fig.5.6: Internal friction peak height versus reciprocal of stress amplitude in the later part of stage II.

CHAPTER 6

CONCLUSIONS

1. The martensitic transformation in the Cu-Zn-Al shape memory alloys is characterized by a peak in internal friction and a minimum in elastic modulus in the temperature range of transformation. The internal friction peak and modulus minimum become reproducible during repeated thermal cycling once the quenched-in vacancies have been removed, provided the upper temperature of thermal cycling is lower than 100°C.

2. There is a finite thermal hysteresis between the forward and reverse martensitic transformation. Independent determinations by DSC (Differential Scanning Calorimeter), DMA (Dynamic Mechanical Analyzer), and metallography have led to a "true value" of about 3°C for the transformation hysteresis.

3. The effects of stress amplitude on the temperature dependence of internal friction due to martensitic transformation strongly depends on the mechanism of the transformation, i.e., whether the transformation is purely thermally-induced or stress-oriented, and whether the martensite re-orientation is taking place. For the specific case where the transformation is stress-oriented ($\sigma_a \gg \sigma_{c2}$), a

theoretical formulation has been developed which gives a inverse relation between the stress amplitude and the internal friction, in good agreement with the experimental results.

4. Different energy dissipation mechanisms predominate in the different microstructural states during isothermal internal friction measurements immediately following the quenching treatment. At holding temperatures in or close to phase transition region, where parent phase is present, stress-induced martensitic transformation can take place isothermally, giving rise to an internal friction peak, a modulus minimum and a step decrease in probe position during isothermal oscillations. The stress-induced martensite can be reverted to the parent phase when the temperature is raised. On the other hand, at holding temperatures where only martensite phase is present, the monotonic decrease of internal friction with time is associated with the progressive pinning of the martensite/martensite interfaces by vacancies.

5. Aging in the martensite state, with or without stress, results in the stabilization of the martensite, as shown by the disappearance of the reversible martensitic transformation peak from both the DSC and the DMA measurements. Aging in the parent phase, especially at temperatures much higher than A_f, results in the precipitation of fine α-phase in the parent matrix, which also suppresses

the reversible martensitic transformation.

6. The internal friction measured simultaneously during the training of the two-way shape memory effect (TWSME) suggests that each training cycle cumulatively contributes to the "training" process by introducing more oriented dislocations and increasing the mobility of the martensite/martensite interfaces. Multiple training cycles are therefore considered necessary to obtain a large and stable TWSME.

REFERENCES:

Ahlers, M., 1986, in Proceedings of ICOMAT-86, Nara, Japan, p.786.

Allan, P., Crellin, E.B. and Bevis, M., 1973, Phil. Mag., **27**, 127.

Arab, A. A. and Ahlers, M., 1988, Acta Metall., **36**, 2627.

Bansal, G.K. and Heuer, A.H., 1972, Acta Metall., **20**, 1281.

Bansal, G.K. and Heuer, A.H., 1974, Acta Metall., **22**, 409.

Batist, R.D., 1972, Internal Friction of Structural Defects in Crystalline Solids, North-Holland Publishing Company, Amsterdam.

Belko, V. N., Darinskiy, B. M., Postnikov, V. S. and Sharshakov, I. M., 1969, Physics of Metals and Metallography, **27**, 140.

Berkowitz, A.E., Donahue, F.J., Franklin, A.D. and Steijn, R.P., 1957, Acta Metall., **5**, 1.

Bidaux, J.E., Schaller, R. and Benoit, W., 1989, Acta Metall., **37**, 803.

Bidaux, J.E., Gremaud, G. and Benoit, W., 1993, Materials Science Forum, **119-121**, 299.

Bilby, B.A. and Christian, J.W., 1956, in Inst. Metals Monograph No.18, London, p.121.

Buehler, W.J., Gilfrich, J.V. and Wiley, R.C., 1963, J. Appl. Phys., **34**, 1475.

Burkart, M.W. and Read, T.A., 1953, J. Metals, 5, 1516.

Cech, R.E. and Holloman, J.H., 1953, Trans. AIME, 197, 685.

Chang, L.C. and Read, T.A., 1951, Trans. AIME, 191, 47.

Christian, J.W., 1965, in Spl. Rep. 93, Iron and Steel Institute, London, p.1.

Clark, H.M. and Wayman, C.M., 1970, in Phase Transformation, American Society For Metals, Cleveland, p.59.

Cohen, M., Olson, G.B. and Clapp, P.C., 1979, in Proc. ICOMAT-79, Intl. Conf. on Martensitic Transformation, Cambridge, Mass., p.1.

Contardo, L. and Guenin, G., 1990, Acta Metall. Mater., 38, 1267.

Cook, J.M. and Brown, L.M., 1978, Scripta Metall., 12, 949.

Daniels, T., 1973, in Thermal Analysis, Kogan Page Limited, London.

Dejonghe, W., Batist, R.D., Delaey, L. and Bonte, M.D., 1975, Shape Memory Effects in Alloys, (Perkins, J., Ed.), Plenum Press, New York.

Dejonghe, W., Batist, R.D. and Delaey, L., 1976, Scripta Metall., 10, 1125.

Dejonghe, W., Delaey, L., Batist, R.D. and Humbeeck, J.V., 1977, Metal Science, 11, 523.

Delaey, L., Suzuki, T. and Humbeeck, J.V., 1984, Scripta Metall., 18, 899.

Delorme, J.E., Schmid, R., Robin, M. and Gobin, P., 1971, J.

De Physique, 32, C2-101.

Dunne, D.P. and Kennon, N.F., 1981, Metals Forum, 4, 176.

Duwez, P. and Taylor, J.L., 1950, Trans. AIME, 188, 1173.

Evsyukov, V.A., Kopylova, V.M., Agapitova, N.V., et al., 1991, Metal Science and Heat Treatment (Translated from Russian), 33, 235.

Friend, C.M., 1991, J. De Phys. IV, 1, C4-25.

Funakubo, H., 1987, in Shape Memory Alloys, Gordon & Breach Science Publishers, New York, p.1 & p.40.

Ghilarducci, A. and Ahlers, M., 1983, J.Phys. F: Met. Phys., 13, 1757.

Gremaud, P.G., Bidaux, J.E. and Benoit, W., 1987, Helv. Physica Acta, 60, 947.

Greninger, A.B. and Mooradian, V.G., 1938, Trans. AIME, 128, 337.

Humbeeck, J.V. and Delaey, L., 1982, J. De Physique, 43, C4-691.

Humbeeck, J.V., Janssen, J., Mwamba, N. and Delaey, L., 1984, Scripta Metall., 18, 893.

Humbeeck, J.V., Hulsbosch, A., Delaey, L. and Batist, R.D., 1985, J. De Physique, 46, C10-633.

Kennedy, S.W., Kriven, W.M. and Fraser, W.L., 1979, Proc. ICOMAT-79, Intl. Conf. on Martensitic Transformations, Cambridge, Mass., p.208.

Koshimizu, S. and Benoit, W., 1982, J. De Phys., 43, C4-679.

Mantel, M., Rapacioli, R. and Guenin, G., 1986a, in Proceedings of ICOMAT-86, Nara, Japan, p.880.

Mantel, M., Guenin, G., Macqueron, J.L., Muntasell, J., Rapacioli, R. and Planes, A., 1986b, Scripta Metall., 20, 803.

Mercier, O. and Melton, K.N., 1976, Scripta Metall., 10, 1075.

Mercier, O. and Melton, K.N., 1979, Acta Metall., 27, 1467.

Morin, M., Guenin, G., Etienne, S. and Gobin, P.F., 1981, Trans. Jap. Inst. of Metals, 22, 1.

Morin, M., 1985, Ph.D thesis, INSA de Lyon, France.

Morin, M., Vincent, A. and Guenin, G., 1985, J. De Physique, 46, C10-625.

Morin, M., Haouriki, M. and Guenin, G., 1987, J. De Physique, 48, C8-567.

Morin, M., Haouriki, M. and Guenin, G., 1989, in Proceedings of The Martensitic Transformation in Science and Technology, (Hornbogen, E. and Jost, N., Ed.), DGM Pub., Bochum, p.325.

Morin, M. and Guenin, G., 1990, Materials Science Forum, 56-58, 499.

Nakata, Y., Tadaki, T. and Shimizu, K., 1985, Trans. JIM, 26, 646.

Nishiyama, Z., 1978, Martensitic Transformation, (Fine, M.E., Meshii, M. and Wayman, C.M., Eds), Academic Press, New York, p.12.

Olander, A., 1932, Z. Kristall., **83A**, 145.

Olson, G.B. and Cohen, M., 1977, Scripta Metall., **11**, 345.

O'Reilly, A.H., 1988, Master's Thesis, McMaster University, Canada.

Ortin, J. and Planes, A., 1988, Acta Metall., **36**, 1873.

Osmond, F., 1895, Bull. Soc. Encour. Ind. Nat., **10**, 480.

Pascheto, W., 1991, Master's Thesis, McMaster University, Canada.

Petty, E.R., 1970, Martensite: Fundamentals and Technology, Longman Group Ltd., London, p.1

Planes, A., Macqueron, J.L., Morin, M. and Guenin, G., 1981, Materials Science and Engineering, **50**, 53.

Poole, D.M. and Hume-Rothery, W., 1955, J. Inst. Metals, **83**, 473.

Purdy, G.R. and Parr, J.G., 1961, Trans. Met. Soc. AIME, **221**, 636.

Rachinger, W.A., 1958, Brit. J. Appl. Phys., **9**, 250.

Rapacioli, R., Chandrasekaran, M. and Delaey, L., 1975, Shape Memory Effects in Alloys, (Perkins, J., Ed.), Plenum Press, New York, p.365.

Rapacioli, R. and Ahlers, M., 1977, Scripta Metall., **11**, 1147.

Rapacioli, R. and Ahlers, M., 1979, Acta Metall., **27**, 777.

Reynolds, J.E. and Bever, M.B., 1952, Trans. AIME, **194**, 1065.

Rios-Jara, O., Morin, M., Esnouf, C. and Guenin, G., 1985, Scripta Metall., **19**, 441.

Ritter, A., Yang, N.Y.C., Pope, D.P. and Laird, C., 1979, Metall. Trans.(A), **10A**, 667.

Rodriguez, P. and Guenin, G., 1990, Materials Science Forum, **56-58**, 541.

Salzbrenner, R.J. and Cohen, M., 1979, Acta Metall., **27**, 739.

Scarsbrook, G. and Stobbs, W.M., 1987, Acta Metall., **35**, 47.

Schofield, D. and Miodownik, A.P., 1980, Metals technology, **7**, 167.

Singh, S.C., Murakami, Y. and Delaey, L., 1978, Scripta Metall., **12**, 435.

Stobbs, W.M., 1983, J. Microscopy, **129**, 307.

Suzuki, T., Kojima, R., Fujii, Y. and Nagasawa, A., 1989, Acta Metall., **37**, 163.

Suzuki, T., Fujii, Y. and Nagasawa, A., 1990, Materials Science Forum, **56-58**, 481.

Swann, P.R. and Walimont, H., 1963, Acta Metall., **11**, 511.

Tadaki, T., Takamori, M. and Shimizu, K., 1987, Trans. JIM, **28**, 120.

Tong, H.C. and Wayman, C.M., 1974, Acta Metall., **22**, 887.

Tong, H.C. and Wayman, C.M., 1975, Acta Metall., **23**, 209.

Wayman, C.M., 1975, Shape Memory Effects in Alloys, (Perkins, J., Ed.), Plenum Press, New York, p.12.

Wayman, C.M., 1990, Materials Science Forum, **56-58**, 1.

West, E.G., 1982, Copper and Its Alloys, Ellis Horwood Ltd., England, p.98.

Xiao, T., 1993, Metall. Trans.(A), **24A**, 1067.

Xiao, T., Johari, G.P. and Mai, C., 1993, Metall. Trans.(A), in press.

Xie, C.Y., Wen, Y.T. and Zhu, X.F., 1988, Acta Metallurgica Sinica (English Edition), **1A**, 83.

Zhao, Z.Q., Chen, F.X. and Yang, D.Z., 1988, Mater. Sci. Prog. Sinica, **2**, 29.

Zhao, Z.Q., Chen, F.X. and Yang, D.Z., 1989, J. Phys.: Condens. Matter, **1**, 1395.

Zhao, Z.Q., Chen, F.X. and Li, S.Z. et al., 1991, Scripta Metallurgica et Materialia, **25**, 669.

Zhu, J.S., Schaller, R. and Benoit, W., 1988, Phys. Stat. Sol. (a), **108**, 613.